Author:
Ali, Sadman Shariar

Title:
Evolution of the UV Upturn in Early-type Cluster Galaxies

Evolution of the UV Upturn in Early-type Cluster Galaxies

Sadman Shariar Ali

A thesis submitted to the University of Bristol
in accordance with the requirements of the degree of
Doctor of Philosophy
in the Faculty of Science

Department of Physics,
H.H. Wills Physics Laboratory,
Tyndall Avenue,
Bristol,
BS8 1TL

September 2018

$\sim 39,000$ words

Abstract

The UV upturn is a rise in the spectra of early-type galaxies below 2500Å down to the Lyman limit. The objective of this thesis is to analyse the stellar population giving rise to this phenomenon and to understand how it evolves with redshift in cluster early-type galaxies.

In chapter 2, using GALEX, UVOT and optical photometry, I explore the prevalence and strength of the UV upturn in the SEDs of quiescent early-type galaxies in several nearby clusters. Even for galaxies with completely passive optical colours, there is a large spread in vacuum UV colour consistent with almost all having some UV upturn component. Combining GALEX and UVOT data below 3000Å, I generate for the first time comparatively detailed UV SEDs for Coma cluster galaxies. Fitting the UV upturn component with a blackbody, twenty six of these show a range of characteristic temperatures (10000–21000K) for the UV upturn population. Assuming a single temperature to explain GALEX-optical colours could underestimate the fraction of galaxies with UV upturns and mis-classify some as systems with residual star formation. The UV upturn phenomenon is not an exclusive feature found only in giant galaxies; I identify galaxies with similar (or even bluer) $FUV - V$ colours to the giants with upturns over a range of fainter luminosities. The temperature and strength of the UV upturn are correlated with galaxy mass. Under the plausible hypothesis that the sources of the UV upturn are blue horizontal branch stars, the most likely mechanism for this is the presence of a substantial (between 4% and 20%) Helium rich ($Y \geqslant 0.38$) population of stars in these galaxies, potentially formed at $z \sim 4$ and certainly at $z > 2$. This plausibly sets a lower limit of $\sim 0.3 - 0.8 \times 10^{10}\ M_{\odot}$ to the *in situ* stellar mass of $\sim L^{*}$ galaxies at this redshift.

In chapter 3, I test the effect of the cluster environment on the UV upturn of member galaxies. To do so, I measure the $FUV - r$ and $NUV - r$ colours of early-type galaxies in 20 2dF clusters of a wide variety of size and richness. These colours are then plotted against the velocity dispersion and X-ray luminosity of the host cluster, as well as the clustercentric distances and line-of-sight velocities of the galaxies, all parameters that are defined by the cluster environment. In all cases, no clear correlation is found, indicating that the strength of the upturn is unaffected by the cluster environment. Furthermore, the $FUV - r$ and $NUV - r$ colours of the 2dF clusters are consistent with those of Coma and Perseus, which suggests that the UV upturn is a ubiquitous feature in all cluster early-type galaxies at low redshift.

In chapter 4, I measure the strength of the UV upturn for red sequence galaxies in the

Abell 1689 cluster at $z = 0.18$, reaching to or below the L^* level and therefore probing the general evolution of the upturn phenomenon. The range of UV upturn strengths in the population as a whole has not declined over the past 2.2 Gyrs. This is consistent with a model where hot horizontal branch stars, produced by a Helium-enriched population, provide the required UV flux. Based on local counterparts, this interpretation of the result implies Helium abundances of at least 1.5 times the primordial value for this HB population, along with high formation and assembly redshifts for the galaxies and at least a subset of their stellar populations.

In chapter 5, I analyse the strength of the UV upturn in red sequence galaxies with luminosities reaching to below the L^* point within four clusters at z = 0.3, 0.55 & 0.7. I find that the incidence and strength of the upturn remains constant up to $z = 0.55$. In comparison, the prevalence and strength of the UV upturn is significantly diminished in the $z = 0.7$ cluster, implying that the stellar population responsible for the upturn in a typical red sequence galaxy is only just developing at this redshift and is essentially fully-developed by ~ 1 Gyr later. Of all the mainstream models that seek to explain the UV upturn phenomenon, it is those that generate the upturn through the presence of a Helium-enhanced stellar subpopulation on the (hot) horizontal branch that are most consistent with this behaviour. The epoch ($z = 0.7$) where the stars responsible for the upturn first evolve from the red giant branch places constraints on their age and chemical abundances. By comparing the results with the prediction made by the YEPS Helium-enhanced spectrophotometic models, I find that a solar metallicity sub-population that displays a consistent upturn between $0 < z < 0.55$ but then fades by $z = 0.7$ would require a Helium abundance of $Y \geqslant 0.45$, if formed at $z_f \sim 4$. Later formation redshifts and/or higher metallicity would further increase the Helium enhancement required to produce the observed upturn in these clusters and vice versa.

Acknowledgements

In memory of my late father – Mohammad Shahed Ali.

Without question, firstly I have to thank my supervisors, Professor Malcolm Bremer and Professor Steven Phillipps, both of whom have been paramount to the completion of my PhD. Malcolm's boundless enthusiasm of the subject has been an inspiration throughout, and his continued guidance in developing and experimenting with new ideas has always pushed me to improve myself. Steve is nothing short of an Astrophysics encyclopedia and if Google didn't exist, I probably wouldn't have had much trouble finishing my PhD with him around. I cannot thank Steve enough for always being there to answer any and all questions I came up with, no matter how simple or complex. Despite the last 4 years being challenging in many instances, it was because of my supervisors that my PhD has overall been a very enjoyable and mentally stimulating experience, one that will remain with me for the rest of my life. Truly, I am grateful to them both.

I also have to extend my gratitude to our close collaborator, Dr. Roberto De Propris, who has been an important third pillar of support during my PhD. During my multiple month-long visits to Finland, he has always been a great host in supporting my research and very entertaining to converse with as well.

It would be remiss of me to not express my appreciation towards Rhys Morris – our resident IT specialist of the Astrophysics group. He is a technical wizard, as simple as that. Rhys' presence meant that I could continue solving actual astrophysics related problems and not have to lose my sanity trying to fix every broken/outdated piece of software that refused to work when installed.

On a more personal level, I cannot thank my mother – Hosne Ara enough for her unequivocal love and care. She is the one who made me realise my passion for astrophysics as a child when she gifted me my first book on the subject – one recounting many curious facts about the moon. At the time the book was too difficult for me to fully understand, but just the pictures alone made me appreciate that there was still so much out there beyond our world, a curiosity that has led me to where I am now. Needless to say, without her moral and emotional support, none of this would have been possible.

Finally and crucially, I am sincerely grateful to God for giving me the capacity to simply

observe and appreciate his cosmos. The Universe is truly grandiose in its nature, and to be able to explore even an iota of its infinite complexity has been nothing short of a blessing, for which I am eternally appreciative.

I acknowledge and thank the Science and Technology Facilities Council (STFC) for providing the funding for my PhD, and the University of Turku for local funding during my visits, where part of this work was carried out. This work was based on observations from SDSS, the funding for which was provided by the Alfred P. Sloan Foundation, the Participating Institutions, the National Science Foundation, and the U.S. Department of Energy Office of Science. Observations made with the NASA Galaxy Evolution Explorer were also used in this project. GALEX is operated for NASA by the California Institute of Technology under NASA contract NAS5-98034. I acknowledge the use of public data from the Swift data archive. This work was also based on observations made with the NASA/ESA Hubble Space Telescope, obtained from the data archive at the Space Telescope Science Institute. STScI is operated by the Association of Universities for Research in Astronomy, Inc. under NASA contract NAS 5-26555.

Declaration

I declare that the work in this dissertation was carried out in accordance with the Regulations of the University of Bristol. This work is original except where indicated by special reference in the text and no part of the dissertation has been submitted for any other degree. Any views expressed in the dissertation are those of the author and in no way represent those of the University of Bristol. The dissertation has not been presented to any other university for examination either in the United Kingdom or overseas.

I note here the publications that have been used in the preparation of the chapters in this thesis, and the contributions from collaborators:

- The abstract of the thesis is largely adapted and reproduced from the abstracts in Ali et al. (2018a,b,c).
- **Chapter 2: The UV Upturn in Coma, Perseus and Fornax clusters** - This work has been published in Ali et al. (2018a) and is largely reproduced from that paper. M. N. Bremer, S. Phillipps and R. De Propris had input in the preparation of the manuscript.
- **Chapter 4: The UV Upturn in Abell 1689 at $\mathbf{z = 0.18}$** - This work has been published in Ali et al. (2018b) and is largely reproduced from that paper. M. N. Bremer, S. Phillipps and R. De Propris had input in the preparation of the manuscript.
- **Chapter 5: The UV Upturn in $\mathbf{z = 0.3, 0.55}$ & $\mathbf{0.7}$ clusters** - This work has been published in Ali et al. (2018c) and is largely reproduced from that paper. M. N. Bremer, S. Phillipps and R. De Propris had input in the preparation of the manuscript.

Contents

List of Figures

List of Tables

1

Introduction

Elliptical and lenticular galaxies, as well as the bulges of early-type spirals, can show a sharp rise in their Ultraviolet spectra below ~ 2500Å, a phenomenon dubbed the 'UV Upturn', despite having finished almost all star-formation activity by $z \sim 2-3$. The purpose of this PhD project is to characterise the UV upturn observed in early-type galaxies, understand how it is affected by cluster environments, and study its evolution through cosmic time - an area of ongoing research that is still not fully understood. By performing photometric analysis of both optical and UV data for a number of galaxy clusters between $z = 0 - 0.7$, the approximate period of onset of the upturn can be determined. These results will allow us to discriminate between the various existing models for the upturn and have important implications on pinpointing the mechanism through which the excess UV flux in such old systems is produced.

1.1 Outline of thesis

The body of the thesis is broken down into 6 chapters. This chapter introduces early-type galaxies and the UV upturn phenomenon observed within them, as well as the various potential sources of the upturn and the key models proposed to explain it. A summary of the observational evidence for the upturn in both early-type galaxies and local globular clusters is also

presented. Chapter 2 will focus on comparing the strength and prevalence of the upturn between Coma, Fornax and Perseus clusters. Furthermore, by fitting models to the observed UV to optical Spectral Energy Distributions (SEDs) of Coma cluster galaxies, the strength of the upturn will be characterised. Chapter 3 will explore the ubiquity of the upturn through an analysis of 20 other low redshift clusters between $z = 0 \sim 0.1$, similar to what is done for Coma, Perseus and Fornax. The effect of the cluster environment on the member galaxies is also investigated. Chapter 4 will present further UV to optical SEDs of early-type galaxies in Abell 1689 at $z \sim 0.2$, which is then compared to the Coma SEDs in order to identify any evolution in the redshift range. Chapter 5 will provide a detailed analysis of the upturn within 4 further clusters between $z = 0.3 - 0.7$, which will once again be compared to lower redshift clusters in order to investigate how the upturn has evolved from low-intermediate redshift. All of these results will then be examined against the predictions of several Simple Stellar Population (SSP) models so as to determine the most likely source of the upturn and to constrain its characteristics. Finally, chapter 6 will include a summary and conclusion of the results, as well as potential future work that could be undertaken on this topic.

1.2 Galaxies in the Universe

Galaxies are some of the fundamental building blocks of the Universe, consisting of billions to trillions of stars, gas, dust and dark matter. Depending on the type of galaxy, the constituent stellar populations can vary strongly. According to the classification scheme of Edwin Hubble (Hubble 1926; Hubble 1936), galaxies in the Universe can largely be divided into two groups based on their morphology - early-type and late-type, in which early-type galaxies are defined by their dominant bulge component (Fig. 1.1) and late-type galaxies by their prominent disk component (Fig. 1.2). Placing the early-type and late-type galaxies in sequence forms the classical 'Tuning Fork' diagram. Galaxies that do not fit into the two aforementioned categories are classified as 'irregulars', which include dwarf galaxies, as well as brightest cluster galaxies (BCGs) found in the centre of galaxy clusters (though BCGs do share physical characteristics with standard early-type galaxies, as will be discussed in later chapters).

Interestingly, the morphology of galaxies also correlates with many of their defining physical properties, such as luminosity, mass, velocity dispersion, optical colours, etc (e.g. Roberts &

Haynes 1994; Pozzetti et al. 2010 and references therein). Most importantly, the rate of star-formation itself is also related to the morphology (Kennicutt 1998) - star-formation activity being nearly non-existent in early-types but increasing significantly in late-type morphologies (Fig. 1.3).

Below is a summary of the key features in the two main galaxy types.

1.2.1 Early-Type Galaxies (ETG)

Early-type galaxies refer to both elliptical and lenticular (also known as S0) galaxies. Elliptical galaxies are characterised by their smooth and featureless ellipsoidal appearance with a continuously declining brightness profile. An example of a typical elliptical, IC2006, can be seen in Fig. 1.1. Hubble assigned a number between 0-7 to indicate the ellipticity of the galaxy, with E0 being perfectly circular and E7 being highly elongated. Ellipticals are generally the biggest and most luminous galaxies in the Universe, with large internal velocity dispersions and optically red colours. Their spectra are dominated by absorption features from the metals present in the atmosphere of their majority old, metal-rich stellar population. S0s on the other hand are considered the mid-point between spirals and ellipticals in that they have both a prominent central bulge and a surrounding disk, but no clear spiral arms. They share most of the physical characteristics of ellipticals such as their smoothness and surface brightness profiles, but most importantly have identical spectral features and optically red colours to ellipticals, and as such are also classified as ETGs (see review by Blanton & Moustakas 2009).

The lack of any prominent features such as central bars or spiral arms, combined with the absence of strong emission features in their spectra and overall optically red colours indicate that the dominant stellar population in ETGs is very old and highly evolved - mostly K-type main sequence and red giant branch stars (Kennicutt 1998; Renzini 2006). In fact, numerous studies of ellipticals in clusters at a range of redshifts suggest that these galaxies formed at very high redshifts and finished the bulk of their star-formation activity at $z \geqslant 3$, and have been passively evolving since then (e.g. Ellis et al. 1997; Stanford et al. 1998; Kodama et al. 1998; Holden et al. 2004). It is thus likely that the progenitors of present day ellipticals are star-burst galaxies such as Lyman-break Galaxies (LBG, Giavalisco et al. 1995; Giavalisco et al. 1996; see also review by Giavalisco 2002) or Ultra-Luminous Infra-red Galaxies (ULIRG, Sanders et al. 1988; Genzel et al. 2001) that underwent rapid star-formation at an early age. S0s on the other hand

[1] $https://www.spacetelescope.org$

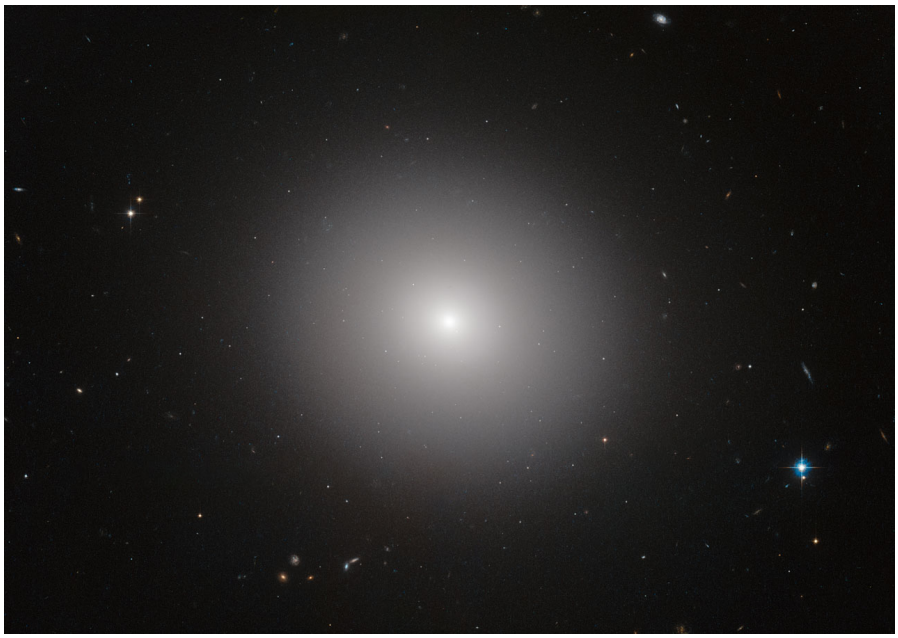

Figure 1.1: Elliptical galaxy IC2006; characterised by its smooth brightness profile and ellipsoidal shape. *Credit: Hubble Space Telescope*

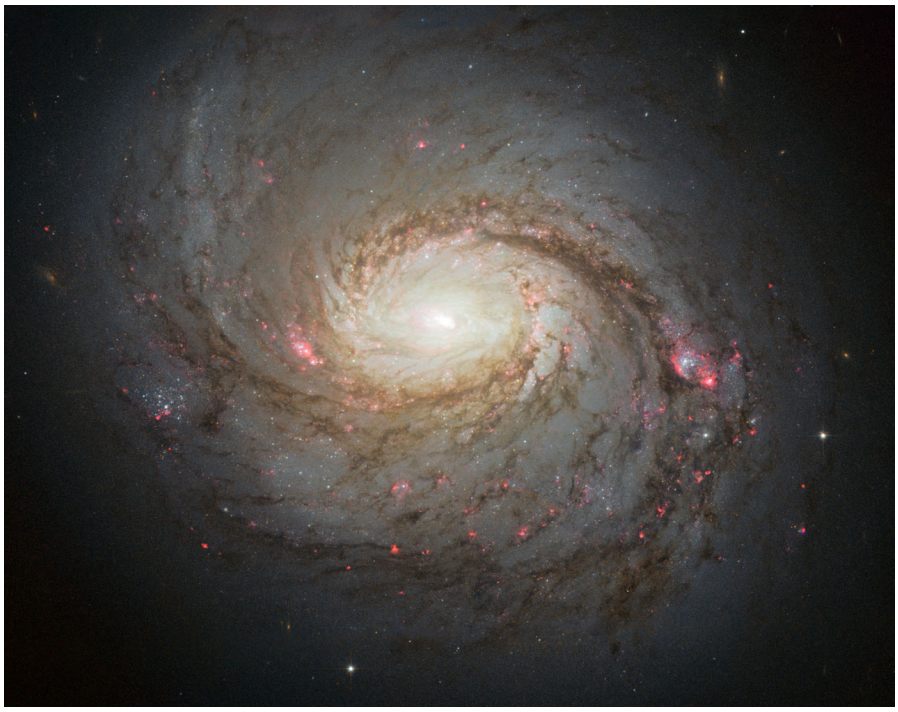

Figure 1.2: Spiral galaxy M77; clearly visible is the central bulge and the surrounding spiral arms. *Credit: Hubble Space Telescope*[1].

are thought to have started off as blue star-forming spirals but later transformed into red S0s through a process of fading (running out of cold molecular gas necessary for star-formation) in low density environments and/or mergers in group or cluster environments. ETGs are most commonly found in galaxy clusters compared to fields due to the role of the environment in the quenching of their star-formation (Dressler 1980a,b et seq.; Rizzo et al. 2018). As noted earlier, there also exist dwarf elliptical galaxies - the most common galaxy-type observed in the Universe, which are much smaller in size, fainter, and exhibit a different surface brightness profile when compared to giant ETGs. (Kormendy 1985; Graham & Guzmán 2003).

1.2.2 Late-Type Galaxies (LTG)

Late-type galaxies are spiral galaxies, characterised by the following key features in their appearance (Sandage 1961; de Vaucouleurs 1963; see also review by Blanton & Moustakas 2009 and references therein):

- A spheroidal bulge in the centre that shares many similarities with elliptical galaxies in both its physical appearance and spectral features, often being dominated by a mostly old stellar population.
- A rotating disk of stars, gas and dust around the central bulge.
- Spiral arms within the disk, which are long lived quasistatic density waves and regions of ongoing star-formation, therefore hosting an overall younger stellar population compared to the bulge.

Hubble assigned letters between a-d to spiral galaxies depending on the pitch angle and shape of the spiral arms, as well as the prominence of the bulge, with Sa galaxies having tightly compacted spiral arms and large bulges and Sd galaxies having much more loosely wound spiral arms and smaller bulges, otherwise called psuedo-bulges. Spirals are further sub-divided into two groups depending on the presence of a central bar structure. Although bars consist of mostly old and evolved populations of stars, they also host nuclear or circumnuclear star-formation and often feature dust lanes, a result of inflowing gas that is required for star-formation (Kormendy 1979, 1982; Gadotti & de Souza 2006). Barred galaxies are also found to have more molecular gas in comparison to unbarred galaxies; as such the presence of a bar is an indication of ongoing star-formation within galaxies (Sakamoto et al. 1999). Roughly 50-70% of all spiral galaxies have a central bar, including our own Galaxy, the Milky Way (e.g. de Vaucouleurs 1963; Barazza et al. 2008). An example of a typical barred spiral is shown in Fig. 1.2.

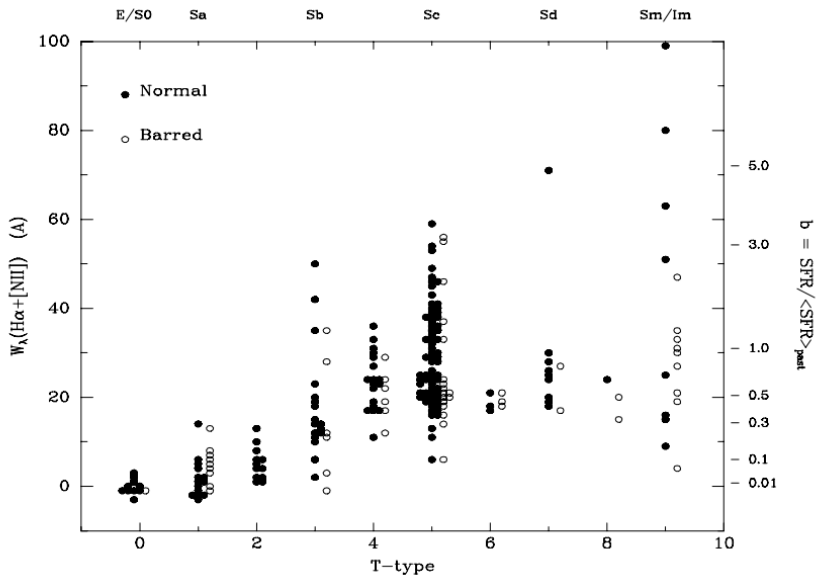

Figure 1.3: The distribution of $H\alpha+[NII]$ emission line equivalent widths, a tracer of the star-formation rate, in a large sample of local galaxies of varying Hubble/T type. A general increase in the average star-formation rate is observed going from early-type to late-type galaxies. Figure taken from Kennicutt 1998.

Unlike elliptical galaxies, spiral galaxies were able to retain their star-formation activity due to an initially slow specific star formation rate. They have overall bluer optical colours compared to ETGs, but their spectra consist of both absorption features due to the older population in the bulge, and also nebular emission lines such as Hα from the star-forming regions in the spiral arms (Kennicutt 1992). LTGs are the most common galaxy type in the field where they evolve secularly without many interactions with other galaxies. Within clusters, their numbers drop significantly in favour of ETGs - a phenomenon commonly known as the 'density-morphology' relation (Dressler 1980a,b et seq.; Moss & Whittle 1993).

1.3 Galaxy Clusters and the Red Sequence

Galaxy clusters are some of the largest gravitationally bound structures in the universe. They formed from the largest overdensities in the initial density field after the Big Bang and increased in size through a process of hierarchical merging and accretion of smaller groups of galaxies, as well as individual galaxies. Observationally, the three main components of a galaxy cluster are as follows (Kravtsov & Borgani 2012):

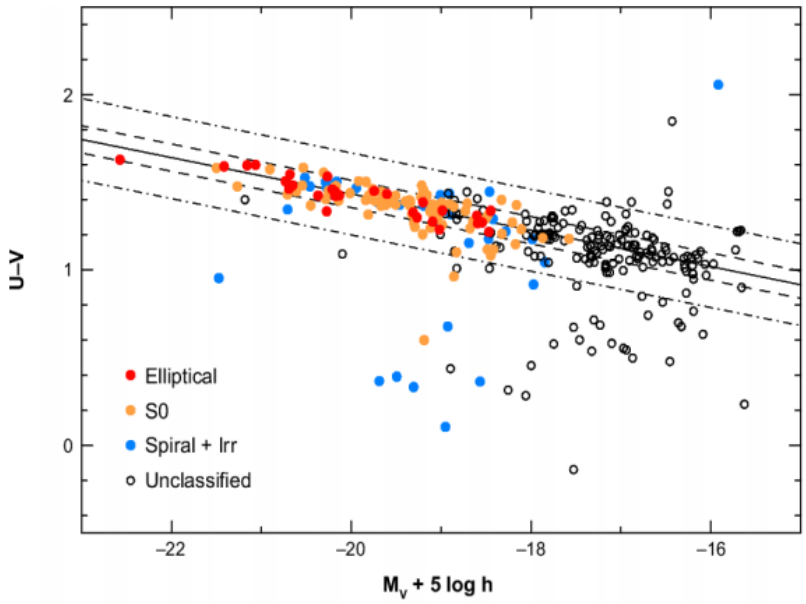

Figure 1.4: Colour-Magnitude diagram of spectroscopically confirmed Coma cluster members. The elliptical and S0s form a tight red sequence, with the spirals and irregulars forming the blue cloud below it. Figure taken from Bower et al. (1999).

- Intracluster light: The light from bright stars in and around galaxies.
- Intracluster medium: Hot primordial gas that permeates through the entire cluster and emits strongly in the X-ray.
- Dark matter: Dark matter is the dominant mass component of the cluster and can be observed indirectly due to its gravitational lensing of background galaxies.

From the perspective of galaxy evolution, the cluster environment has a strong effect on the star-formation activity within member galaxies. Galaxy clusters, in particular the cluster cores, are dominated by passively evolving elliptical or S0 galaxies with little to no ongoing star-formation. Spirals are mostly found towards the outskirts of clusters and even then their star-formation rates are lower in comparison with field spirals. It is thus believed that the cluster environment quenches star-formation and transforms spirals into S0s. This idea is further strengthened by the observation of an increasing amount of blue spiral population in clusters compared to S0s at increasing redshift, from $z = 0 \sim 0.5$, a phenomenon known as the 'Butcher-Oelmer' effect. While the number of true ellipticals in clusters has remained roughly constant with redshift, galaxies that started off as star-forming spirals have been transformed into passive

S0s by the present day, leading to the majority early-type population in local clusters (Butcher & Oemler 1978a,b; Dressler 1980a,b et seq.; Rizzo et al. 2018).

Galaxies in the local universe, in particular cluster galaxies, follow a standard bimodal colour-magnitude relation (Baum 1959; Visvanathan & Sandage 1977; Sandage & Visvanathan 1978a,b). When the optical colour of galaxies is plotted against their magnitude, the ETGs form a very tight sequence, dubbed the 'red sequence' due to their red colours. The spirals in general have much bluer colours, forming the 'blue cloud'. Fig. 1.4 shows the colour-magnitude diagram (CMD) for the well studied Coma cluster for which the members have been confirmed spectroscopically (Bower et al. 1999). The elliptical and S0s form a tight red sequence with a small amount of contamination from likely edge-on or dusty spirals. Studies of clusters out to $z = 1 \sim 2$ have found the presence of tight red sequences at even such high redshifts (Newman et al. 2014; Glazebrook et al. 2017, see also references in Renzini 2006), meaning that any appreciable star-formation in cluster ellipticals must have been completed even earlier (over ~ 10 Gyrs ago).

Since the red sequence appears to be a ubiquitous feature of all clusters in the local Universe and out to very high redshifts, it is a reliable method in identifying early-type cluster members. Given that ETGs are mostly found in clusters than in the field, there is little contamination in the red sequence from non-cluster members. Spirals that are part of the cluster, as well as field spirals and irregulars together form the blue cloud in the colour-magnitude diagram. CLASH-VLT spectroscopy of rich clusters found that $> 95\%$ of bright red sequence members are also genuine cluster members (De Propris et al. 2016). This method of identifying red sequence members is particularly useful in higher redshift clusters for which a complete spectroscopic survey may not exist - a process that will be used throughout the studies presented in this thesis.

1.4 The UV Upturn in Early-type Galaxies

The UV upturn is the rise in the spectrum of ETGs (and the bulges of early-type spirals) shortward of 2500Å, down to the Lyman limit. This phenomenon was first discovered by Code & Welch (1979) through UV observations of 7 E/S0 galaxies and the bulge of M31 using the *Orbiting Astronomical Observatory* (OAO-2), as shown in Fig. 1.5. de Boer (1982) confirmed detections of two of the objects from the OAO-2 sample and detected the upturn in 11 further elliptical galaxies using the *Astronomical Netherlands Satellite* (ANS). The phenomenon was

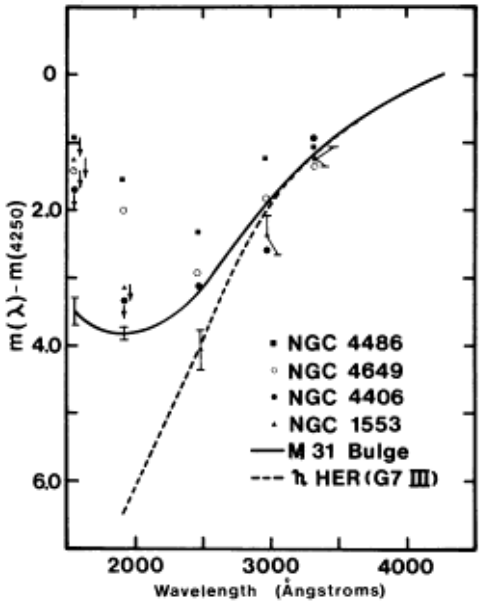

Figure 1.5: Original observations of the UV upturn using OAO photometry by Code & Welch (1979). A clear rise in the flux can be seen shortward of ~ 2500Å in the elliptical galaxies and the bulge of M31 - a phenomenon dubbed the UV upturn.

also re-affirmed by Bertola et al. (1982) through *International Ultraviolet Explorer* (IUE) observations of the elliptical galaxy NGC4649. Among all of these observations, the upturn showed a large scatter in the UV despite these galaxies having nearly identical optical/near-IR spectra. Burstein et al. (1988) combined the IUE spectra of 24 quiescent ETGs and the bulge of M31 to show that the $1550 - V$ (the canonical $FUV - V$ used to measure the upturn strength) colour was anti-correlated to the Mg_2 index, which is a proxy of the metallicity of a system. Therefore, more metal-rich galaxies, which in turn are also brighter and more massive (due to the mass-metallicity relation - Ferrarese et al. 2016) demonstrated stronger upturns. They also found that all of the ETGs demonstrated an upturn component and the $1550 - V$ showed a large scatter of ~ 2.5 magnitudes that was clearly absent from the optical colour. As such, the stellar population responsible for the upturn in the UV is completely separate from the majority old MS and RGB populations that dominate the optical in these galaxies. Bureau et al. (2011) later confirmed the negative correlation between the $FUV - V$ colour and the Mg_2 index using GALEX data of SAURON ETGs, once again suggesting that the upturn is stronger in more massive, metal-rich galaxies. Another important feature of the upturn, first discovered by Ohl et al. (1998) in a sample of 8 ETGs observed using the UIT and then later reconfirmed by Carter et al. (2011) in Coma

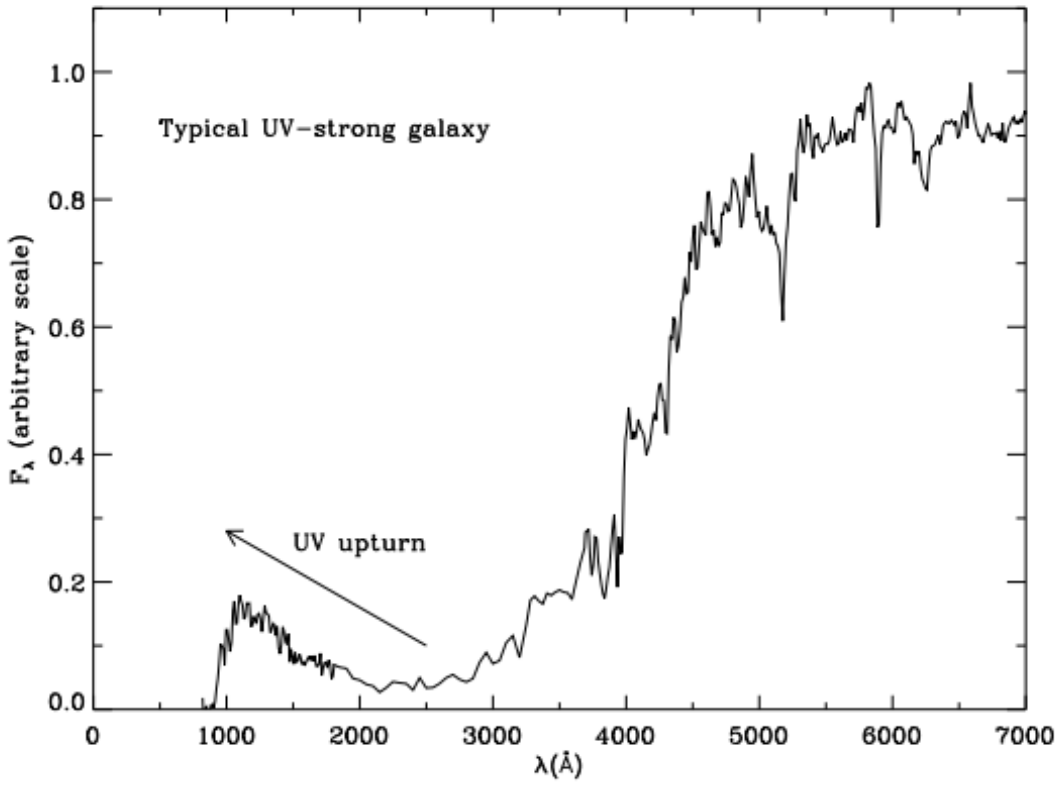

Figure 1.6: Composite spectrum of the elliptical galaxy NGC4552 from Yi et al. (1998) created using observations from HUT (FUV), IUE (NUV) and ground-based optical observations. The galaxy spectrum demonstrates a sharp decline shortward of the 4000Å break but then starts to rise again below $\lambda \approx 2500$Å.

red sequence galaxies is the gradient in the $FUV - optical$ colours found in these galaxies. The UV light in ETGs is more centrally concentrated compared to the optical, so the $FUV - optical$ colour is bluer in the centre and becomes redder radially outwards.

An example of a strong upturn galaxy spectrum of NGC4552 (taken from Yi et al. 1998) can be seen in Fig. 1.6. As expected, the flux of the galaxy drops significantly going from the optical to the UV, but shows a sudden increase shortward of ~ 2500Å until the Lyman limit.

The rise in the UV spectrum of ETGs came as a genuine surprise to both theorists and observers, since these galaxies were previously thought to be dominated by a purely old and cool stellar population, which would practically have almost no output in the UV. As discussed previously, studies show that ETGs formed between $z = 2 \sim 6$ with most star-formation activity

having stopped by $z \gtrsim 3$. Therefore UV-bright young hot stars (found predominantly in star-forming regions) are not expected to be present in such 'red and dead' systems. The absence of these stars was proven explicitly through high resolution UV imaging with HST in the centres of M31 and M32 (e.g. Bertola et al. 1995; Lauer et al. 1998), as well as the nuclei of ETGs (Maoz et al. 1996). Furthermore, IUE observations of bright ETGs showed that the FUV light has a smooth and extended profile similar to the optical band profiles, even in the case of M87, which has a prominent AGN in the centre (Bertola et al. 1980; Norgaard-Nielsen & Kjaergaard 1981; Oke et al. 1981; Bertola et al. 1982; Oconnell et al. 1986). Such a smooth and extended profile is contrary to both star-formation and AGN activity being the source of the upturn, as star-forming regions tend to be clumpy in nature and AGN activity is concentrated in the nuclei of galaxies. Instead, this suggests that the upturn must originate from an old stellar population in these galaxies.

Of the majority main sequence and red giant branch stars that dominate ETGs, canonically, the stellar component with the hottest temperature in these galaxies is the main sequence turnoff, with $T_e \sim 6000$K, clearly insufficient to make any significant contribution to the FUV flux. This led to the conclusion that the FUV flux must be coming from a highly evolved minority population of hot, low mass stars in these galaxies. Greggio & Renzini (1990) proposed the following highly evolved candidates:

- Post-Asymptotic Giant Branch (P-AGB) stars: These are shell Helium burning stars that leave the AGB after undergoing their first thermal pulse, with temperatures over 100,000K, before finally descending down the white dwarf cooling curve. Due to their very short life-times, they are expected to burn $\sim 0.003 M_{\odot}$ of Hydrogen in this phase and thus are unlikely to have a significant output in the UV.
- Post-Red Giant Branch (P-RGB) stars: These stars lose most of their envelope in the RGB and fail to ignite core Helium burning, thus directly becoming Helium white dwarfs. P-RGB burn even less Hydrogen than P-AGB stars and as such are going to have even more of a negligible UV output. Recent observations of solar metallicity open cluster, M67, have found a lack of a substantial population of Helium core white dwarfs (Williams et al. 2018), which are the end product of P-RGB stars, indicating that such stars may not exist in old metal-rich systems.
- Post-Early Asymptotic Giant Branch (P-EAGB) stars: Unlike P-AGB stars, these stars are unable to ignite any thermal pulses due to having lost most of their hydrogen envelope, and

leave the AGB before any pulsations can occur, before finally descending the white dwarf cooling curve. P-EAGB stars burn $\sim 0.025 M_{\odot}$ of Hydrogen in this phase. Although more promising than their P-AGB counterparts, P-EAGB stars are also too short-lived in this phase to be the primary source for the upturn.

- Hot (or Extreme) Horizontal Branch (HB) stars: Core Helium-burning stars located on the blue end of the HB beyond the RR Lyrae gap in the HR diagram. They have high effective temperatures due to a thin outer shell. Depending on the amount of mass loss they have undergone before reaching the HB, they can also become 'AGB-manqué', i.e. the stars skip the AGB phase entirely and become Carbon-Oxygen core white dwarfs. Hot HB stars burn $\sim 0.05 M_{\odot}$ of Hydrogen (or $\sim 0.5 M_{\odot}$ of Helium), a number significant enough such that if only $\sim 20\%$ of the stellar population in ETGs underwent this phase, that would account for the UV output from the bluest (and strongest) upturn galaxies. As such, hot HB stars are generally accepted to be the most plausible source of the upturn.

By developing simple spectral synthesis formulations for the evolution of stars from the zero-age main sequence to the white dwarf cooling track, including all other evolutionary phases in between, Dorman et al. (1995) found that without EHB stars, systems with $[Fe/H] \geqslant 0$ could not produce the blue $1500 - V$ and $2500 - V$ colours observed in their sample of local globular clusters (GC) and elliptical galaxies. Using their models, they calculated that for strong upturn systems, the EHB stars provide up to $\sim 80\%$ of the FUV flux in these systems, the rest coming from P-AGB stars. Through spectral fitting of the HUT spectra of 6 ETGs, Brown et al. (1997) also came to the conclusion that the FUV of those galaxies was dominated by emissions from stars evolving through the hot HB and AGB-manque phase. Similar results were also obtained in Brown et al. (1998a) for the central regions of M31 and M32. Subsequently, Brown et al. (2000b) presented HST STIS imaging of the core of M32, which for the first time resolved hot HB stars and gave direct evidence for the existence of these UV-bright stars. They found that the UV emission was almost entirely dominated by a small fraction of hot HB stars, that accounted for $\sim 5\%$ of the overall population and there were many fewer UV-bright P-AGB stars than expected, despite the UV-to-optical flux of M32 being weak enough such that in theory it could have been entirely explained by the UV emissions from such P-AGB stars.

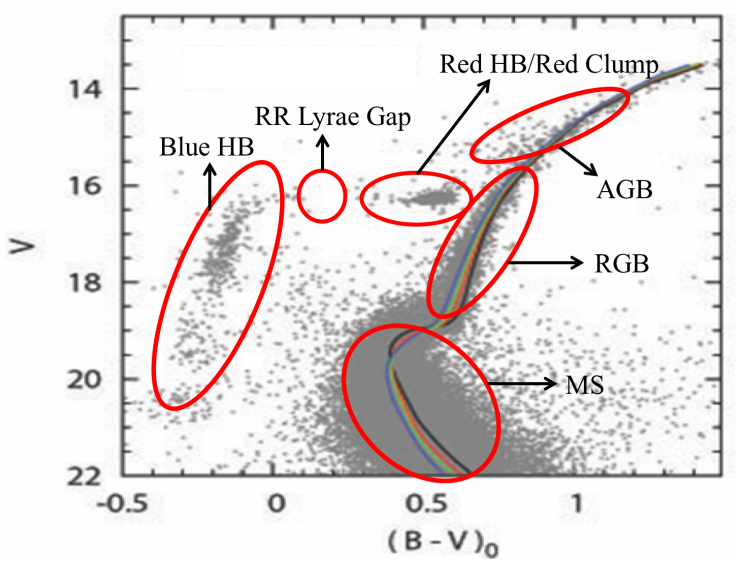

Figure 1.7: Hertzsprung-Russell diagram of the globular cluster NGC2808 from Lee et al. (2005b) showing the showing the main stellar evolutionary phases within old, non-starforming systems - a rough proxy of ETGs despite the difference in metallicities. Of particular note is the extended horizontal branch and its two components that are separated by the RR Lyrae gap - i) The red clump with colours/temperatures similar to the MS; ii) The blue horizontal branch, which is much hotter and is the main source of the UV upturn.

1.5 Models of the UV Upturn

In the canonical stellar population synthesis models for elliptical galaxies (e.g. Conroy et al. 2009), the HB consists of mostly cool stars that are part of the red clump (i.e. the red end of the HB) to the right of the RR Lyrae gap, with temperatures around $\sim 5000K$, similar to the RGB and MS stars. However, in systems with upturn, the HB extends past the RR Lyrae gap to form a blue horizontal branch on the left of the gap. An example of this can be seen in Fig. 1.7, where the red HB and the blue HB are clearly separated by the RR Lyrae gap in NGC2808, a Milky Way globular cluster with a clearly extended HB - a rough proxy to UV upturn ETGs due to its old age and quiescent star-forming history, despite being a lower metallicity system.

Given that the source of the upturn was determined to be hot HB stars and their progeny, the fundamental question then became: What processes gave rise to these hot HB stars? The following hypotheses were proposed to explain how HB stars can become hot and UV-bright (see reviews by O'Connell 1999 and Yi 2008 for a more detailed summary):

1.5.1 Metal-poor HB

Low metal content on the surface of a HB star means that there are fewer opportunities for photons from deeper within the star to excite electrons to higher energy levels and subsequently be radiated away when the electron falls back down to a lower energy level, making the star appear hotter. As such, metal-poor stars have much higher effective surface temperatures than metal-rich stars. Furthermore, metal-poor stars naturally have shorter evolutionary timescales compared to their metal-rich counterparts, and as such could realistically reach the hot HB within the current age of the Universe, even with cosmological Helium abundance. Thus, given low enough metallicities and very old ages, metal-poor HB stars can naturally become hot and UV-bright. Even though ETGs are observed to have high metallicities ($Z_{\odot}$ or higher), all galaxies have a metallicity distribution. According to the models of Park & Lee (1997), if $\sim 20\%$ of the overall population in elliptical galaxies was very metal-poor and old, the UV observations could be matched by the models. This would indicate that the anti-correlation between $FUV - V$ and Mg_2 is a non-causal correlation, as the $FUV - V$, which represents the strength of the upturn is dominated by the minority metal-poor population, while the Mg_2 index is driven by the majority metal-rich population. Since the oldest stars in a galaxy are expected to be metal-poor and in the core, as is the case with the Milky Way (e.g. García Pérez et al. 2013; Howes et al. 2014; Howes et al. 2015), this would also explain the upturn being strongest in the core of galaxies.

However, this hypothesis has several glaring problems. Observations of bright ETGs suggest that a $\sim$20% population of very metal-poor stars is far too high in such galaxies and is incompatible with the strength of the metallicity indicators (and hence the integrated metallicity) from their optical spectra (Bressan et al. 1994). Furthermore, given that metal-poor stars need very old ages for them to become UV-bright, the upturn would need to completely fade away at a relatively low redshift if such stars were the primary source of the phenomenon. As will be discussed in the upcoming sections, this is found to be untrue in cluster galaxies at higher redshifts.

1.5.2 Mass-loss in the RGB

Metal rich HB stars can become very hot and UV-bright by losing a significant amount of their envelope mass during their ascent up the RGB due to the opacity effect, leading to the hot HB and AGB-manqué phase (Greggio & Renzini 1990). This would allow them to remain as low mass

blue HB stars for a long period of time and skip the AGB altogether, directly becoming Carbon-Oxygen core white dwarfs. The mass loss as given by the Reimer's mass loss parameter, η_R (Reimers 1975, 1977). is assumed to be enhanced in these systems, up to 2-3 times the normal rate. To explain the wide range in upturn strengths in these galaxies, a Gaussian distribution in η_R is used. The mass loss is assumed to increase with metallicity in order to explain the $FUV - V$ vs. Mg_2 relation and $\Delta Y/\Delta Z$ is also expected to be enhanced compared to the solar neighborhood, i.e. > 2.5. The model predicts that the upturn should disappear at a moderate redshift when the stars have not yet evolved on to the RGB, where they are expected to lose their envelope mass rapidly over a relatively short period of time (Yi et al. 1997, 1998, 1999).

Although the model does reproduce the observed $FUV - V$, there is no observational evidence or theoretical explanation as to why a small sub-population of stars would undergo a sudden episode of large mass over a short period of time in the RGB, or why the mass-loss should increase with metallicity. In fact, studies of local clusters (that exhibit an upturn) show that the mass loss on the red giant branch does not have any clear dependence on metallicity (Miglio et al. 2012; Salaris et al. 2016).

1.5.3 Binary interactions

The hot subdwarf stars found in our Galaxy (e.g. Saffer et al. 1994 and references within) appear to be remarkably similar to the blue HB population that is thought to be the source of the upturn in ETGs. Observations suggest that over half of all such stars in our Galaxy are part of binary systems and possibly formed from binary interactions (e.g. Reed & Stiening 2004 and references within). Han et al. (2007) thus proposed binary models for the formation of hot HB stars based on their models for the formation of hot subdwarf stars in our Galaxy (Han et al. 2002; Han et al. 2003). There are three main formation channels for hot HB stars through binary interactions - i) Merger of two Helium white dwarfs to form a hot HB star; ii) Mass overflow from a star at the tip of the first giant branch (FGB) on to a MS companion, in the case of long orbital periods; iii) Ejection of the common envelope shared by very close contact binaries due to unstable Roche Lobe overflow to form a hot subdwarf/HB star, where the companion can either be a white dwarf or MS star. The binary model suggests that the upturn appears at very high redshifts (within ~ 1.5 Gyrs of the galaxy forming) and remains constant since then.

The main caveat to this model is that unlike the single star evolutionary models, it predicts virtually no evolution in the strength of the upturn unless at very high redshift. As will be shown

in later sections, this prediction does not seem to hold true and the upturn does show evolution outside of very high redshifts. Furthermore, recent studies of clusters in the Galactic bulge show that the binary fraction decreases with metallicity (Badenes et al. 2017), which would give the opposite effect of the upturn becoming stronger with metallicity as originally shown by Burstein et al. (1988).

1.5.4 Helium-enhancement (Y)

One of the most promising mechanisms that gives rise to the UV upturn is Helium enhancement in HB stars (with $Y > 0.4$ in the most extreme cases). Normally, the temperature of a stellar population decreases with increasing metallicity due to an increase in the opacity of the stellar envelope. However, a higher Helium abundance leads to a decrease in the opacity, which in turn increases the effective surface temperature of the star and shortens its MS lifetime. For HB stars in which the envelope is already thinned, an increase in the Helium content can lead to extremely high surface temperatures - allowing even metal-rich systems to have a hot HB component, which can explain the UV upturn in ETGs (e.g. Norris 2004; Lee et al. 2005b; Chung et al. 2017).

There is a lot of direct and indirect evidence for He-enhanced stars in the globular and open clusters within the Galactic bulge, as well as other galaxies such as M87, which will be discussed in further detail shortly. Perhaps most importantly, as will be shown through the work presented in this thesis, He-enhancement can best explain the overall evolution of the upturn strength in cluster ETGs above all other proposed models. Despite the observational evidence supporting this model, there still does not exist a clear theoretical framework that can explain how such extreme values of Y (> 0.4) can be reached. However, even though not fully confirmed through observations, a few mechanisms to explain the He-enhancement in ETGs have been proposed:

- **Cluster Disintegration Scenario:** Bekki (2012) proposed the *'Cluster Disintegration Scenario'* (CDS), in which all stars in the system are formed in Giant Molecular Clouds (GMC) as part of either bound or unbound star clusters (SC). The first generation of stars that originally form from the GMCs (as observed in typical HII regions, e.g Peimbert et al. 2007) have primordial Helium abundances (Y=0.23) and the canonical $\Delta Y/\Delta Z \sim 2$ - denoted as Helium Normal Stars (HNS) in the model. Once this first generation of stars undergoes stellar evolution, the ejecta from AGB stars (which are known to be He-enriched, e.g. D'Antona et al. 2010) allow for a second generation of stars to form with much higher Helium abundances,

if the ejecta does not significantly mix with and is not diluted by the Interstellar Medium (Renzini 2008). The aforementioned condition is extremely important because in the canonical models of chemical enrichment, the ejecta from stars is assumed to mix well with the ISM, forming new stars that are not significantly He-enriched. In the CDS however, the second generation of stars, referred to as Helium-rich stars (HRS), can have $Y \geq 0.35$. The model requires massive SCs with deep potential wells to retain the AGB ejecta and create high density gaseous regions for star-formation, without dilution of the ejecta by the ISM. To achieve this, Bekki (2012) assume that the parameter m_{sc}/m_{gmc} (mass of SC/mass of GMC) is constant for all SCs and that the mass of the GMC must exceed a threshold mass, m_{thres}, which is estimated from numerical simulations (D'Ercole et al. 2008; Bekki 2011). In GMCs where $m_{gmc} \leq m_{thres}$, only HNS are formed as the potential wells are not deep enough to hold the AGB ejecta. The HNS can later become field stars if the cluster is disintegrated due to dynamical friction within the host galaxy, or become part of bound SCs with normal He abundances. In GMCs with $m_{gmc} > m_{thres}$, the AGB ejecta is retained due to the deeper potential wells and HRS are formed. Once again, if the SCs are disintegrated, the HRS become field stars, or alternatively become part of massive SCs. In CDS, the He-rich field stars are the source of the upturn in ETGs.

Given the above scenario, the model can explain some of the key features of the UV upturn. The study showed that top-heavy IMFs formed more HRS in ETGs as there is a greater amount of AGB ejecta to form such stars. An important feature of the upturn is the $FUV-V$ vs. Mg_2 relation. In the CDS, more massive galaxies can retain ejecta from supernovae efficiently and hence have higher metallicities. If such galaxies also have top-heavy IMFs (though recent observational studies of massive ETGs suggest a bottom-heavy IMF in the centre - van Dokkum et al. 2017), they would also have larger fractions of He-rich stars and hence a stronger upturn, leading to the strength of the upturn (as measured through $FUV-V$) increasing with metallicity (Mg_2 index). Another observed feature of the upturn is the positive gradient in $FUV-optical$ colours with radius, i.e. the strength of the upturn decreases with increasing radius (as $FUV-V$ becomes redder outwards), as shown in the Coma cluster galaxies by Carter et al. (2011). In the CDS, HRS form in massive SCs that can survive multiple interactions with other SCs and naturally sink to the centre of the galaxy where they are finally disintegrated due to dynamical friction with field stars or interactions with other massive SCs. This leads to more HRS from massive clusters becoming field stars

in the inner region of the galaxy than the outer regions, and hence the radial gradient in $FUV - optical$ colours. It is however important to note that there does not yet exist any observational evidence for the CDS.

- **Dissolved massive metal-rich globular clusters:** An alternative hypothesis for the He-enriched populations in ETGs was recently proposed by Goudfrooij (2018). His study showed a strong anti-correlation between the specific frequency of red GCs and $FUV - V$, i.e. the strength of the upturn increases with increasing number of large metal-rich GCs. Given that a decrease in the surface density of red GCs is observed in the central regions of massive ETGs (Forbes et al. 2006; Peng et al. 2006; Harris et al. 2017), Goudfrooij (2018) proposed that He-rich stars were initially formed in large metal-rich GCs as observed in M87 - the central BCG of the Virgo cluster (Sohn et al. 2006; Kaviraj et al. 2007; Peacock et al. 2017), which were eventually dissolved by the strong tidal forces in the central regions of the ETG during their long ~ 10 Gyr lifetimes. This hypothesis predicts an enhancement in the light element abundance ratios in ETGs, which has recently been observed through a spectroscopic survey of massive ETGs by van Dokkum et al. (2017), who found enhancements of [Na/Fe] and [O/Fe] in the central regions of their galaxies.

  The range in upturn strengths in this model is explained by the range in truncation mass, M_c (as described by Schechter 1976) of metal-rich GCs in galaxies. The anti-correlation of $FUV - V$ and Mg_2 index is explained by the sensitivity of Mg_2 index to age, [Z/H] and [α/Fe], which all also anti-correlate with $FUV - V$ (Jeong et al. 2012). Recent studies have shown that both GCs and field stars in our Galaxy are [α/Fe] and N-enhanced, potentially lending evidence for the hypothesis suggesting that the upturn population in ETGs originated from now dissolved GCs (Chantereau et al. 2018; Bastian & Lardo 2018).

1.6 Evolution of the UV upturn

The evolution of the UV upturn with redshift has been a key area of research ever since the discovery of the phenomenon, as the nature of its evolution can constrain the proposed models for the upturn. If a metal-poor population is responsible, the upturn should disappear at relatively low redshift. Conversely, in the case of a binary origin, the upturn should exist to very high redshifts. If mass loss on the RGB is the driver of the upturn, then the upturn should slowly become weaker at low redshift before disappearing completely at moderate redshift. In the case

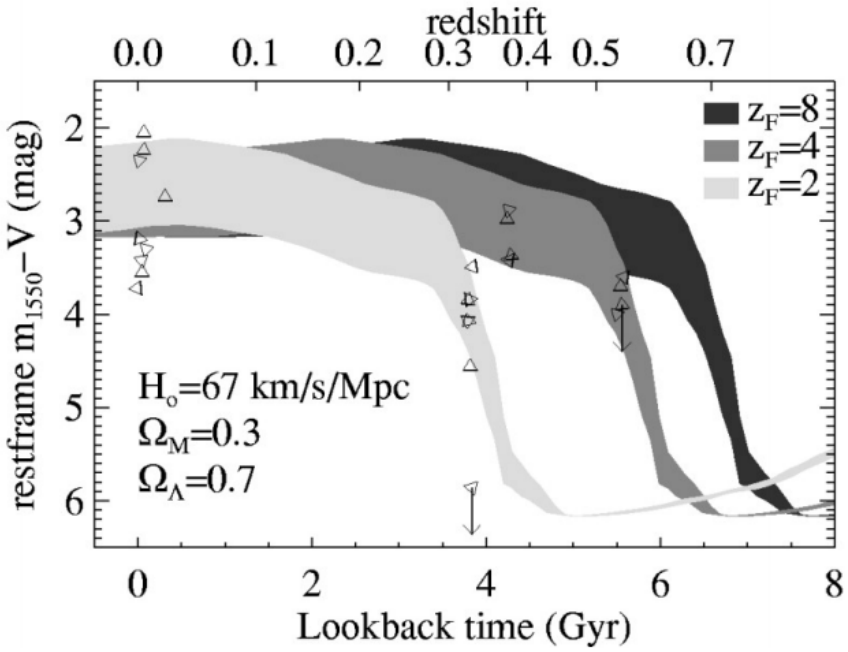

Figure 1.8: Models of Tantalo et al. (1996) showing the evolution of the $FUV - V$ colour (given in Vega magnitudes) as a function of redshift/lookback time for galaxies between 3×10^{12} and $10^{12} M_{\odot}$. The $FUV - V$ colour is very red and the scatter is small at high redshift (after the epoch of star-formation) when the upturn has yet to develop, but the colour becomes blue and the scatter increases as the upturn 'turns on' at moderate redshift - an epoch that is strongly dependent on the formation redshift (z_f) of the galaxy. Plotted on top are the observed colours of BCGs and very bright ellipticals from Brown et al. (1998b, 2000a, 2003), which show some fading between $z = 0 \sim 0.30$, but remain relatively consistent thereafter between $z = 0.30 \sim 0.55$. Figure taken from Brown et al. (2003).

of He-enhancement, the upturn should remain roughly constant out to a moderate redshift (the specific z being dependent on the value of Y) before disappearing quickly within a short window of time (1$\sim$2 Gyrs). All of these hypotheses can be tested by measuring the $UV - optical$ colours at a range of redshifts and comparing both their exact values, as well as the scatter with the predictions from the models.

With the launch of the *Galaxy Evolution Explorer* (GALEX), deep imaging surveys of entire galaxy clusters have been performed in the UV at the low redshift regime. Clusters in particular provide an excellent avenue for exploring the upturn as they're mostly dominated by ETGs with little to no star-formation activity. The galaxies are also contained within a relatively confined volume of space and are at approximately the same distance, minimising any line-of-sight and distance related effects from galaxy to galaxy. Boselli et al. (2005) performed an analysis of the upturn in ETGs in the Virgo cluster, going all the way down to the dwarf elliptical regime. They found a similar anti-correlation between $FUV - V$ and metallicity as Burstein et al. (1988) in bright ETGs and a spread of ~ 1.5 magnitudes in $FUV - V$. However, even though the $FUV - V$ tended to become bluer with increasing mass/luminosity for the giant ellipticals, the same relation did not hold true for dwarf ellipticals, in which the $FUV - V$ colour became bluer with decreasing mass/luminosity. Boselli et al. (2005) concluded using the results from spectroscopy of a number of dwarfs in their sample that the opposite behaviour demonstrated by dwarfs compared to giants was due to recent episodes of star-formation in those galaxies as opposed to simply being a metallicity effect, and that overall the stellar populations dominating the UV in the two galaxy types were completely different. Smith et al. (2012) recovered similar results from a large sample of optically selected red sequence galaxies in the Coma cluster, which also showed comparable values and large scatter in the $FUV - i$ of giant ellipticals as Virgo. As before, the upturn became stronger on average with increasing mass/luminosity in the bright ETGs.

Numerous other studies have been performed on large samples of ETGs in the nearby Universe, i.e. $z < 0.1$ (e.g. Rich et al. 2005; Lee et al. 2005a; Donas et al. 2007; Rawle et al. 2008; Jeong et al. 2009; Yi et al. 2011; Schombert 2016), all of which unanimously recovered similar values of the $FUV - optical$ and $NUV - optical$ as those of Virgo and Coma clusters, as well as comparable scatters of $\sim 1.5 - 2$ and $\sim 1 - 1.5$ magnitudes in each colour respectively in all samples. A handful of these studies (e.g. Yi et al. 2011; Loubser & Sánchez-Blázquez 2011) also found that the upturn is unaffected by the environment in which the galaxies reside. In

general, all studies also concluded that the upturn is best explained using the hot HB hypothesis as proposed by Greggio & Renzini (1990).

Pioneering work on extending the analysis of the upturn into moderate redshifts was first undertaken by Brown et al. (1998b, 2000a, 2003), in which they analysed the strength of the upturn in a small sample of the the most luminous galaxies in three clusters between $z = 0.3 \sim 0.6$. They found that the upturn exists in galaxies out to $z = 0.55$, although the strength of the upturn shows some fading between galaxies at $z = 0$ and $z = 0.3$, but remains consistent thereafter out to $z = 0.55$ (corresponding to 5.6 Gyrs in lookback time). The observations are shown in Fig. 1.8. It should be noted that Brown et al.'s sample only consisted of a handful of the brightest cluster members from each cluster and so the results are likely to suffer from stochasticity, especially given the naturally large scatter observed in $FUV - optical$ colours of upturn galaxies. Ree et al. (2007) also performed a study of the BCGs of Abell clusters at $z < 0.2$ and found a decrease in the upturn strength in the past 2 Gyrs. However, a similar analysis by Donahue et al. (2010) on 32 BCGs between $z = 0.06 - 0.18$ from the XMM-Newton Cluster Structure Survey (REXCESS) and by Boissier et al. (2018) on a sample of BCGs out to $z = 0.35$ behind the Virgo cluster showed no evolution in the upturn strengths at these redshifts. A much larger spectroscopic analysis of BOSS Luminous Red Galaxies (LRG) was undertaken by Le Cras et al. (2016), who found evidence for the upturn out to $z \sim 1$; although the frequency of upturn galaxies fades at higher redshifts, particularly at $z > 0.6$. It should also be noted that there is potentially a large fraction of post-starburst galaxies in Le Cras et al.'s LRG sample as demonstrated by Roseboom et al. (2006).

In summary, the various studies performed over the past decades seem to have yielded contradictory results in a few instances, but most of these can be attributed to small sample sizes due to detector limitations of performing UV observations at increasing redshift, and the stochastic nature of the upturn itself. In general, there is agreement between most studies that the upturn persists to a moderate redshift ($z \sim 0.6$) in the very brightest cluster ETGs. The fact that the upturn exists beyond low redshifts ($z \sim 0.2$) already excludes the metal-poor model for the upturn, which predicts that the upturn should disappear beyond low redshifts. Furthermore, since the strength of the upturn shows fading at least at moderate redshift ($z = 0.5 \sim 1$), this contradicts the prediction from the binary model, in which the upturn should remain constant out to very high redshifts. Mass loss and He-enhancement are the only remaining hypotheses that are not clearly falsified by the observations thus far on the evolution of the upturn.

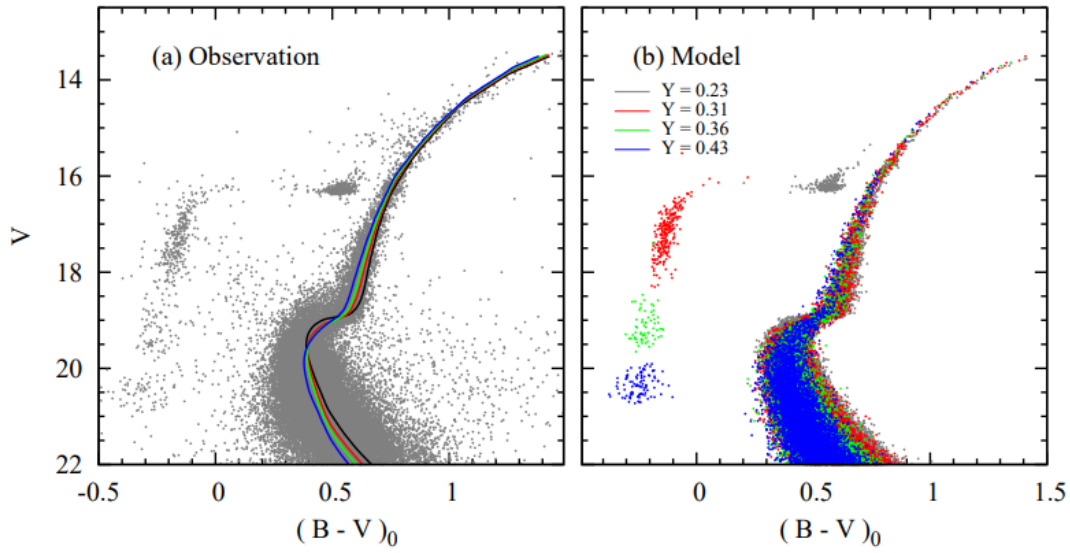

Figure 1.9: *Left:* Observed colour-magnitude diagram of the Galactic globular cluster NGC2808. The GC has an extended horizontal branch due to the large range in temperatures in this population of stars. *Right*: Modeled colour-magnitude diagram of NGC2808, which almost exactly reproduces the observations by assuming a range of Helium abundances. Figure taken from Lee et al. (2005b).

1.7 Helium-enhanced populations in Globular Clusters

Globular clusters are compact collections of stars bound together tightly in a spherical shape by gravity. They are mostly found in the halo of galaxies, but can also exist in the centre. GCs are some of the oldest objects observed in the Universe, similar in age to their host galaxies themselves and provide a unique window into exploring a host of astrophysical questions, such as the formation and evolution of galaxies, age of the Universe and the epoch of reionization, as well as the theories of stellar evolution, just to name a few. Due to their very old ages and quiescent stellar populations, GCs can act as good proxies for understanding the stellar populations of spheroids (ETGs and spiral bulges). In particular, the GCs in the Galactic Bulge are close enough such that the stars can be individually resolved, allowing for the different stellar evolutionary phases to be studied in detail. Although GCs were originally thought to host Simple Stellar Populations (i.e. all of the stars in the system formed at the exact same time, in the same volume of space and with homogeneous chemical composition), it is now accepted that these systems are far more complex and host multiple stellar populations with different chemical abundances (Forbes et al. 2018; see also reviews by Brodie & Strader 2006

and Bastian & Lardo 2018 and references therein). While a full account of the work that has been done over the past two decades on understanding the multiple stellar populations in GCs is outside the scope of this thesis, in this section I will summarise a few of the key studies of GCs that lend further evidence for the existence of highly evolved He-rich stars in old stellar systems - the same stars that are believed to be the primary source of the upturn in ETGs. See reviews by Carretta (2012), Charbonnel (2016) and Bastian & Lardo (2018) for a complete breakdown of our current understanding on this topic.

Multiple stellar populations in GCs were first discovered in ω Centauri, the largest GC in the Milky Way, which showed a minority population of bluer/fainter MS and RGB stars that was separated from the majority redder/brighter MS and RGB stars (Lee et al. 1999; Piotto et al. 2002; Bedin et al. 2004, Piotto et al. 2005). Later observations also found a much hotter population of HB stars that was completely separate from the normal HB stars (Ferraro et al. 2004; Sollima et al. 2005). By using a range of Helium abundances, Norris (2004) was able to reproduce the multiple MS/RGB/HB populations simultaneously in ω Centauri. Similarly, Lee et al. (2005b) were able to fit models with a large range of He-enhancements to the colour-magnitude diagram (CMD) of NGC2808, another massive Galactic GC that was found to host discrete multiple stellar populations (Piotto et al. 2007). The model fits to the observed CMD of NGC2808 are shown in Fig. 1.9, requiring extremely large He abundances, with $Y > 0.4$ for the bluest population of stars - ones that were also very bright in the UV. Of particular interest was the fact that the bluest MS population was spectroscopically found to be more metal-rich than the others, thus requiring the extremely high He content. Calculations by D'Antona et al. (2005) suggested that the blue extension to the standard MS consisted of $\sim 20\%$ of the entire population. These findings were followed up by studies on many other Milky Way GCs that were also found to host multiple stellar populations (see references in Chung et al. 2017). Milone et al. (2018) also demonstrated a clear correlation between the cluster mass and the level of He-enhancement in GCs, similar in nature to the $FUV - V$ vs Mg_2 relation in ETGs. Furthermore, Buzzoni et al. (2012) reported the presence of UV-bright blue HB stars in the Galactic open cluster NGC6791, with $Y = 0.3 \pm 0.04$. The open cluster is old, ~ 8 Gyrs (Chaboyer et al. 1999) and has a supersolar metallicity of $[Fe/H] \approx 0.4$ (e.g. Boesgaard et al. 2009), making it a good proxy for UV upturn galaxies.

Most of the studies mentioned thus far concluded the need for high He abundances through

fitting models to CMDs. Even though the excellent model fits (as seen in Fig. 1.9) all unanimously suggested high Helium as the obvious solution, this conclusion was still indirect and there existed the potential for alternative hypotheses to explain the blue HB stars. However, non-cosmological He abundances have now been directly measured through spectroscopy using the He I 10830Å line strength in RGB and HB stars in both ω Centauri and NGC2808 (Dupree et al. 2011; Pasquini et al. 2011, Dupree & Avrett 2013; Marino et al. 2014), with $\Delta Y \gtrsim 0.17$ between stars belonging to two different sub-populations. These direct measurements thus left no doubt on the existence of He-rich stellar populations.

Extending the search beyond our own Galaxy, which hosts GCs with mostly low metallicities, numerous UV-bright GCs with much higher metallicities comparable to ETGs were discovered in M87, the BCG of the nearby Virgo cluster (Sohn et al. 2006; Kaviraj et al. 2007). These massive metal-rich GCs have values/scatter in $UV - optical$ colours comparable to those of ETGs with upturn, much bluer than what is predicted by canonical SPS models, due to a significant fraction of their HB population (up to 50%) being He-enhanced to counteract the overall cooler temperatures caused by the higher metallicities, just as in ETGs. Similar metal-rich clusters were also found in other galaxies, such M31 and M81 (Peacock et al. 2017).

1.8 Summary

ETGs are dominated by a majority old and quiescent stellar population that emits strongly in the optical but is expected to have little output in the UV according to canonical stellar population synthesis models, due to no ongoing star-formation activity. However, UV observations of such systems show a sharp rise in their spectrum shortward of ~ 2500Å, down to the Lyman limit - a phenomenon dubbed the UV upturn. Practically all bright ETGs are found to have a component of the upturn and their $FUV - V$ colour anti-correlates with the Mg_2 index, i.e. the strength of the upturn increases with metallicity. Another important feature of the upturn is that it is concentrated in the centre of galaxies and becomes weaker radially outwards. The $FUV - V$ colour, which is the standard measure of the upturn strength is found to have a large scatter of ~ 2 magnitudes in nearby cluster ETGs, despite the same galaxies exhibiting minimal scatter (< 0.2 magnitudes) in their optical colour. This lends credence to the idea that the optical output from ETGs is dominated by the canonical old and quiescent stellar population, while the upturn is caused by a minority sub-population of hot stars. The upturn is found to exist in a subset of

the brightest cluster galaxies potentially up to $z \sim 1$, although its prevalence appears to decrease at higher redshifts, particularly $z > 0.6$.

Of all the possible sources, hot Horizontal Branch stars were found to best explain the UV observations in ETGs. To explain how HB stars can have such high temperatures and become UV-bright, several models have been proposed - metal-poor HB stars, mass loss in the RGB, binary interactions and finally Helium enhancement. The metal-poor hypothesis predicts that the upturn should disappear at a relatively low redshift ($z \sim 0.25$). This has been proven to not hold true as the upturn is observed out to at least moderate redshifts. The binary origin of the HB stars predicts that the upturn should remain constant out to very high redshifts ($1 \sim 2$ Gyrs after the galaxies form), which once again has observationally been proven to be unfeasible as the strength of the upturn is found to evolve with redshift. The mass loss hypothesis has recently been brought into question through observations of RGB stars in local star clusters with upturn, where mass loss is not found to depend on metallicity, hence the $FUV - V$ vs Mg_2 relation did not hold true. Also, there is no observational or theoretical basis for why enhanced mass-loss (2-3 times the observed amount) should occur in a subset of RGB stars suddenly at moderate redshift. The most plausible theory for the hot HB is thus He-enhancement, a conclusion that was reached via the discovery of multiple stellar populations in Galactic GCs with extended hot HBs, which could only be explained by high He abundances. Subsequently, RGB stars with extreme He abundances above the cosmological value have also been spectroscopically confirmed in ω Centauri and NGC2808.

Both observations and theoretical models have left no doubt on the existence of He-enhanced hot HB stars. However, there does not yet exist fully self-consistent mechanisms that can explain how such high He abundances can be reached. A few hypotheses have recently been suggested, such as the cluster disintegration scenario in which He-enhanced stars are produced within massive stellar clusters that eventually become disintegrated by tidal forces in the inner regions of the host galaxy, leaving behind field stars with high He abundances (Bekki 2012). Another hypothesis suggests that He-rich stars were formed in dissolved metal-rich clusters, the likes of which are currently observed in M87 and other galaxies (Goudfrooij 2018). Further observational and theoretical work is necessary to answer many of the questions raised by these scenarios.

In the upcoming chapters in this thesis, I will characterise the strength of the upturn population in ETGs within low-z galaxy clusters, as well as testing any potential effects of the cluster environment on the upturn. Most previous work on the evolution of the upturn at higher redshifts

have only been performed within BCGs, which may have different properties when compared to normal ETGs due to their complicated formation channels (as will be discussed in later chapters). Throughout this thesis, I will analyse in detail the evolution of the upturn in cluster red sequence galaxies down to L^* and beyond, out to $z \sim 0.7$. The results will then be tested against various SSP models of the upturn to determine which model can best explain the UV observations in the general ETG population in clusters, not just the BCGs.

2

The UV Upturn in Coma, Fornax and Perseus clusters

Previous studies of the UV upturn have involved characterising the population of hot HB stars that gave rise to the phenomenon by fitting models to the UV spectra of bright ellipticals, or BCGs. However, due to the acute lack of high resolution spectroscopy and the requirement of space based instrumentation in order to perform UV observations, the fitting could only be performed on a handful of galaxies in the nearby Universe. In this chapter, the strength of the upturn will be analysed and compared between galaxies in the Coma, Fornax and Perseus clusters, beyond the L^* point in each case, demonstrating that the feature is ubiquitous in all ETGs regardless of luminosity/mass. The population giving rise to the upturn will then be characterised through model fitting of the galaxies' UV-to-optical SEDs, which are generated by combining photometric data from several space and ground based telescopes.

This chapter has been published in and is largely reproduced from Ali et al. (2018a).

2.1 Introduction

Despite their generally old and metal rich stellar populations, ETGs often show excess flux at $\lambda < 2500$Å above what is expected from conventional stellar evolution (Code 1969, Bertola

et al. 1982). It is now generally accepted that the UV-excess originates from hot horizontal branch (HB) stars (e.g., see review by O'Connell 1999; Yi 2008). Two general conditions must apply to this upturn population. First, any hot HB population giving rise to an upturn in a massive ETG cannot be metal-poor because the broadband colours and line indices of ETGs clearly show that they are dominated by a metal-rich stellar population (e.g. Burstein et al. 1988; Pastorello et al. 2014). Second, as HB stars represent the late core Helium burning phase of low mass stars, the upturn directly probes the properties of stars that reached the zero age main sequence at relatively high redshift and therefore provides a window to the conditions within galaxies at very early times. Brown et al. (1997) calculated the temperatures of the hot HB population in 6 bright ETGs through model fitting of the galaxy spectra. They recovered a range of temperatures between 20,000$\pm$3000K for the hot HB population, which is much higher than the average temperature of $\sim 5000 - 6000K$ of the majority MS/RGB population that dominate ETGs.

The upturn, as measured by the $FUV - V$ colour, appears to be correlated with metallicity (more properly, Mg_2 strength) and velocity dispersion, in the sense that more massive and metal-rich galaxies have bluer UV-optical colours (Burstein et al. 1988, Bureau et al. 2011). However, it shows very weak correlation with the Iron-abundance indices (Fe5015), suggesting that the source of the upturn is related to the α-enriched older stellar populations (O'Connell 1999, Bureau et al. 2011). In a sample of bright passively evolving ETGs (some with weak AGN activity), as well as early-type spirals, Carter et al. (2011) demonstrated a clear positive gradient in the $FUV - NUV$ colour with increasing galactocentric distance, thus concluding that the UV emission in upturn galaxies is centrally concentrated.

Boselli et al. (2005) for the first time performed a cluster-wide survey for the upturn in all ETGs in the Virgo cluster, going all the way down to dwarf ellipticals. They recovered the correlations between $FUV - V$ and metallicity as with Burstein et al. (1988) in the brightest galaxies, however this correlation did not necessarily hold true for the fainter galaxies. Even though the upturn tended to get stronger with increasing mass (or luminosity) in giant ellipticals, they found that the opposite was true for dwarf ellipticals, possibly due to residual star-formation activity in the dwarf population. Smith et al. (2012) recovered a similar result when looking at a large sample of optically-selected giant red sequence galaxies in the Coma cluster and found a reddening in the $FUV - i$ colour as the galaxy luminosity decreased (i.e. mass decreased). Schombert (2016) also carried out multi-colour photometry for a large sample of local ellipticals

using a combination of GALEX, SDSS, 2MASS and Spitzer data. He found that the NUV-optical colours in particular were a direct measure of the UV upturn and changed with galaxy luminosity. These colours could only be reproduced by using models with a range of blue HB populations.

This chapter has two main objectives. First to expand upon the initial work of Brown et al. (1997) by fitting the SEDs of ETGs to derive key physical parameters of the hot HB population that gives rise to the upturn. For Coma cluster galaxies, UV observations have been made by both GALEX and UVOT, which when combined together with their optical SDSS dataset, allows for comparatively deep UV-to-optical SEDs to be generated. The approach that is taken is as follows: I construct the most detailed UV SED possible from the available photometry for red sequence galaxies drawn from the Coma cluster, combining each with their optical SED. I then fit the entire SED with a combination of a conventional old stellar population and a blackbody. The conventional stellar population does not include a UV-luminous post-main sequence population with which to explain the UV upturn; the additional blackbody is used to model and characterise this. The best fit temperature of this blackbody component could be interpreted as the luminosity-weighted temperature of any population that gives rise to the UV upturn. Using the derived temperature and taking local globular clusters as a benchmark, the fraction of stars that evolve on to the hot HB relative to the turnoff stars is estimated. This work has the obvious advantage of surveying a much larger sample of galaxies, but also a wider range of luminosities down to at least the L^* point in Coma - so the standard elliptical population is explored, not just a handful of the brightest galaxies in the cluster.

Second, I expand upon the work of Boselli et al. (2005) and Smith et al. (2012) by performing a photometric analysis of optically selected quiescent galaxies in Coma, Fornax and Perseus clusters. Due to their relative proximity ($0 < z < 0.025$) and richness (Bautz-Morgan classes II/II-III; Bautz & Morgan 1970), all three clusters provide excellent astrophysical laboratories to explore the upturn in galaxies with a wide range of luminosities/masses. I compare the $FUV - optical$ colours of the Coma galaxies with those in Fornax and Perseus clusters in order to analyse the strength of the upturn in all three. Lee et al. (2005a) carried out photometry of some of the brightest galaxies in the Fornax cluster, however given the subsequent availability of much deeper GALEX data, it is now possible to detect a larger number of galaxies and present a more comprehensive study of this cluster. Perseus has not been explored in the UV despite having a large number of bright ETGs in its core (Kent & Sargent 1983), mainly due to the high galactic

extinction along the line-of-sight. However, the GALEX UV dataset is deep enough such that the UV emission from Perseus ETGs can be clearly detected and analysed despite the large line-of-sight extinction.

In the following chapters all magnitudes quoted are in the AB system, and the cosmology used assumes $h = 0.7, \Omega_m = 0.3, \Omega_\Lambda = 0.7$. Corrections for Galactic extinction in all bands are made using the extinction maps provided by Schlafly & Finkbeiner (2011). For the Perseus cluster in particular, due to the large amount of extinction present in the UV bands, and the possibility of there being slightly varying amounts of extinctions along different lines of sight, there is a small yet intrinsic uncertainty in the extinction-corrected UV photometry for the Perseus galaxies.

2.2 Data

2.2.1 Optical

The main focus of this chapter is on the Coma cluster, but I also carry out a comparison with the Fornax and Perseus clusters. Optical data for Coma and Perseus was taken from the latest release (DR12) of the Sloan Digital Sky Survey (SDSS; Alam et al. 2015; York et al. 2000). Given that the optical cluster red sequence is known to host the majority of cluster members and to consist of mainly 'red and dead' E/S0 galaxies (Bower et al., 1992), these galaxies are the main focus of this study. Only those red sequence members were selected which have uncertainties of < 0.05 magnitudes in their relevant optical colours. A metric 7.5kpc diameter aperture was used to measure UV-optical colours in each cluster. For Fornax the the B and V data was taken from Karick et al. (2003) [1] and for Coma and Perseus, the SDSS g and r band magnitudes were converted to equivalent V magnitude using the equations from Jester et al. (2005). Galaxies on the red sequence were assumed to be cluster members, as is usually the case, but I have also used published catalogs to check membership (Coma: Hammer et al. 2010; Michard & Andreon 2008 and Trentham et al. (priv. comm.); Fornax: Drinkwater et al. 2000; Ferguson & Sandage 1988; Perseus: Brunzendorf & Meusinger 1999). The red sequences are plotted in Fig. 2.1.

[1] In this case the Kron (model) apertures was used.

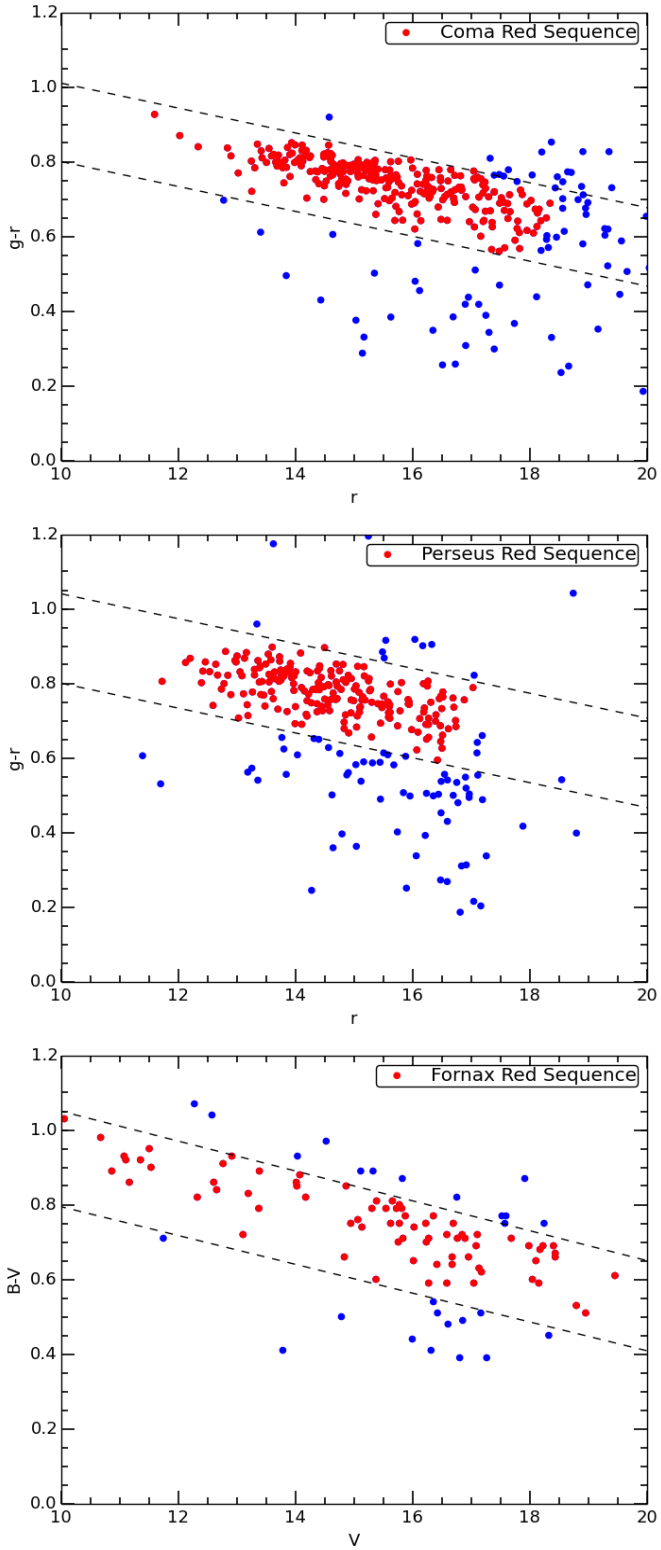

Figure 2.1: Optical colour-magnitude diagrams ($g - r$ or $B - V$ vs. r or V) for the Coma, Perseus and Fornax clusters (top to bottom). The red sequence is denoted by the dashed lines in each case. Galaxies used in this analysis are those red sequence objects with photometric uncertainties in their optical colour < 0.05 magnitudes. All colours are corrected for foreground extinction as described in the main text. However, varying levels of extinction along the line-of-sight to Perseus (which was not accounted for) could cause a slightly different spread in the Perseus red sequence compared to Coma, even though the same colours are used in each case.

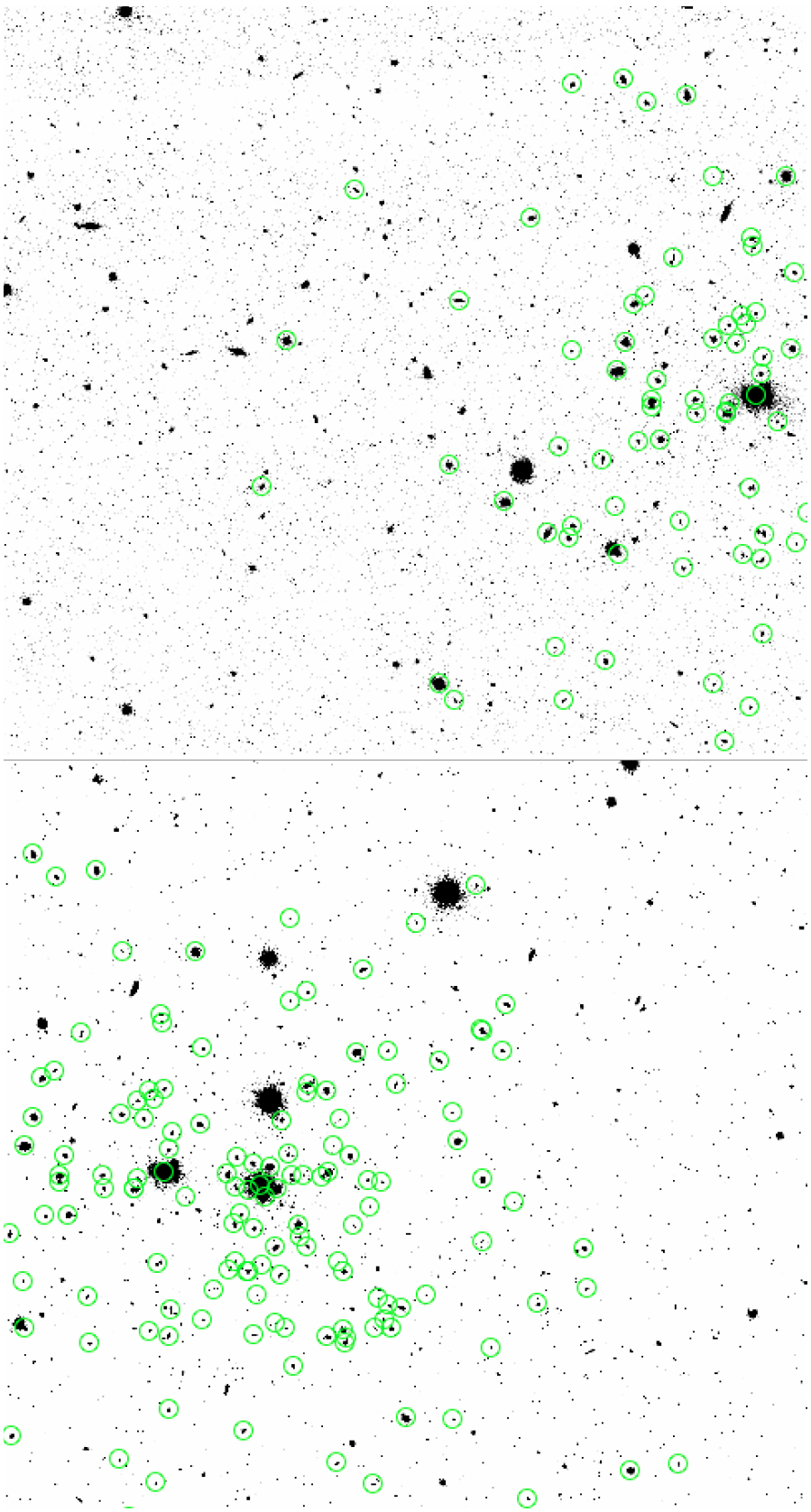

Figure 2.2: Exemplar SDSS r-band images of Coma, covering its central region. Highlighted are a subset of the red sequence galaxies detected in the GALEX FUV band and plotted in Fig. 2.4.

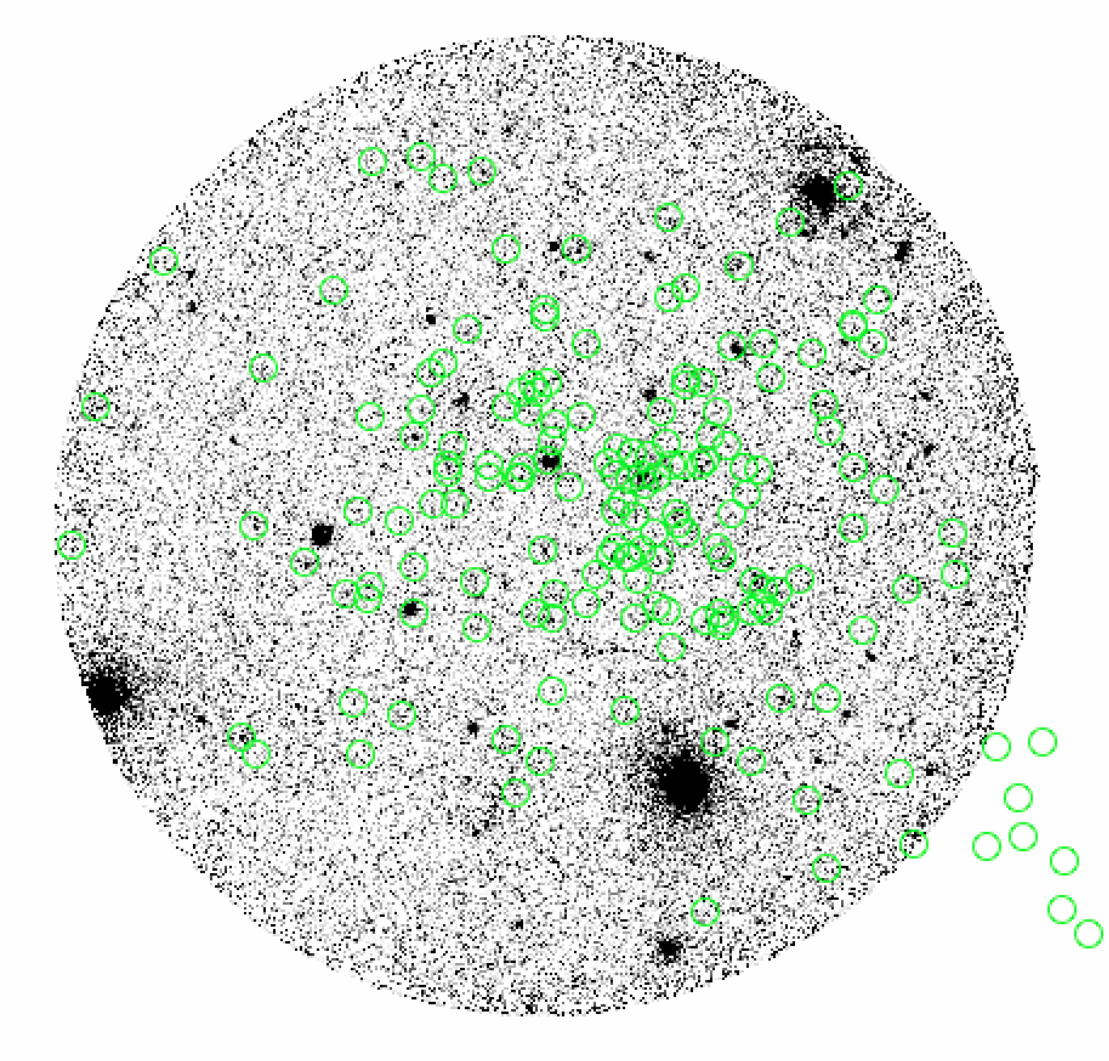

Figure 2.3: Exemplar GALEX FUV image of Coma, covering its entire central region. Highlighted are a subset of the red sequence galaxies detected in this band and plotted in Fig. 2.4. The extra galaxies in the southwestern region of Coma belongs to the 'Coma-3' field as detailed in the text.

2.2.2 GALEX

Galaxy Evolution Explorer (GALEX) is an orbiting 50 cm Ritchey-Chretien telescope with two UV imaging channels and a selectable CaF_2 g/mm grism for slitless spectroscopy over the whole field-of-view. The UV images for the Fornax, Perseus and Coma clusters were obtained from archived GALEX data available through the Multi-Mission Archive at the Space Telescope Science Institute (MAST). Images were taken with both GALEX filters: FUV and NUV which have central wavelengths 1526Å (range of 1344-1786Å) and 2329Å (range of 1771-2831Å) and image resolution FWHM of $4.3''$ and $5.3''$. The two filters also have slightly different field of views of 1.28° and 1.24° respectively, with a very large pixel scale of $1.5''$/pixel. See Martin et al. (2005) and Morrissey et al. (2007) for full technical specifications of GALEX. SDSS and GALEX images of Coma are shown in Figs. 2.2 and 2.3 as examples.

All images were retrieved as calibrated intensity maps (plus their relative σ images) from the GalexView tool[2]. Both the cluster core of Coma as well as the southwestern 'Coma-3' field was observed by GALEX, where the latter shows a secondary X-ray peak (White et al. 1993) and is associated with the infalling NGC4839 galaxy group (e.g. Colless & Dunn 1996; Komiyama et al. 2002). Exposure times for the Coma (central) and Coma-3 images were 19ks and 30ks respectively in the FUV band (Hammer et al. 2010). For Perseus the exposure times in FUV were 14.9ks and 8ks (O'Connell 2005), and for Fornax I used a deep exposure of 34ks in the centre and a 'ring' of 12 2.5ks exposures in the outer regions (NGS - Nearby Galaxy Survey, Gil de Paz et al. 2007). The majority of the Fornax optically selected red sequence members were found to be in the central FUV frame, with only four galaxies in the outer 'ring' of lower exposure frames. Of these 4, only one was clearly undetected. The remaining red sequence members were outside the field of view of the UV images and hence could not be analysed.

The FUV and NUV magnitudes of red sequence galaxies in these clusters were measured through 7.5kpc (diameter) apertures, centred on the optical position. Only objects with $> 5\sigma$ detections were considered, and their reality was verified by eye. This process ensured that all red sequence Coma galaxies to 2 magnitudes below M^* in the H-band (Eisenhardt et al. 2007) would be included in the sample.

[2]https://galex.stsci.edu/galexview

2.2.3 UVOT

UVOT (Ultraviolet Optical Telescope) is an ancillary 30cm telescope on the SWIFT satellite. It has a field of view of $17' \times 17'$ with a pixel scale of $0.502''/pixel$ and a PSF FWHM of $2.5''$. Technical descriptions of the SWIFT UVOT telescope and its photometric calibrations are given in Roming et al. (2005) and Poole et al. (2008). UVOT images for Coma were taken through the $UVW2$ (central wavelength 1928Å), $UVM2$ (2246Å), $UVW1$ (2600Å) filters, as well as optical filters. Only the $UVW2$ and $UVW1$ data was used in conjunction with the optical U, B and V UVOT images, given that the $UVM2$ band largely overlaps with the GALEX NUV band and has a far shorter total exposure time in comparison.

For Coma, I was able to find images in the Swift UVOT archive from multiple programs (Markwardt et al. 2005; Brown et al. 2014). These covered a subset of the Coma galaxies observed with GALEX and depending upon the number and/or depth of individual exposures, resulted in a variety of effective exposure times. The deepest exposures came from overlapping pointings that targeted the centre of the cluster. Most of the UVOT-targeted galaxies ($\sim$24 out of 42) were drawn from this region and consequently had deeper ($\sim$2.7-3.4ks in $UVW2$ and $\sim$0.8-1.3ks in $UVW1$) exposure times. For the galaxies outside of this region, exposure varied between $\sim$0.8-2.7ks in $UVW2$ and $\sim$0.15-0.8ks in $UVW1$. Despite the variation in exposure times, all galaxies detected by GALEX and targeted by UVOT were detected. However while the GALEX observations sampled passive galaxies down to $M_v = -18$ (Fig. 2.4), the UVOT pointings only targeted one galaxy fainter than $M_v > -19$.

The images were aligned and averaged together using the *imcombine* function in *IRAF* to create final images with longer exposure times to perform photometry on. Similar to GALEX, photometry was carried out in all UVOT bands through 7.5kpc diameter apertures centered on the optical positions of red sequence galaxies. When combined with GALEX FUV and NUV, this creates essentially contiguous coverage of the entire ultraviolet region of the spectrum between $\sim$1000Å and $\sim$3000Å.

2.3 Results

2.3.1 The UV upturn in Coma, Fornax and Perseus

To analyze and compare the UV upturn in Coma, Fornax and Perseus clusters, I plot the $FUV - V$ colour, the standard measure for the strength of the UV upturn, in fixed 7.5 kpc diameter apertures of all the cluster red sequence galaxies against their absolute V band magnitudes in Fig. 2.4. The brightest giant ellipticals tend to have the bluest colours and as such the strongest upturn. This is (as will be shown) because they have hotter and more prominent extended HBs. We see a general trend of the $FUV - V$ colour getting redder with decreasing luminosity (mass). At $M_v \gtrsim -18$ however, as seen in Fornax galaxies, the $FUV - V$ trend with V is reversed and becomes bluer with decreasing luminosity. Obviously, the lack of systems with comparatively red $FUV - V$ colours at these magnitudes is simply a reflection of the FUV magnitude limit. However, the presence of galaxies with colours significantly bluer than $FUV - V < 5.5$ indicates that a significant fraction of the fainter dwarfs either have ongoing star-formation or a UV upturn population with different characteristics to those of the more luminous galaxies, perhaps unsurprising given the mass and overall metallicity for these galaxies.

So far, these observations confirm the conventional view of the upturn as shown in Burstein et al. (1988) and Bureau et al. (2011). Note that the data for Perseus is subject to a comparatively large and therefore less certain Galactic extinction correction, and as a consequence there may be an uncertain offset in the $FUV - V$ colours between Perseus and the other clusters. However, the range in $FUV - V$ colours is largely unaffected by this and is consistent with that found in the Coma and Fornax clusters (and Virgo; Boselli et al. 2005).

Focusing only on the giant ellipticals, i.e. galaxies with $M_v \lesssim -18$, even with the brightest (most massive) galaxies tending to be somewhat bluer than their fainter counterparts, there is still significant stochastic variation of $1.5 \sim 2$ magnitudes in range in the $FUV - V$ colour between the majority of galaxies in all three clusters, ignoring the few outliers. Where they have bands in common, the photometric behaviour for each of the cluster populations appears consistent to the fidelity of the data, indicating that the results are most likely applicable to the general population of quiescent cluster ETGs in the local Universe. However, this can only be verified with studies involving larger sample of low redshift clusters (chapter 3).

The photometric range in UV-optical colour observed here agrees with that seen in the results of Boselli et al. (2005), who also found approximately 2 magnitudes of scatter in the $FUV - V$

colour in red sequence Virgo cluster galaxies. As such the variation in the UV upturn strength appears to be a ubiquitous feature present in all low redshift early-type cluster galaxies. This may be interpreted as a variation in the temperature and/or strength of an extended blue HB component in these galaxies.

If the blue colours at fainter magnitudes are due to an extended HB population in fainter galaxies rather than star-formation, these may be relatively low metallicity stars. In this case the observed trend of $FUV-V$ becoming bluer with decreasing luminosity could simply reflect the lower mean metal abundance of the stellar population of dwarf galaxies (i.e. the conventional first parameter of HB morphology).

2.3.2 The UV SEDs of Coma galaxies

To properly investigate the nature of the sources of the UV upturn, we would need detailed UV spectra of the galaxies in question, data that is not available at present. The broad consensus is that the UV flux is produced by hot HB stars. Brown et al. (1997) obtained UV spectra of some bright galaxies from Ultraviolet Imaging Telescope (UIT) and found their temperatures to be consistent with a hot HB with $T_{eff} \sim 20000$K. Imaging of the resolved sources of the UV upturn in M31 and M32 (Brown et al., 1998a) confirms their nature as stars in the extended HB.

GALEX and UVOT data could be combined for the Coma cluster to build a detailed spectral energy distribution for red sequence galaxies within the UVOT and GALEX images, covering between 1000 and 3000 Å uniformly for these objects. From GALEX, I used data from both the FUV and NUV bands and from UVOT data from the $UVW2$ and $UVW1$ bands, which when combined gave a contiguous coverage in the UV. I have also made use of the UVOT U, B and V data to give coverage in the optical all the way up to approximately 6000Å. Plotted in Fig. 2.5 are all colours relative to V.

176 confirmed early-type cluster members were detected in the GALEX bands as shown in Fig. 2.4, i.e. all Coma galaxies brighter than $M_v \leq -18$ in the region covered by GALEX. Of these 44 were also targeted in UVOT pointings and all were detected. A colour cut was then made at $U-V=2.1$ (this was done in addition to the $g-r$ red sequence selection), and all galaxies with colours bluer than this limit were rejected in order to ensure that no systems with significant residual star formation were included. This left 42 galaxies altogether, which are shown in Fig. 2.5 (both red and cyan points in the plot combined).

I also plot the SED of IC4040, a known star-forming galaxy within Coma, and the SED of

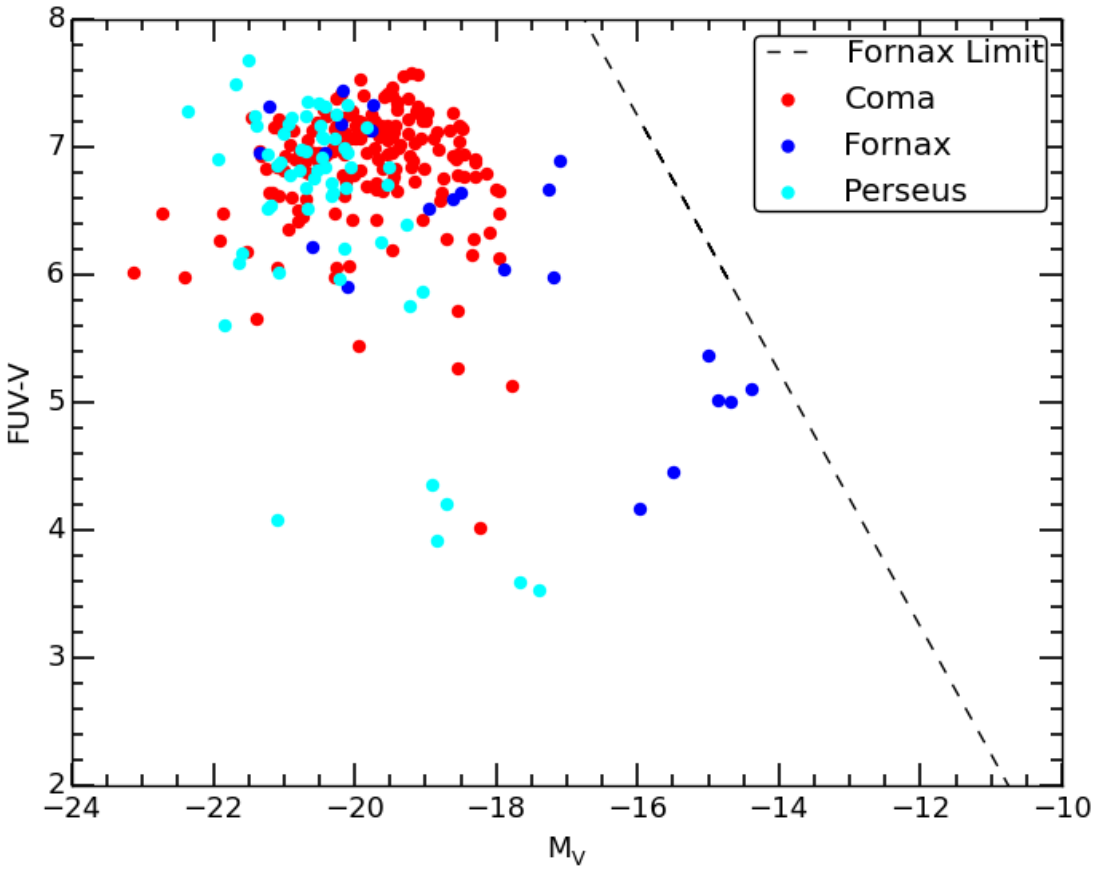

Figure 2.4: GALEX $FUV-V$ vs M_v colour-magnitude diagram for red sequence galaxies in Coma, Fornax and Perseus clusters. The black dashed line shows the GALEX FUV detection limit ($> 5\sigma$) for Fornax. Photometric error in colour is < 0.1 magnitudes.

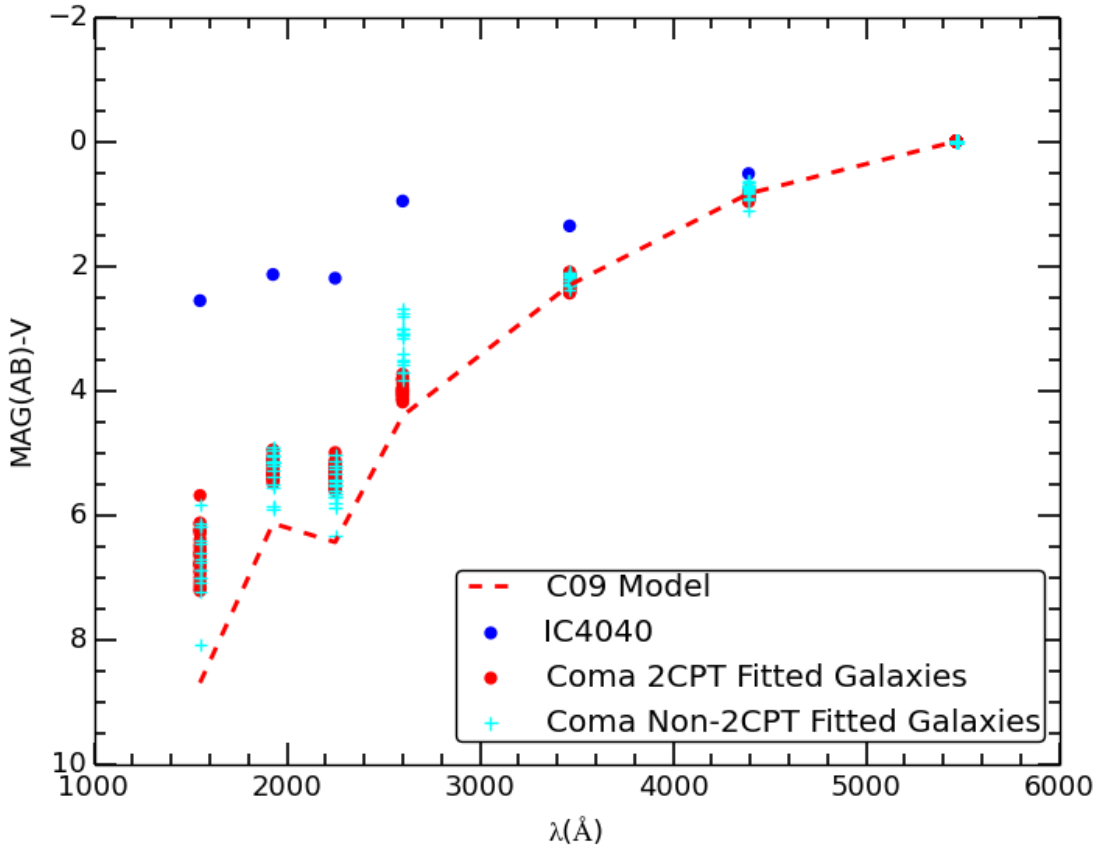

Figure 2.5: UV to optical SEDs of Coma red sequence galaxies, IC4040 (a starforming galaxy) and an old metal-rich SSP (no starformation) from the C09 model. The colours plotted (from left to right) are $FUV - V$, $UVW2 - V$, $NUV - V$, $UVW1 - V$, $U - V$ and $B - V$. Photometric error in colour is $\lesssim 0.1$ magnitudes.

a 'red and dead' galaxy as given by the Conroy et al. (2009) (C09 henceforth) model, as these two SEDs represent the extreme cases of strong ongoing star formation and no star formation at all to compare with my sample of red sequence galaxies. As one would expect, the spectrum of IC4040 is much flatter going from the optical to the ultraviolet when compared to the red sequence galaxies. This is due to the IMF of a star-forming system producing stars of a range of temperatures from faint M types all the way to OB supergiants, which emit strongly at all wavelengths between optical and ultraviolet, leading to a flat spectrum. Compared to this, the upturn galaxies have a bimodal population, consisting of a majority of low temperature stars (mostly K giants by luminosity) superimposed with a relatively small but very hot sub-population of (likely) blue/extreme HB stars.

Unlike optical colours, the UV colours show considerable scatter. This is due to the different strengths, and temperatures (as will be shown) of the hot HB component. While the scatter increases towards bluer colours, as one would assume, unexpectedly, there is also large scatter in the $UVW1$ (2600 Å)-V colours, even though this filter is the reddest of the UV filters used. This will be discussed further when fitting blackbody curves to the UV SEDs.

a) Blackbody Fitting

To model the SEDs, it was assumed that the galaxies consist of a conventional old stellar population (with no attempt to model a hot post-MS phase) plus a secondary hot HB component. For the old SED, a standard quiescent stellar population from C09 is chosen, with solar metallicity and a formation redshift of $z_f = 4$ (low redshift UV-optical colours change very little between $z_f = 3$ and $z_f = 6$ in these models). This was found to reproduce the optical colours of ETGs well and produces 'normal', very red UV colours ($FUV - V \sim 8.5$) that are consistent with the expectations of conventional stellar evolution models. Importantly, this SED also matched the UV colours of 47 Tucanae, (Dalessandro et al., 2012) and other metal-rich globular clusters, as well as the reddest (but un-reddened) ETGs with a HB nearly all confined to the red clump and with only a minor contribution from secondary populations with small He spreads. These are all old systems that have little to no UV upturns.

The hot HB was then modeled with a single blackbody (of a given temperature) plus variable extinction following the Milky Way law (Cardelli et al., 1988), to fit the UV SED of Coma ETGs. I minimized least squares to fit the UV SEDs over a grid of reasonable values for temperature and extinction - $T = 5000 - 40000$K with 1000K intervals and $A_V = 0 - 1$ in 0.1 intervals.

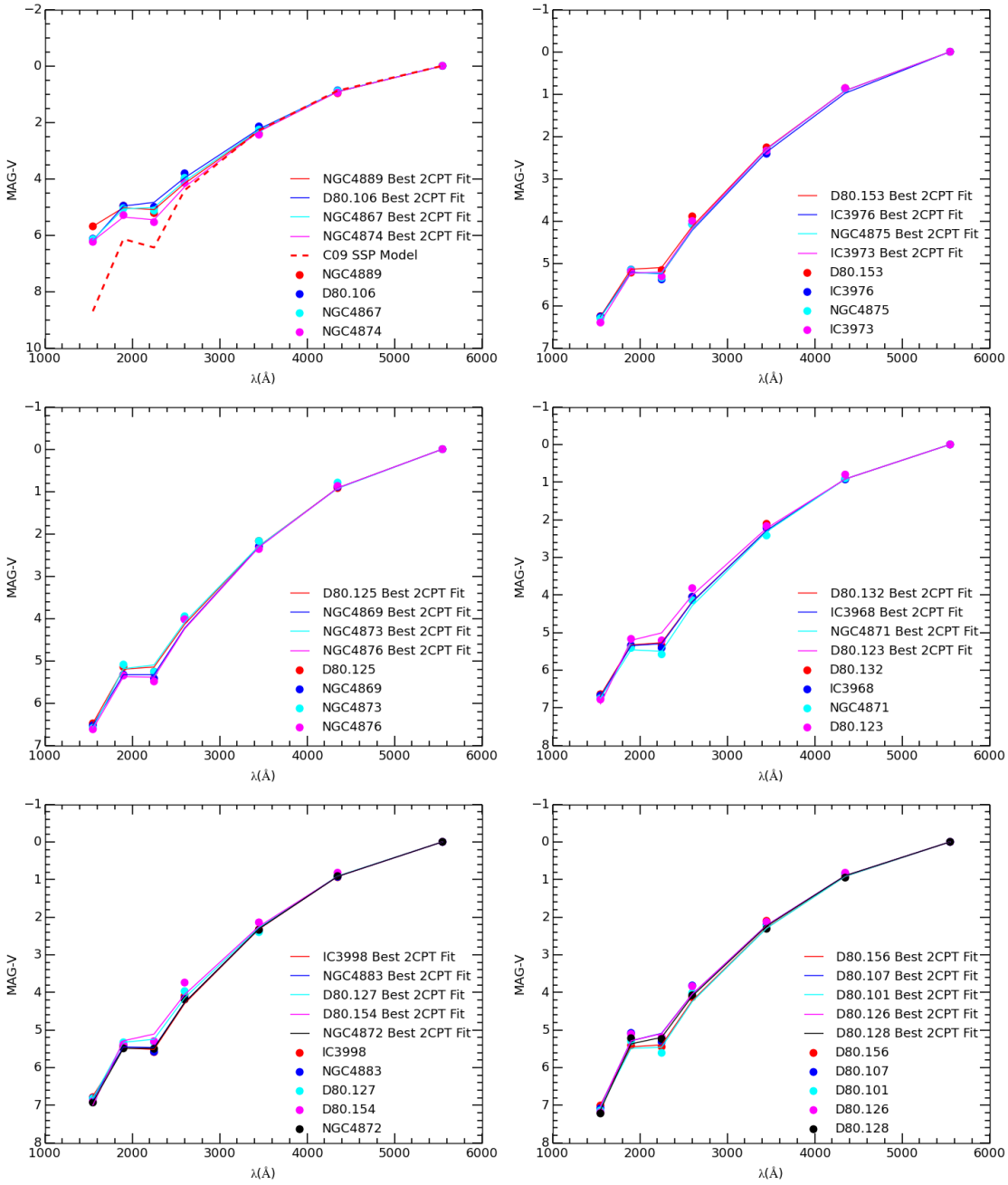

Figure 2.6: UV to optical SEDs of 26 Coma red sequence galaxies that were well fitted with 2 component (C09 + Blackbody) models. Galaxies are identified in the figure caption, by their NGC/IC numbers or their number in Dressler (1980a,b)'s catalog. Once again, the colours plotted (from left to right) are $FUV - V$, $UVW2 - V$, $NUV - V$, $UVW1 - V$, $U - V$ & $B - V$. Photometric error in colour is $\lesssim 0.1$ magnitudes. The dashed red line in the first panel indicates the baseline SED derived fromConroy et al. (2009) upon which the blackbody component is added to fit the individual galaxy SEDs.

Galaxy	M_r [mag]	BB Temp [K]	A_V [mag]	Normalisation [%]
NGC4889	-23.48	21000	0	340
D80.106	-19.82	13000	0	468
NGC4867	-21.14	15000	0	374
NGC4874	-23.05	19000	0	216
D80.153	-20.00	15000	0	340
IC3976	-20.59	15000	0.2	478
NGC4875	-20.47	16000	0	287
IC3973	-21.00	15000	0	298
D80.125	-19.75	14000	0	322
NGC4869	-21.48	15000	0	255
NGC4873	-20.95	12000	0.1	454
NGC4876	-20.82	15000	0	236
D80.132	-19.71	13000	0	278
IC3968	-19.78	13000	0	268
NGC4871	-21.17	15000	0	204
D80.123	-19.97	10000	0.1	500
IC3998	-20.52	15000	0	198
NGC4883	-20.96	14000	0	215
D80.127	-19.32	12000	0	291
D80.154	-19.53	10000	0.1	448
NGC4872	-20.89	13000	0	210
D80.156	-19.34	12000	0	238
D80.107	-19.87	10000	0	351
D80.101	-20.19	12000	0	220
D80.126	-19.61	10000	0	349
D80.128	-19.66	10000	0	307

Table 2.1: Table showing the derived parameters (Blackbody temperature, A_V, Normalisation) from model fitting as shown in Fig. 2.6. The 'Normalisation' parameter gives the relative percentage normalisation of the blackbodies to the base C09 model at the GALEX NUV band (i.e. 100% indicates that the blackbody flux is equal to the C09 flux at this wavelength). The error in the black body temperature is $\pm 1000K$ (see text for further details).

The blackbodies were normalised to the base C09 model in the GALEX NUV band and the normalisation parameter (which is the relative percentage normalisation of the blackbodies to the C09 model) was allowed to vary between 1-500% with 1% intervals, i.e. 100% indicates that the blackbody flux is equal to the C09 flux at the NUV waveband. NUV was chosen in particular to allow for finer adjustments to the model fits. It is important to note that the fitting was carried out in the UV part of the spectrum (i.e. GALEX FUV, UVOT $UVW2$, GALEX NUV, UVOT $UVW1$) since it is most affected by the upturn. Nevertheless, I added the contribution of this component to the SED of the old stellar population at every wavelength considered through to the V band. The actual contribution longward of 3000Å is negligible. This works under the assumption that the spread in optical colours is small and the base C09 model chosen reflects the observed optical colours very well, which can be seen to be the case in Fig. 2.5. Furthermore, the interstellar extinction in these galaxies would also need to be very small and this is found to be the case just from fitting to the UV part of the spectrum (see later).

Of the 42 total galaxies, I obtained very good fits to a single temperature blackbody (which is interpreted as the mean blue HB stellar temperature) for 26 galaxies, from which I also derived a value for the interstellar extinction, which was generally low ($Av \lesssim 0.2$). However, some galaxies appear to show excess flux in the $UVW1$ filter (2600 Å), such that it is not possible to obtain a good fit (especially given the small number of points). These sources are represented by the SED points plotted in cyan in Fig. 2.5; clearly the spread in the 2600Å photometry is much wider than that for the other UV points. I have checked the date of observations and find no correlation with those galaxies giving a poor fit. The objects that are clearly discrepant in the $UVW1 - V$ colour are randomly distributed in all other colours. It simply appears that there is anomalous behaviour in the $UVW1$ band for a subset of these galaxies.

The galaxies with a poor fit to the models were rejected based on a least squares criterion. The distribution of this value across the sample is strongly bimodal (i.e. the good fits are fitted very well while the bad fits are significantly and clearly worse). The majority of poorly-fit galaxies have very blue $UVW1 - V$ colours. So although I do not do this, had I chosen to make a colour cut at approximately $UVW1 - V = 3.8$ (see Fig. 2.5) and a priori rejected all galaxies with a bluer colour, the majority of the poorly-fit galaxies would have been rejected purely on this criterion.

The discrepant objects were largely (but not exclusively) found in a single UVOT $UVW1$ image (PSNJ13003230+2758411) which contains a few galaxies with a good fit. This may point

to systematic problems with this particular image (it appears to be just a single bad frame in Coma), though the fact that good fits were obtained with it and bad fits also occurred elsewhere means that this is not certain. In Fig. 2.5, IC4040 also shows a comparatively high flux in this band, perhaps indicating that this may be a signature of residual star formation dominating in the UV. To explore this, I created composite SEDs from a C09 model supplemented with a scaled version of the IC4040 SED to generate SEDs with star formation that acted to increase the $U-$band flux of the simulated SED by 1 to 20 % above that of the C09 value. Given the tightness of the range ($\sim$ 0.1 mag) in $U-V$ colours of the selected objects, the models with up to a 10% increase in $U-$band flux were plausible fits to the *optical* data. Looking at the UV part of these simulated SEDs, only the model with the smallest component of star formation (1%) gave a plausible fit with the C09 plus RSF model, even then it is far redder in UV-optical colours than all of the well-fitted galaxies - the star forming component only increases the UV brightness relative to C09 alone by a few tenths in magnitude. All others fail largely because of their $NUV-UVW1$ colour being too steep for any C09 plus BB model. Consequently, from this exercise it is clear that star formation models do not generate the UV upturns we see in the galaxies with good fits. Any one colour could be fit, but not the entire UV-optical SED.

I also attempted to fit the SEDs of the poorly fit (C09+BB) galaxies with the C09+RSF models, but fail to get good fits to their SEDs. However, the possibility that this subset of galaxies has UV emission due to some residual star formation cannot be completely ruled out, as they may be accounted for by more sophisticated residual star forming (or upturn+RSF) models.

Furthermore, I also note that HST WFC3 $F336W$ imaging data for red sequence galaxies in Abell 1689 (which is close to rest-frame $\sim$2600Å) does not show the abnormally large spread in equivalent colour as seen in the UVOT data for Coma (chapter 4), indicating that this is likely an issue with some of the $UVW1$ data and not a genuine feature of some UV SEDs. As this discrepancy can not be explained and it appears to be a problem with a subset of a single band's photometry, the affected objects are excluded from further analysis and discussion.

There is no intrinsic reason why the best blackbody fits could not contribute significant flux in the optical bands, because the fit is not constrained there. The fact that the blackbody fits never do this strongly supports the idea that the UV is dominated by the component modeled here as a blackbody while the optical is completely dominated by the conventional old metal-rich stellar population. As a consistency check the entire model fitting process was performed for the whole spectrum (UV and optical points), allowing both blackbody and C09 components to vary across

the wavelength range. I find that although there are some minor changes to the individual results obtained for each galaxy, the overall trends and conclusions remain intact.

All major derived parameters for the good fit galaxies are given in table 2.1. Fig. 2.6 shows the galaxies with their corresponding best fit models. The first panel also includes the underlying C09 model showing the contribution of the purely old population, clearly demonstrating that the extra blackbody component only contributes to the UV part of the SED. The fitted blackbody component usually has a temperature between 10,000 and $\sim 21,000$K, consistent with the earlier UIT observations of Brown et al. (1997) and the indices derived by Le Cras et al. (2016) for massive BOSS galaxies. The derived temperature is plotted vs. M_r (a good proxy for stellar mass) in Fig. 2.7 and shows a potential correlation between temperature and mass (and therefore metal abundance), in the sense that more massive (and metal rich) galaxies have hotter (and stronger) HB components. This also recovers the $FUV - V$ vs. V (or Mg_2) anti-correlation, as observed by Burstein et al. (1988) and Bureau et al. (2011). It should be noted here that since the hot component does not have a single temperature for all galaxies, one cannot use a single UV-optical colour, e.g. $FUV - V$ to measure the upturn in a uniform manner and classify sources as in Yi et al. (2005, 2011), a point also made by Smith et al. (2012).

It is worth noting that the two brightest galaxies in Coma - NGC4889 and NGC4874 also have the largest blackbody temperatures. This is interpreted as these galaxies exhibiting the strongest upturns, per the $FUV - V$ vs Mg_2 relation. However, NGC4889 and NGC4874 are also known to host prominent AGNs in their cores, which act as bright X-ray sources (e.g. Sanders et al. 2014). Hence the AGN may also contribute to the FUV flux of the overall galaxy, potentially leading to in part the higher overall blackbody temperatures derived for these galaxies. However, previous studies of the IUE spectra of galaxies with well known bright AGNs such as M87, NGC4278 and NGC1052 have shown that such objects only contribute a small fraction of the overall FUV flux in these galaxies - up to $\sim 10\%$ (Ohl et al. 1998; Møller et al. 1995). The UV light in general demonstrated an extended profile that appeared similar to the optical light, unlike what one would expect from an AGN or massive star-forming regions. Furthermore, UV-bright AGNs should be identifiable from the presence of characteristic broad, high-excitation emission lines, which was not found to be the case in the IUE spectra of nearby bright ellipticals and spiral bulges (e.g. Johnson 1979;Oke et al. 1981; Bertola et al. 1982; Oconnell et al. 1986). As such, while a small fraction of the FUV flux in NGC4889 and NGC4874 (which also demonstrate an extended UV light profile) may originate from their AGNs, it is unlikely that the

AGNs contribute to the FUV in any significant manner. Hence the derived blackbody temperature should be a reasonably accurate representation of the hot horizontal branch temperature in these galaxies.

Nelan et al. (2005) and Thomas et al. (2005, 2010) demonstrated through a spectroscopic analysis that both metallicity and age are correlated with the velocity dispersion and therefore mass of ETGs, with Price et al. (2011) demonstrating similar behaviour in Coma ETGs. The variation in the $FUV - V$ colour of the C09 models with age beyond 8 Gyrs does not change their contribution to the UV spectrum, therefore validating the decision to use a single age model for all of the fits to the optical photometry regardless of the luminosity. Similarly, for the $g - r$ selection, metallicity is expected to vary between $1 - 2Z_{\odot}$. However, as a test of consistency, the fitting procedure was duplicated using a C09 model with $Z = 0.56Z_{\odot}$, in particular to check whether such a sub-solar model yields a better fit for the lowest luminosity galaxies in my sample. I find that for all such galaxies, using a base sub-solar metallicity model gives worse fits to the optical colours than using a solar metallicity model. Furthermore, the most reasonable fits of the sub-solar metallicity models required very large values of interstellar extinction ($A_v \sim 0.7$), which are clearly unphysical for these systems. Conversely, for the most luminous galaxies in the sample - which are likely to be of super-solar metallicity - a base solar metallicity C09 model is already overestimating the contribution from the underlying conventional stellar population, given that the super-solar metallicity models have redder UV-optical colours.

To test the effect of a super-solar metallicity model, the entire fitting procedure was repeated using a base C09 SSP with $Z = 1.78Z_{\odot}$ (the next highest Z available after Z=$Z_{\odot}$), likely to be appropriate for the top 50% of the brightest galaxies in the sample. I find that the best fit temperatures decreased by on average $\sim 1000K$, but the blackbody normalisations increased significantly between $\sim 200 - 500\%$ to compensate for the combination of a decrease in blackbody temperature and the underlying super-solar SSP being redder in the UV. However, despite the change in temperatures and normalisations when using a base super-solar metallicity model, the overall trend seen in Fig. 2.7 (top) still remained intact.

Given the high metallicity and old ages (and therefore the restricted range of both) for the conventional stellar populations in all of these galaxies, neither their metallicity nor age can therefore be driving the correlations seen in Fig. 2.7. Note that the claim here is not that there is no correlation between overall age and strength of UV upturn in the actual systems. What is merely being stating is that the C09 models include no component that specifically attempts to

replicate anything that may give rise to a UV upturn, unlike e.g. the Yi et al. (1999) models. The parameters of the blackbody components that have been used to fit the upturn may correlate with overall age but I do not attempt to make this explicit.

2.4 Discussion

2.4.1 Hot HB stars as the source of the UV upturn

I have measured vacuum UV colours and the UV SEDs for quiescent ETGs in three low redshift clusters, reaching to the L^* point and beyond. Across this entire luminosity (mass) range I find evidence for a UV-bright stellar population that can be related to the classical upturn (O'Connell 1999). Reflecting the scatter in $FUV - V$, all of the galaxies undergoing the fitting presented in this chapter require an extra blackbody component on top of the C09 model to account for their UV SED. Moreover, the temperature of this component seems to increase with optical luminosity, albeit with some scatter. The need for this component is already clear in the scatter of $FUV - V$ colour in the absence of similar scatter in the optical colours.

Residual star formation does not produce an SED consistent with the observations (cf. discussion of IC4040 above). The most likely source of the excess UV flux is a hot HB component, as earlier argued by Brown et al. (1997); Greggio & Renzini (1990); O'Connell (1999). While blue HBs are commonly observed in metal-poor star clusters, it is very unlikely that the observations made here can be explained in this fashion. The galaxies in my sample are largely metal-rich and their HB should largely coincide with the red clump at temperatures of around 4000-5000K: too cool to provide the observed UV emission in the upturn galaxies. Given the small fraction of the lifetime that stars live on the HB, it would require a significant low metallicity main sequence population to exist within these galaxies, which is explicitly ruled out by many studies determining the metallicities of such galaxies (as explained in the introduction). The explanation of these UV upturn galaxies lies in the understanding gleaned from observations of the resolved stellar populations in high metallicity open clusters and so-called 'second parameter' globular clusters (Catelan 2009; Peacock et al. 2017).

The most likely mechanism to explain the presence of hot HB stars in comparatively metal-rich systems (by globular cluster standards, i.e. where the HB should not extend beyond the RR Lyra gap according to canonical models) involves Helium enrichment. In Milky Way globular clusters such as ω Centauri and NGC2808, multiple main sequences are found to correspond

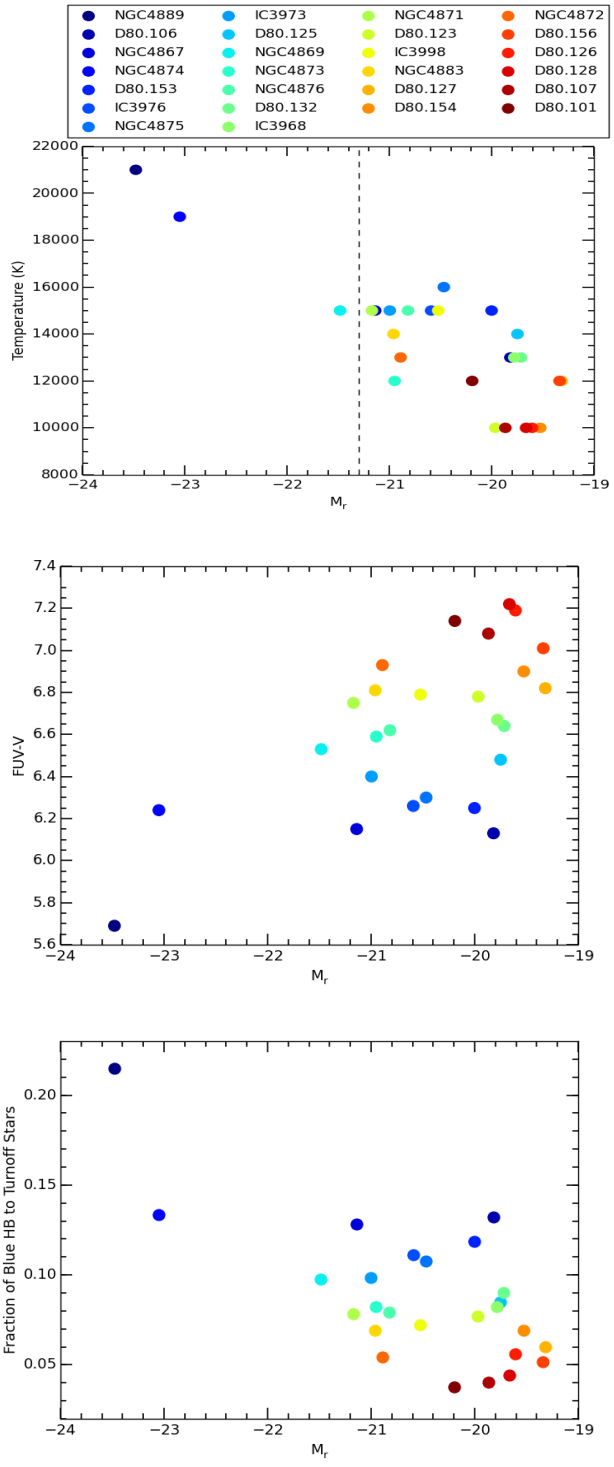

Figure 2.7: *Top:* The best fit blackbody temperature vs. M_r (absolute r-band magnitude) for galaxies in Coma. There is a potential trend of higher T_{eff} with increasing luminosity (and hence increasing mass and metallicity). Dashed line shows M^* for Coma (Eisenhardt et al. 2007). Typical errors in temperature are of the order $\pm$1000K, the quantisation used in the fitting process. *Middle:* $FUV - V$ vs. M_r for these same galaxies, showing how the increasing temperature drives the bluer colours. Photometric error in colour is < 0.1 magnitudes. *Bottom:* The estimate of the ratio of blue HB stars to turnoff stars within each galaxy as a function of M_r for these objects.

with multi-modal blue HBs and spectroscopic evidence shows that the bluer stars are more metal-rich than the red ones (Piotto et al. 2005, 2007; Bragaglia et al. 2010). The only way for this to be possible is for the bluer stellar population to be enriched in Helium relative to the redder population. There is indirect evidence of this in the selective abundance patterns of the proton-capture elements, which indicates processing through the Mg-Al chains during hot bottom burning, a process that may also dredge up Helium to the surfaces (e.g, see Charbonnel 2016; Gratton et al. 2012 for reviews). The He abundance may be as high as Y=0.43 for the most extreme population in NGC2808 (Milone et al., 2015). In other words the anomalously hot HB stars in Galactic globular clusters arise from a population with significantly enhanced Helium abundance.

Some of the more metal-rich globular clusters in the bulge, such as NGC6388 and NGC6441 (which have [Fe/H] ~ -0.5, at the high metallicity tail of the distribution in the Galaxy), also have extended HBs. Tailo et al. (2017) show that these stars have temperatures of up to 14,000K for a Y of 0.38. A specific Galactic system that provides a possible model for a Helium enriched high metallicity and old population is the open cluster NGC6791 (cf. Dorman et al. 1995 for a similar remark). In many ways this resembles a miniature version of elliptical galaxies. Buzzoni et al. (2012) demonstrate that it has a single stellar population with an age of 9 Gyr and [Fe/H] of +0.3. It is also considerably α element enhanced and has $Y = 0.30 \pm 0.04$ (Linden et al. 2017, though see Boesgaard et al. 2015). Its HB contains a significant blue population and its integrated SED is essentially indistinguishable from strong UV upturn elliptical galaxies. Buzzoni et al. (2012) argue, given this similarity, that He-enriched HB stars are therefore an extremely strong candidate to explain UV upturns in elliptical galaxies. Despite it being a single and possibly unusual object (but cf. Berkeley 17, Bragaglia et al. 2006), NGC6791 represents the *only* resolved stellar counterpart to the sources of the upturn in external galaxies and therefore remains the best heuristic model with which to interpret this UV excess in galaxies.

While He-enhanced HBs have been directly observed, there are other theoretical possibilities for producing a UV upturn population. These include scenarios where there is extra mass loss in the red giant branch (Yi et al. 1999; Yaron et al. 2008), possibly due to binary interactions (Carraro & Benvenuto, 2017; Han et al., 2007). However, in this case the degree of mass loss or the close binary fraction would somehow (e.g. via metallicity, Yi et al. 1999) have to depend strongly on galaxy mass and neither explanation would account for the observations in globular clusters, where the blue HB segments are clearly related, by chemical tagging, to the multiple

main sequences (Milone et al., 2015). This would be in contrast with recent observations by Badenes et al. (2017), where the binary fraction *decreases* with increasing metallicity, opposite to what would be needed to explain the observed trends. Moreover, there is no observational evidence for enhanced mass loss on the RGB depending on metal abundance in local stellar clusters (e.g. see Salaris et al. 2016, Miglio et al. 2012). In any event, most of the mass loss would be expected to happen at the AGB, i.e. after the horizontal branch phase.

All this points to the presence of a He-rich subpopulation in these galaxies producing hot HB stars at the end of their MS lifetime. Given that stars spend a small fraction of their lifetimes in the HB ($\sim 1\%$), they represent a much larger number of He-enhanced stars within the galaxy.

2.4.2 Implications for galaxy formation

Using the blackbody fits to the UV upturns as detailed earlier in combination with UV photometry of individual hot HB stars in local globular and open clusters could allow for the properties of the upturn populations to be estimated. Using the observed absolute luminosities of local hot HB stars with the same temperatures as my blackbody fits (e.g. NGC1904 from Recio-Blanco et al. 2006), it was possible to deduce the number of such stars needed to account for the galaxies' FUV outputs.

To relate this to a global population fraction, I adopted a HB lifetime of ~ 100 Myr and ~ 1 Gyr for stars to evolve from the main sequence turnoff to the Helium flash. In order to estimate the fraction of blue HB stars (i.e. the He-rich population), via the initial mass function, it is necessary to assume an age for the 'normal' and He-rich populations. The YEPS spectrophotometric models for He-enhanced stellar populations (Chung et al. 2017) were used to determine the age since formation of the stellar populations investigated in this analysis. To match the observed UV colours of all cluster galaxies in my sample, the models predict at least a $Y \sim 0.38$ and an age of ~ 12 Gyrs, assuming Z=$Z_{\odot}$ and $z_f \sim 4$ (plausible given the recent estimates by Jørgensen et al. 2017). That is, with this level of He-enrichment, it takes ~ 12 Gyr for the upturn to become apparent in the YEPS models' simulated colours (see also Tantalo et al., 1996). Using this estimate of age, the relevant masses for the turn-off stars, etc, could be determined and the relative numbers of HB and total stars could also be calculated from the IMF.

In fact, if we assume that both the He-enriched and 'normal' populations are formed in effectively simultaneous coeval bursts, we should expect the main sequence lifetimes of the He-rich population stars to be shorter than those of the normal population (Chantereau et al., 2015).

Consequently, at any given time, the He-rich stars reaching the HB should be of lower mass than those of the other population. If we assume that HB luminosities are largely independent of mass (as observed in NGC2808, Piotto et al., 2007), then as time goes on, given a normal IMF, an increasing number of stars enter the blue HB. If this is not matched by a shorter HB lifetime, the overall UV luminosity contributed by the He-rich HB population will increase. Thus the base estimate of the fraction of He-rich stars, from above, will be an *over*estimate.

A full treatment of this would require a detailed study of the relevant isochrones and is beyond the scope of this work. However, to progress we can make the (incorrect) assumption that the MS lifetimes of the two populations are the same (leading to the same mass stars joining the HB at the same time) and thereby determine an upper limit to the fraction of stars in the He-rich population for each of my galaxies. Then, by making an estimate of the correction to the relevant mass of the He-rich population and assuming a standard slope for the IMF, it is possible to estimate a correction to this upper limit, thereby indicating whether the derived upper limits are likely to be close to the true values.

However, it should be noted that the YEPS He-enhanced SSP models imply a constant UV luminosity with time once a blue HB is formed, rather than one where the UV luminosity increases. This may be because, in their models, the time spent on the HB decreases with stellar mass, compensating for the increasing rate of stars entering the blue HB with time due to the slope of the IMF. If this is the case then we should expect the upper limits derived here to be close to the real values.

Given the above, I consider ages since formation of both stellar populations to be 12 Gyr. This value is in broad agreement with spectrophotometric and spectroscopic measurements on ETGs with masses similar to those used here, where red sequence galaxies are found to evolve passively and with no increase in colour spread at least to $z \sim 2$, and probably higher, with quiescent galaxies observed to $z \sim 4$, including in the Dark Energy Survey data (C. Maraston, priv. comm.) and elsewhere (e.g. Glazebrook et al. 2017).This points to high redshifts of star formation and no significant further episodes at later times (see also Thomas et al. 2010). Assuming these ages, I find that a range of between 4 and 20% of stars in my galaxy sample evolve onto the blue HB. This is a similar fraction as that suggested by Dorman et al. (1995) and observed in some local stellar clusters (see below), and also as estimated by Le Cras et al. (2016) for massive BOSS galaxies. The fractions and temperatures of these stars appear to depend on the luminosities of their parent galaxies (Fig. 2.7; bottom), suggesting that the origin of the hot

HB population is related to the internal chemical evolution of galaxies.

Similar behaviour is seen in a minority of local globular and open clusters which have a wide spread in Helium abundances within their stellar populations (with NGC2808 and ω Centauri being the prime examples). In these cases 10–30% of stars seem to have $Y \sim 0.34$–0.40 (Buzzoni et al., 2012; Piotto et al., 2007; Tailo et al., 2017). Note that a significant fraction of the population may also be more He-rich than the cosmological value but do not produce hot HB stars because of their high metallicities; this appears to be the case for the objects studied by Tailo et al. (2017), where 2/3 of the stars may have $Y > 0.24$.

Individual HB stellar temperatures appear to correlate with Helium abundance e.g., for NGC2808 T_{eff} of nearly 40,000K for stars with $Y = 0.43$. Most of my galaxies are fitted with an average $T_{eff} \sim 15,000$K indicating that any He-enhanced population within them have lower Y than this, similar to that of NGC6791. This allows us to assess any correction required to the fraction of stars in this He-enhanced population due to the assumption of equal stellar mass used in the estimation of the upper limit. In Chantereau et al. (2015) a $Y = 0.4$ star with 0.6 $M_{\odot}$ has a main-sequence lifetime of 11.1 Gyrs, compared to 11.9 Gyr for a 0.8$M_{\odot}$ counterpart with cosmological He abundance. If we assume that stars of these masses reach the HB at the same time, then for a typical IMF slope, this implies twice as many He-enriched stars than if we assumed (as above) that the MS lifetime was independent of Y. Consequently, assuming that the increased rate of entry onto the HB by He-enriched stars is not matched by a decrease in their HB lifetime *and* that HB luminosity does not vary overly with stellar mass, this difference implies that the true fraction of stars with enhanced He abundances should be within a factor ~ 2 of the simple (upper limit) estimate calculated above. Given that all except the most massive of my galaxies are likely to have $Y < 0.4$, even this factor ~ 2 is likely to be itself an upper limit. One final *caveat* on this estimate is that even though we might expect a $Y-$related variation in turn-off mass and main sequence lifetime, no difference in the MS turnoff mass has been reported for any of the stellar populations with varying Y in NGC2808 (Milone et al. 2015).

a) Effect on early evolution

Assuming that the blackbody component can be interpreted as a He-enhanced population, this population appears to be more enriched and more abundant as a function of galaxy mass. As galaxy mass and metallicity are in general thought to be correlated in ETGs, this may suggest a relation between Y and Z, unsurprising given the predictions of many models of stellar

nucleosynthesis. This suggests that these objects originate from the normal process of galaxy chemical evolution and are formed in situ. We know from Carter et al. (2011) that the hot HB component is centrally concentrated, as expected if the He-enrichment comes from the same processes of chemical evolution. Given that my observations are similar to those of Buzzoni et al. (2012), the results therefore imply a rapid enrichment for a large mass of stars in situ, and therefore rapid formation of massive halos at high redshifts (in agreement with e.g., Glazebrook et al. 2017; Jørgensen et al. 2017).

Using the same assumptions as those in Chung et al. (2017), if we take $\sim$ 12 Gyr as a typical age for my stellar populations (as above), the data allows for a lower limit to be set to the stellar mass of these galaxies at $z \sim 4$. Assuming 4-20% of the stars to be sufficiently He-rich to evolve to the hot HB (Fig. 2.7; bottom), a L^* galaxy must have a stellar mass of at least $0.3 - 0.8 \times 10^{10}$ $M_{\odot}$ in place at $z \sim 4$ or earlier, with all the caveats noted above. This in turn implies that the bulk of the stellar population may be even older. Varying the assumed age of the stellar population by 2 Gyrs only changes the fraction of He-rich stars by $\sim 1.5\%$. In any event, there needs to be an earlier population to produce the extra Helium. The only way this argument may be incorrect is if the Y value of this population is even more extreme, in which case the stars can reach the HB in a significantly shorter period of time. Given the abundance yields of any prior population that gives rise to the enhanced He fractions of the hot HB stars, it is likely that this earlier population must be an order of magnitude more massive than the values estimated above (D'Antona et al., 2016). This would imply that nearly all of the stellar mass observed today in these galaxies is in place at high redshift. I note that even if my assumption of $Y \sim 0.38$ and therefore 12 Gyrs as an age for stellar populations of my typical galaxies is incorrect, the lack of evidence for appreciable star formation at $z < 2$ (Jørgensen et al. 2017 find formation redshifts for cluster galaxies between $2 < z < 6$ depending on the diagnostics used) limits their age to > 10 Gyrs (requiring higher Y). Even then, similar arguments can be made as to how much stellar mass needs to be present by this time.

There have been alternative models invoked to explain an increased Helium abundance in galaxies, for example those involving Helium sedimentation in galaxy-cluster scale halos (Peng & Nagai, 2009). Here, the results in this chapter seem to run counter to the predictions of Helium sedimentation. The most massive galaxies in my sample appear to have the highest He-enhancement and likely contain the oldest stellar populations. Helium sedimentation acts to increase the He-enhancement with increasing time and over timescales of billions of year.

If a He-enhanced sub-population is not accounted for, it is possible that galaxy properties derived from photometry and spectroscopy may be misleading or misinterpreted. Interpretation of spectral indices, particularly those involving Balmer lines may be incorrect if the Helium abundance and the presence of a hot HB is not correctly accounted for (De Propris, 2000; Percival & Salaris, 2011; de Freitas Pacheco & Barbuy, 1995) and so derived quantities such as ages and metallicities of old stellar populations might appear self consistent, yet be inaccurate. The YEPS models (Chung et al., 2017) show the required behaviour for late-time evolution, showing UV upturns, but imply that for reasonable metallicities, most broad-band optical colours are unaffected by varying He abundance over the range modelled at intermediate ages. However, stellar populations younger than 1 Gyr are not presented and so the effect on the colours of *e.g.* Lyman break galaxies and other young systems is unclear.

2.5 Conclusions

I have shown that the UV upturn is a common phenomenon in quiescent ETGs to luminosities well below the L^* point. All galaxies appear to show at least some fraction of a UV-bright population. Characterising this upturn with a blackbody component, the temperature and mass of this population appears to vary with the mass (and therefore metallicity) of the galaxy, in the sense that brighter and more metal-rich systems have the hottest and more luminous UV fluxes. I interpret this, in common with other studies, as evidence for the presence of hot HB stars in these galaxies. This interpretation of my results indicates that the more massive galaxies have the most extreme HBs. An explanation of this, consistent with the findings of local stellar populations (e.g. in star clusters) is that these stellar populations are systematically enriched in Helium. If this is the case, then, noting the caveats discussed in section 4.2, I estimate that up to 4-20% of the turnoff stars (galaxy-dependent) must be so enriched as to evolve on to the blue HB, with Y of about 0.38 to explain the observations of typical galaxies.

Interpreting my results via the recent YEPS stellar population synthesis models of Chung et al. (2017) implies that at least $\sim 0.5 \times 10^{10}\ M_{\odot}$ from the He-enriched sub-population alone needs to be in place, certainly by $z = 2$ and by $z \sim 4$ if the assumption of $Y \sim 0.38$ is reasonable. This interpretation implies that there is an upper limit to the redshift at which upturns are easily detectable, given the main sequence lifetimes of the He-enriched stars that go on to

become hot HB stars. This limit may itself be dependent on galaxy mass through the correlation between this quantity and the current-day UV upturn properties. I will explore this in the upcoming chapters.

3

The Effect of Environment on the UV Upturn in $z \leqslant 0.1$ clusters

In the previous chapter, the strength and characteristics of the UV upturn were analysed in detail for Coma red sequence galaxies, as well as comparing their UV-to-optical colours to those of Fornax and Perseus. In this chapter, I expand further on the work done in chapter 2 by analysing the upturn strength in red sequence galaxies from 20 more low redshift clusters between $0 < z < 0.1$ and investigating whether the cluster environment plays any role in driving the upturn within its constituent galaxies.

3.1 Introduction

The mass composition of galaxy clusters is $\sim$ 2% galaxies, $\sim$ 13% hot primordial gas and $\sim 85\%$ dark matter. As such the majority of baryonic matter is contained within the hot gas that permeates the entire cluster, known as the 'Intracluster Medium' (ICM), which emits strongly in the X-ray with temperatures reaching tens of millions of Kelvins, and forms an integral part of the cluster environment (Kravtsov & Borgani 2012; Lima Neto et al. 2014). This environment plays a fundamental role in the evolution of cluster galaxies. It can drive morphological evolution, as well as significantly affecting a galaxy's star-formation history. For example, clusters are

generally dominated by early-type galaxies. In particular, the core of clusters where the density is the highest hosts the most massive ellipticals and S0s with little to no ongoing star-formation, while more disky star-forming spirals are found with increasing clustercentric distance. Furthermore, the rate of star-formation is found to be much higher in isolated field galaxies compared to their cluster counterparts. It is believed that the cluster environment quenches star-formation within members and transforms disky, blue spirals into 'red and dead' ellipticals and S0s (Butcher & Oemler 1978a,b; Dressler 1980a,b; Dressler 1984; Dressler et al. 1997). This can happen through multiple processes, such as ram pressure stripping of the cold gas within galaxies by the ICM (Gunn & Gott 1972; Abadi et al. 1999), 'harassment' - galaxy-galaxy interactions in which the tidal gravitational force can rip apart the arms of spiral galaxies (Gallagher & Ostriker 1972; Moore et al. 1996), or via 'strangulation' - the removal of fresh gas from the galactic halo by the ICM or the cluster potential (Larson et al. 1980; Mamon 1987; McCarthy et al. 2008). All of these processes work to halt the formation of new stars within cluster galaxies and cause the stellar population within them to dim and redden with age (Taranu et al. 2014).

Given that the environment plays a vital role in the transformation and evolution of cluster ETGs in which the UV upturn is primarily observed, an important question to investigate is the the effect of the cluster environment on the upturn itself. The Helium sedimentation model of the UV upturn by Peng & Nagai (2009) predicted three key environmental dependencies of the upturn in the BCGs of clusters:

1. The upturn should correlate with the mass of the cluster.
2. The upturn should be stronger in clusters with cooling flows.
3. The upturn should be stronger in dynamically relaxed clusters.

All three of these predictions were proven to not hold true in observations of a sample of 36 nearby BCGs by Loubser & Sánchez-Blázquez (2011) and in another sample of REXCESS BCGs between $z = 0.06 - 0.18$ by Donahue et al. (2010), who found no correlation between the X-ray temperature/velocity dispersion of clusters (which act as proxies of the cluster mass) and the $FUV - NUV$ colour (a measure of the upturn strength) of their BCGs. Clusters with or without cooling flows also showed a similar range in upturns in their BCGs. Finally, they found no correlation between the offset of the X-ray peak of the cluster and its BCG, where a smaller offset indicates a more dynamically relaxed system. A similar study by Boissier et al. (2018) on a sample of BCGs behind the Virgo cluster up to $z = 0.35$ showed no dependence of the $FUV - NUV$ colour on cluster properties, such as the number of members, etc. Yi et al.

(2011) also found no evidence of cluster environment affecting the strength of the upturn in a sample of SDSS-selected BCGs.

Besides BCGs, given that the general early-type population of galaxies across multiple clusters (Virgo - Boselli et al. 2005; Coma - Smith et al. 2012, Chapter 2; Perseus and Fornax - Chapter 2) show similar UV-optical colours across a range of luminosities, this would indicate that the upturn in all early-type cluster galaxies, not just BCGs, is an intrinsic feature of those galaxies and unrelated to the cluster environment.

In this chapter the dependence of the UV upturn in the general early-type population (not just BCGs) on the cluster environment is investigated. To do this, a sample of 20 2dF clusters of various sizes (ranked by cluster members) between $0 \leq z \leq 0.1$ is used and the strength of the upturn (as given by their UV-optical colours) in red sequence members is checked against various cluster properties to account for any correlations. The results are then compared to those of Coma and Perseus to both demonstrate the ubiquity of the upturn in all low redshift cluster galaxies, and any potential dependence of the phenomenon on cluster environment.

3.2 Data

For this study, the following 20 clusters from the 2dF Galaxy Redshift Survey (De Propris 2017) were used: Abell 930, Abell 954, Abell 957, Abell 1139, Abell 1189, Abell 1238, Abell 1364, Abell 1620, Abell 1663, Abell 1692, Abell 1750, Abell 2660, Abell 2734, Abell 3094, Abell 3880, Abell 4053, Abell S0003, Abell S1043 and EDCC119. These clusters have a wide range of properties (velocity dispersions, X-ray luminosities and Bautz-Morgan types), details of which are given in Table 3.1. They also have highly complete redshift coverage ($> 80\%$) for all galaxies to at least ~ 2 magnitudes below the L^* point. To determine cluster membership, the galaxies with velocities (cz) ± 1500 kms^{-1} of the cluster recessional velocity were chosen to be members. For all galaxies this value corresponded to approximately 1-3σ. In a plot of cz vs. r-band magnitude, the cluster members generally grouped together uniformly and were easily distinguishable from non-cluster members.

Optical data for each galaxy was either obtained from SDSS (Alam et al. 2015) or the Supercosmos photometry of the UKST plates. From SDSS, g and r band Model magnitudes were extracted from the database, and from UKST the B_J and R_F magnitudes were obtained from the WFAU SSA service. To determine the red sequence, plots of either SDSS $g - r$ vs. r or

Cluster	RA/°	DEC/°	$\mathrm{cz/kms^{-1}}$	$\sigma/\mathrm{kms^{-1}}$	$L_X/10^{44}\,\mathrm{erg\,s^{-1}}$	Bautz-Morgan
Abell 930	151.693	-6.188	17293	1033	0.061	3
Abell 954	153.437	-0.12	28312	830	-	2
Abell 957	153.41	-0.925	13499	718	0.638	1.5
Abell 1139	164.824	1.154	11711	463	0.256	3
Abell 1189	167.55	1.224	28780	786	0.155	3
Abell 1238	170.726	1.114	22145	573	0.309	3
Abell 1364	176.119	-1.835	32058	469	0.071	3
Abell 1620	192.516	-1.54	25644	1042	0.036	3
Abell 1663	195.878	-2.233	24921	751	0.99	2
Abell 1692	197.903	-0.483	22526	1073	0.561	2.5
Abell 1750	202.796	-1.727	25484	1051	3.189	2.5
Abell 2660	356.856	-25.199	15919	719	0.054	1.5
Abell 2734	2.84	-28.854	18318	914	2.416	3
Abell 3094	47.854	-26.931	20355	804	0.578	3
Abell 3880	336.977	-30.576	17322	733	1.453	2
Abell 4053	358.185	-28.571	20195	1656	-	3
Abell S0003	0.796	-27.878	18984	939	-	1
AbellS0084	12.345	-29.52	32866	905	2.562	1
Abell S1043	338.411	-24.764	11143	1449	-	1
EDCC119	334.086	-25.67	25400	1015	-	-

Table 3.1: Key parameters of the 20 2dF galaxy clusters used in this study as given in De Propris (2017). The X-ray luminosities (L_X) are from the ROSAT band, taken from the BAX catalogue (Sadat et al. 2004).

UKST $B_J - R_F$ vs. R_J were made. The selected red sequences have a tight optical spread in colour of ~ 0.2 magnitudes. The optical red sequence selection for each cluster can be seen in Figs. 3.1-3.4.

For all the red sequence cluster members, a search was made on the GALEX (Morrissey et al. 2007; Martin et al. 2005) MAST database to obtain wherever possible the GALEX FUV and NUV MAG_AUTO (Kron 1980) magnitudes. I find FUV and NUV magnitudes for at least a subset of the members in each cluster, but it is important to note that some of the clusters in this study only have 20-30 confirmed members, and as such have little available UV data. In total, there were 198 red sequence galaxies with available FUV data and 382 galaxies with NUV data across the entire sample of clusters. Extinction corrections to both the UV and optical data were made using Schlafly & Finkbeiner (2011).

3.2.1 k-corrections

Due to most of the clusters in my sample being at $z > 0.05$, a k-correction to the photometry was necessary for the UV data, while for the optical colours its effect was negligible. No evolutionary corrections were required for such a small redshift range.

Proper k-correction of both the FUV and NUV data requires a priori knowledge of the spectra of upturn galaxies and crucial model-dependent corrections. Given that upturn galaxies by their nature have a range of different slopes in the UV part of their spectra depending on the strength of the upturn, it can be difficult to find a correct model for each individual galaxy. However, in chapter 2, it was found that C09+blackbody models of various temperatures fit the SEDs of upturn galaxies in the Coma cluster remarkably well, and that there was a temperature range between 10,000-22,000K in the fitted blackbodies, which model the hot HB sub-populations that give rise to the upturn.

Assuming that the models fitted to the Coma galaxies are applicable to all low redshift cluster galaxies, for a C09+BB with $T = 16,000K$ (approximately the median of the Coma sample) the largest k-correction at $z = 0.1$ in FUV and NUV are ~ 0.2 and ~ 0.3 magnitudes respectively. Increasing or decreasing the temperature to the maximum and minimum of 22,000K and 10,000K respectively brings about a change of $\sim \pm 0.15$ magnitudes, which is added to the uncertainty of the plotted results. Regardless, the k-correction is relatively small in the UV bands at $0 < z < 0.1$.

3.3 Results

To analyse the strength of the upturn, the $FUV - r$ and $NUV - r$ colours for all 2dF red sequence cluster galaxies in the sample are plotted against their absolute r-band magnitudes in Fig. 3.5. The $FUV - r$ colours mostly range between $5.5 - 7.5$ mags. This observed ~ 2 magnitude range in colour is similar to that of Coma and Perseus (from Chapter 2), as well as Virgo red sequence galaxies (Boselli et al. 2005). The $NUV - r$ varies between $5.0 - 6.5$ mags and once again, the ~ 1.5 magnitude range seen in this colour is typical of the aforementioned low redshift cluster galaxies. This consistent range in $FUV - r/NUV - r$ observed between all low redshift cluster galaxies indicates that the upturn is a universal feature among all such old, passively evolving systems and also that the environment must not have any significant influence on this phenomenon, since the clusters studied here have a wide variety of properties as seen in Table 3.1.

The following plots further explore the effect of the environment on the upturn:

- $FUV - r$ & $NUV - r$ vs. σ: Fig. 3.6 is a plot of the upturn strength against the velocity dispersion of each cluster. As can be seen in the case of both $FUV - r$ and $NUV - r$, there is no correlation with σ.
- $FUV - r$ & $NUV - r$ vs. L_X: Similarly, Fig. 3.7 shows a plot of the upturn strength against the X-ray luminosity of each cluster from ROSAT (Truemper 1993) taken from the BAX catalogue[1] (Sadat et al. 2004). Once again, there is no correlation between $FUV - r/NUV - r$ and L_X.
- $FUV - r$ & $NUV - r$ vs. r/r_{200}: In Fig. 3.8, r is the physical distance in Mpc between each galaxy and the core of the cluster (taken to be the BCG) as given by the RA and DECs in Table 3.1. r_{200} is defined as the radius at which the mean density of the cluster is 200 times that of the critical density of the universe and is related to the velocity dispersion, σ and Hubble's Constant, H_0 through the following equation (Carlberg et al. 1997):

$$r_{200} = \frac{1.732 \times \sigma}{10 \times H_0}$$

The r/r_{200} for each galaxy is thus scaled to the size of its host cluster, so that it may be directly compared between galaxies from different clusters. Plots of $FUV - r$ and $NUV - r$ against r/r_{200} allow us to determine whether the strength of the upturn varies with cluster-centric distance. There is no correlation between these parameters as seen in Fig. 3.8 and

[1] http://bax.ast.obs-mip.fr/

there is a similar scatter in the UV-optical colours with increasing distance from the centre of the cluster. It should however be noted that as mentioned in section 3.2.1, the same k-correction is applied uniformly to the UV-optical colours of all galaxies at a given redshift. In reality, the k-correction in the UV bands from galaxy to galaxy will vary slightly at a given redshift due to the inherent stochasticity of the UV upturn, which is difficult to replicate without a detailed study of the UV spectra of these galaxies. As such, while the k-corrections applied here are reasonable estimates, they may also introduce a small but noticeable offset to the UV-optical colours of some galaxies. The spread in the colours should however be largely unaffected.

- $FUV - r$ & $NUV - r$ vs. $\Delta v/\sigma$: In Fig. 3.9, Δv is the difference between the velocity of each galaxy within a cluster and the cluster recessional velocity. Δv is divided by the velocity dispersion to account for the different velocity spreads between clusters and scale for cluster properties. As can be seen from the plots, there is once again no correlation between the upturn strength and the velocities of galaxies in clusters.
- $\Delta v/\sigma$ vs r/r_{200} vs. $FUV - r$ and $NUV - r$ (colour-coded): Fig. 3.10 shows caustic plots of the line-of-sight velocity against the cluster-centric distance (Diaferio et al. 2005; Serra & Diaferio 2013), with a colourmap of $FUV - r$ and $NUV - r$. This is done for all of the 2dF cluster galaxies (top left and right), as well as Coma and Perseus (bottom left and right). Caustic plots are generally used as a more robust method of determining cluster membership than using just velocities, and given that all of the galaxies in my sample have both $\Delta v/\sigma$ and r/r_{200} of < 3, they are highly likely to be cluster members. From the colourmap of $FUV - r$ and $NUV - r$, we see a mostly random distribution of colours with both line-of-sight velocities and cluster-centric distances.

3.4 Discussion

From the analysis of red sequence galaxies from a sample of 20 clusters from the 2dF galaxy redshift survey, the $FUV - r$ and $NUV - r$ colours showed approximately ranges of 5.5-7.5 and 5.0-6.5 respectively, consistent with the colours observed in other low redshift clusters such as Coma, Perseus and Virgo. As with those clusters, the results obtained here can be interpreted with the presence of a He-enhanced sub-population of hot HB stars giving rise to the upturn, superimposed on top of the majority 'red and dead' population that makes up ETGs. The range

in colours can then be explained by varying amounts of He-enhancement. Using the YEPS Stellar Population Synthesis models of Chung et al. (2017) that incorporate He-enhancement, a $Y \geqslant 0.38$ was necessary to explain the entire range in UV-optical colours seen in Coma cluster galaxies (chapter 2). Given that with the 2dF clusters only a slightly higher redshift range is being probed (up to $z \approx 0.1$) compared to Coma, a $Y \geqslant 0.39$ is predicted by the YEPS models (assuming Z=$Z_{\odot}$ and $z_f = 4$ as in chapter 2) to account for the full range in $FUV - r$ and $NUV - r$ colours seen in all of these clusters below $z = 0.1$. The derivation of the Y values from the YEPS models will be discussed in further detail in the upcoming chapters. For now, the focus will be on the effect of the cluster environment on the strength of the upturn.

Under dynamical equilibrium the velocity dispersion (e.g. Munari et al. 2013; Saro et al. 2013) and X-ray luminosity (e.g, Kravtsov et al. 2006; Stanek et al. 2010) of a cluster directly correlate with its mass. Figs. 3.6 and 3.7 demonstrate that the upturn strength has no correlation with either velocity dispersion or X-ray luminosity, and by proxy the mass of the cluster. As such, clusters of all sizes can have a component of upturn in their early-type population.

Within galaxy clusters, star-formation is quenched very strongly in the centre due to processes such as ram-pressure stripping, harassment and strangulation (as discussed in the introduction). The rate of star-formation in cluster galaxies thus tends to increase with increasing cluster-centric distance (Dressler et al. 1997 et seq.). If star-formation was the driving mechanism behind the UV emission in the galaxies in my sample, one would expect to see the $FUV-r$ and $NUV - r$ colours to become bluer with increasing r/r_{200}. However as seen in Fig. 3.8, the UV-optical colours show no correlation with cluster-centric distance. This reinforces the idea that the UV emission in these galaxies is indeed from an old, hot HB subpopulation and not from any residual star-formation. Similarly, there appears to be no correlation between the line-of-sight velocity of galaxies and the upturn strength, in Fig. 3.9. Therefore, the influence of the cluster's gravitational potential - the main driving force behind the velocities - does not affect the strength of the upturn. We can see from Fig. 3.10 that the majority of cluster members are centred around the core of the cluster ($r/r_{200} < 1$; $\Delta v/\sigma < 2$), yet these central galaxies show the full range of $FUV - r$ and $NUV - r$ colours as seen from the the entire population of galaxies. This suggests that there is no gradient in colour with either cluster-centric distance or line-of-sight velocity.

These results are in line with a He-enhanced HB origin for the UV upturn, in which case the cluster environment should have no effect on the emergence and prevalence of the upturn.

In a hierarchical model of structure formation, galaxies form first at $z \sim 2-6$ and the star-formation in ETGs rapidly comes to an end by $z \sim 2$ (Jørgensen et al. 2017). Galaxies then accrete in highly over-dense regions of the universe to form clusters at $z \lesssim 1.5$ (e.g. Wen & Han 2011). Studies have shown that cluster red sequences are already established between $z \sim 1-2$ (Newman et al. 2014). This indicates that the majority of star-formation in ETGs was completed and a mostly passively evolving stellar population, that is observed at present, was already established before these galaxies became part of clusters, or shortly thereafter. This is particularly important as the oldest stars in ETGs, ones that formed at $z \sim 4$ (before the galaxies became part of clusters) are the ones that would have the necessary time required to evolve from the main sequence on to the red giant branch, and then eventually to the horizontal branch, where they become UV-bright given sufficient He-enhancement. Since the cluster environment particularly works to quench the star-formation within galaxies, the main sequence population in ETGs, which is already red and passively evolving, is largely unaffected. Hence, the upturn develops intrinsically within these galaxies irrespective of the cluster environment, as seen in the analysis presented in this chapter. This also indicates that the large He-enhancement that leads to the eventual UV upturn in a sub-population of the main sequence in ETGs must also occur intrinsically within the galaxies and at a very early redshift ($z \sim 4$), when the galaxies first form.

The final test to prove that the upturn is an intrinsic feature in all ETGs would be to look at a large sample of non-star-forming early-type field galaxies and analyse their UV output. If these galaxies also show an upturn component despite having no visible traces of star-formation within their spectra, that would prove that this phenomenon does indeed develop within all red and dead galaxies given enough time for their stellar population to become old enough to start evolving on to the HB.

3.5 Conclusions

By analysing the GALEX UV-optical colours of a large sample of red sequence galaxies from 20 clusters in the 2dF Galaxy Redshift Survey at $z \lesssim 0.1$, the strength and prevalence of the upturn was found to be consistent with ETGs from other low redshift clusters, such as Coma and Perseus. Since the sample of clusters had a wide range of properties, the effect of the cluster environment on the upturn could be tested. To do so the velocity dispersions and X-ray luminosities of all clusters, as well as the clustercentric distances and line-of-sight velocities of

all galaxies in the sample were plotted against the $FUV - r$ and $NUV - r$ colours. In each case, the results were also compared to those of Coma and Perseus and found to be roughly identical to those of the 2dF clusters. No correlation was found between the upturn strength and any of the aforementioned parameters, all of which are directly related to the cluster environment. Therefore, the conclusion is that the UV upturn phenomenon is an intrinsic feature of ETGs, irrespective of their cluster environment.

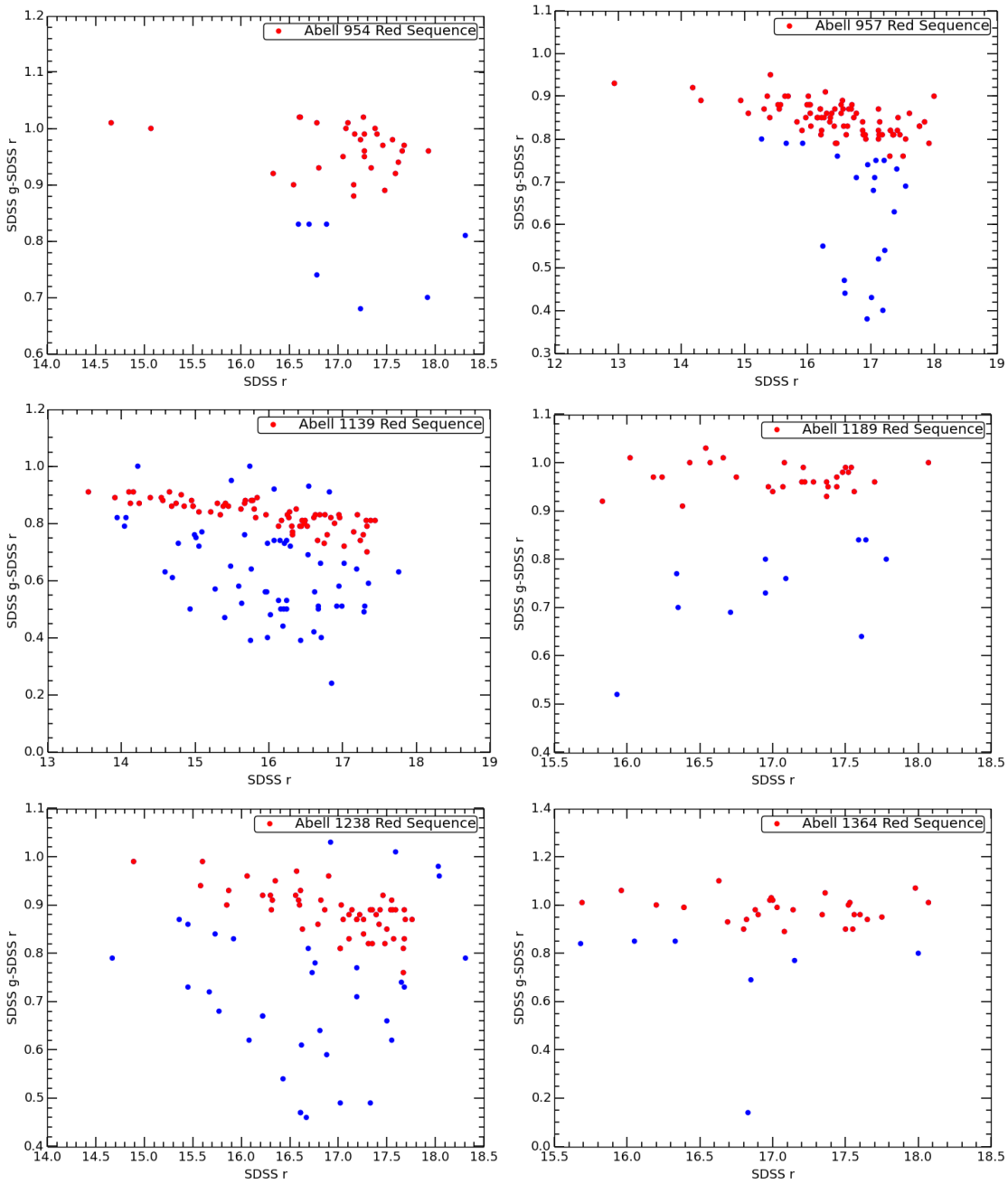

Figure 3.1: Optical colour magnitude diagrams ($g - r$ vs, r) for Abell 954, Abell 957, Abell 1139, Abell 1189, Abell 1238 and Abell 1364. The red sequence is denoted by filled red circles. Photometric uncertainty in colour is < 0.05 magnitudes.

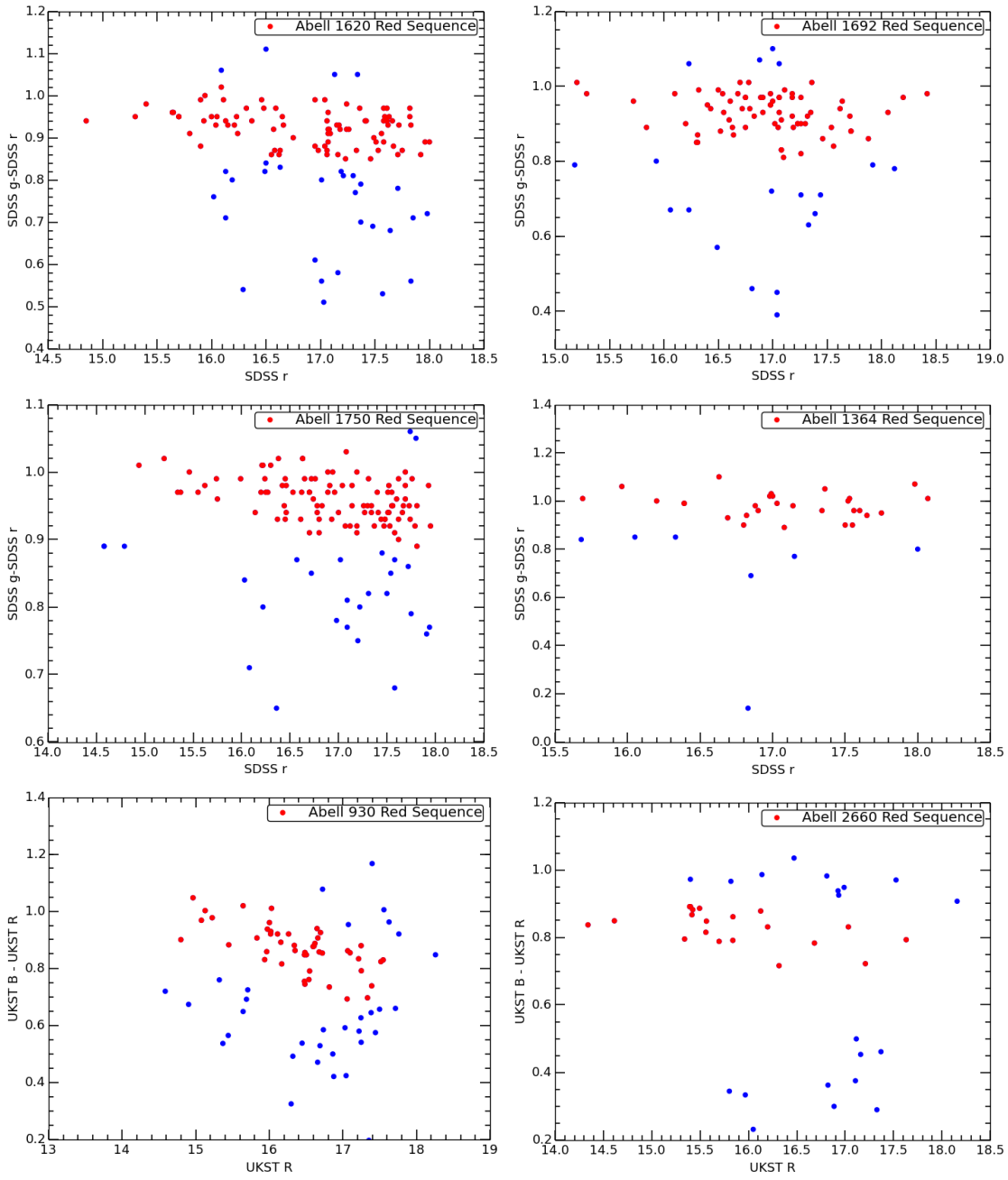

Figure 3.2: Optical colour magnitude diagrams ($g - r$ or $B - R$ vs. r) for Abell 1620, Abell 1692, Abell 1750, Abell 1364 and Abell 930 and Abell 2660. The red sequence is denoted by filled red circles. Photometric uncertainty in colour is < 0.05 magnitudes.

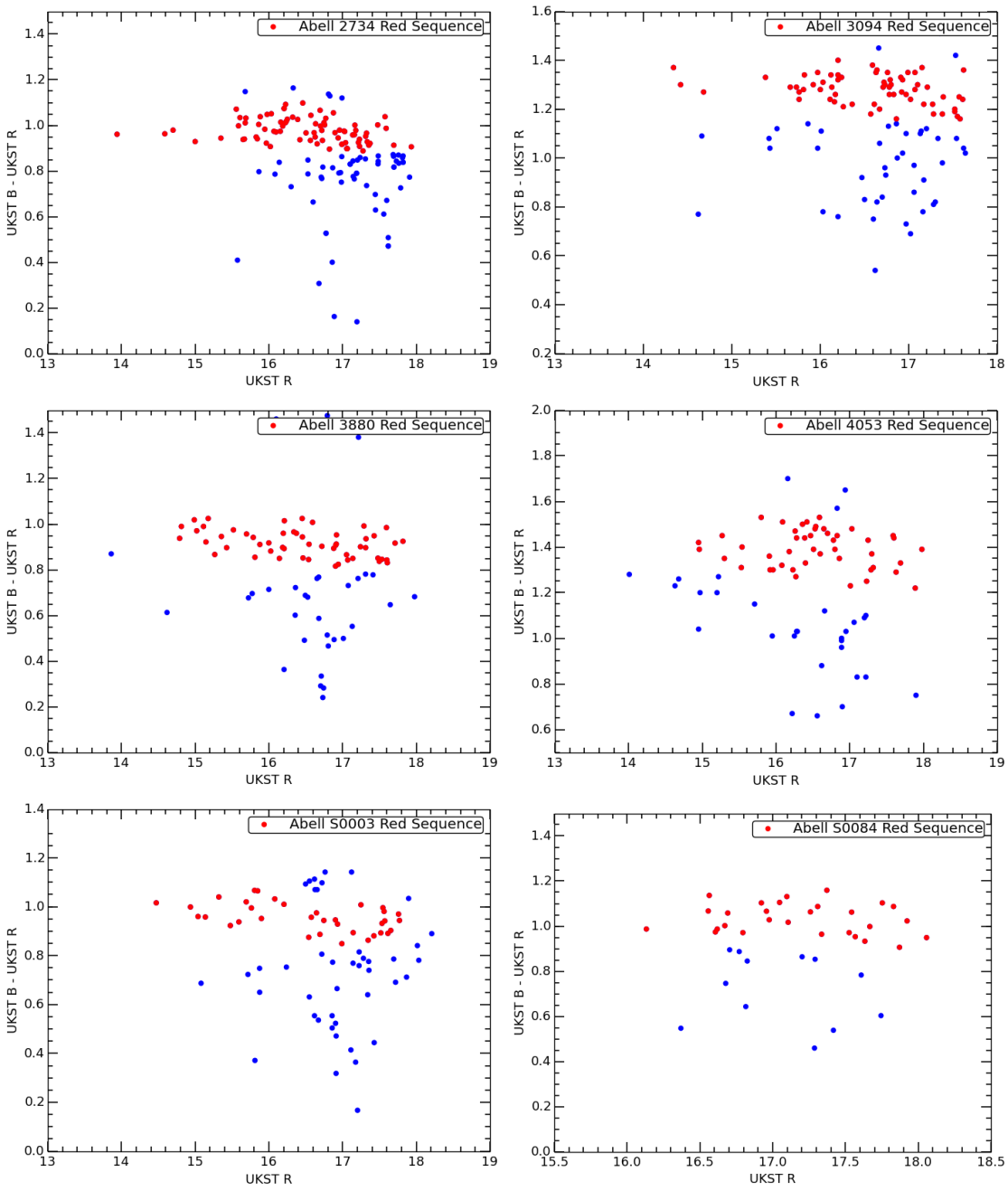

Figure 3.3: Optical colour magnitude diagrams ($B - R$ vs. R) for Abell 2734, Abell 3094, Abell 3880, Abell 4053, Abell S0003 and Abell S0084. The red sequence is denoted by filled red circles. Photometric uncertainty in colour is < 0.05 magnitudes.

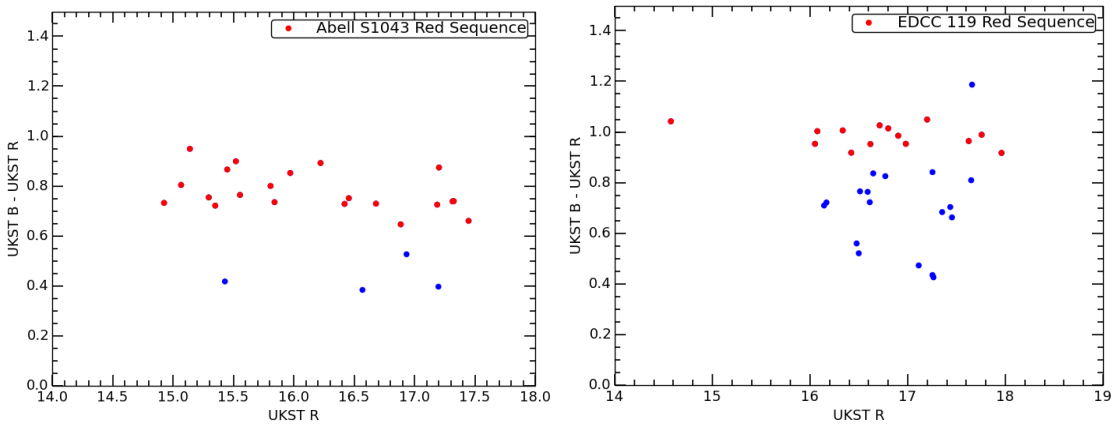

Figure 3.4: Optical colour magnitude diagrams ($B - R$ vs. R) for Abell S1043 and EDCC119. The red sequence is denoted by filled red circles. Photometric uncertainty in colour is < 0.05 magnitudes.

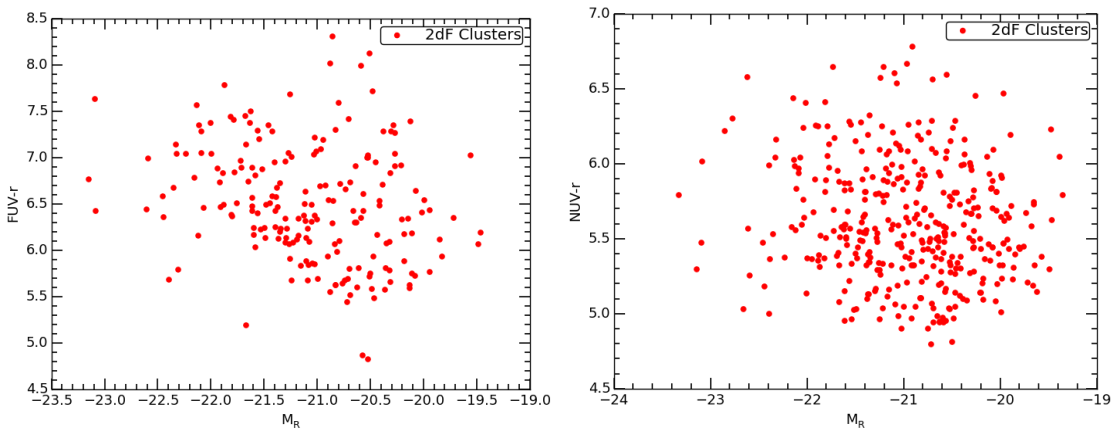

Figure 3.5: GALEX $FUV - r$ (left) and $NUV - r$ (right) vs. M_R for all 2dF red sequence cluster galaxies in the sample. Photometric uncertainty in colour is $\lesssim 0.2$ magnitudes. As can be seen in the plots, the scatter in the colours (> 1 mag) is much larger than the errors $\lesssim 0.2$.

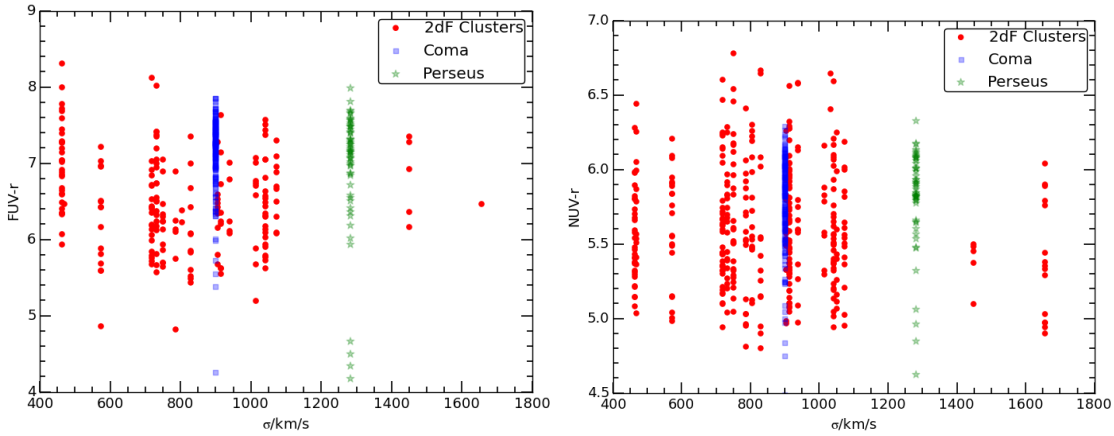

Figure 3.6: GALEX $FUV - r$ (left) and $NUV - r$ (right) vs. σ (of clusters) for all 2dF red sequence cluster galaxies in the sample. Also plotted are Coma and Perseus for comparison, the velocity dispersions for which were taken from Danese et al. (1980). Photometric uncertainty in colour is $\lesssim 0.2$ magnitudes.

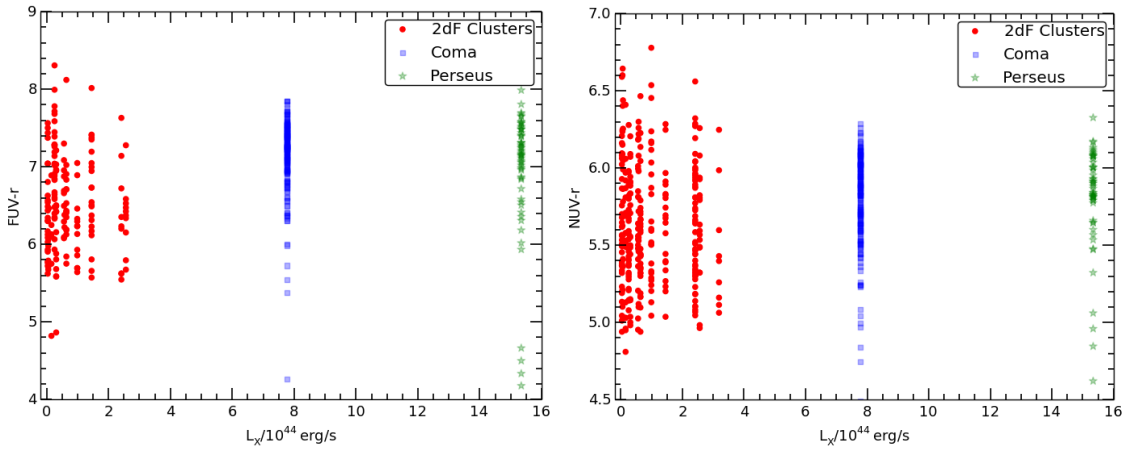

Figure 3.7: GALEX $FUV - r$ (left) and $NUV - r$ (right) vs. X-ray Luminosity (of clusters) for all 2dF red sequence cluster galaxies in the sample. Also plotted are Coma and Perseus for comparison, the L_X for which are from ROSAT and taken from the BAX catalogue. Photometric uncertainty in colour is $\lesssim 0.2$ magnitudes.

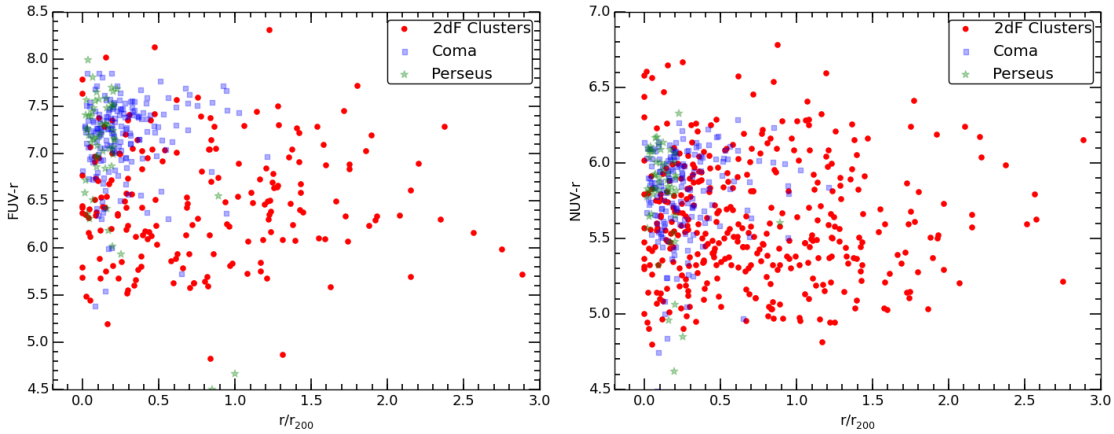

Figure 3.8: GALEX $FUV - r$ (left) and $NUV - r$ (right) vs. r/r_{200} for all 2dF red sequence cluster galaxies in the sample. Also plotted are the Coma and Perseus red sequences for comparison. Photometric uncertainty in colour is $\lesssim 0.2$ magnitudes.

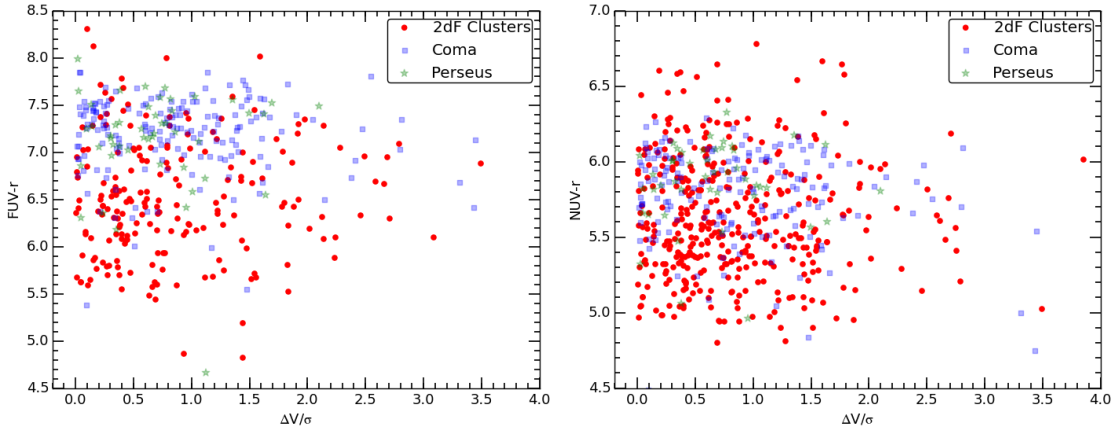

Figure 3.9: GALEX $FUV - r$ (left) and $NUV - r$ (right) vs. $\Delta v/\sigma$ for all 2dF red sequence cluster galaxies in the sample. Also plotted are the Coma and Perseus red sequences for comparison. Photometric uncertainty in colour is $\lesssim 0.2$ magnitudes.

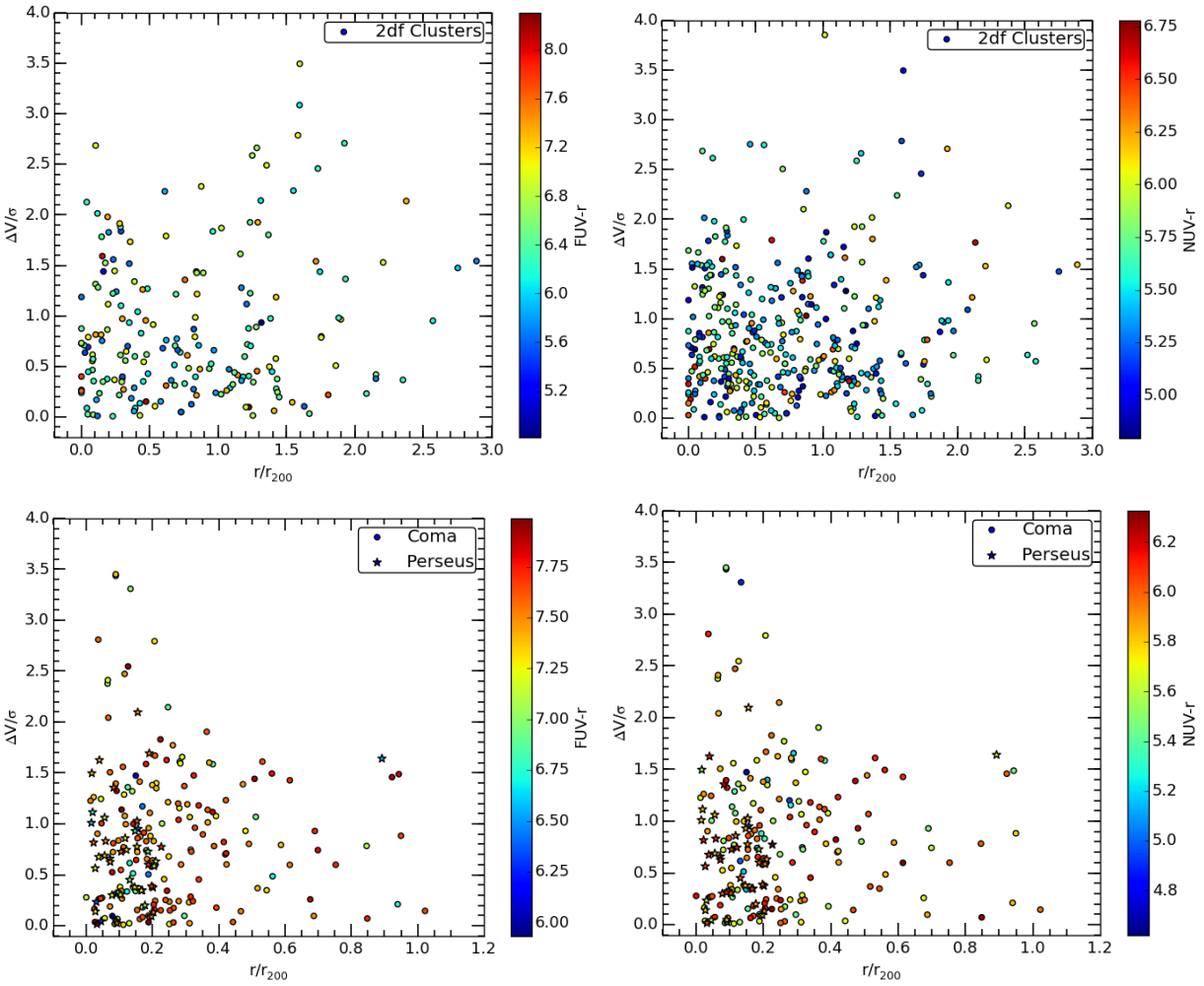

Figure 3.10: Caustic plot of r/r_{200} vs. $\Delta v/\sigma$ with GALEX $FUV - r$ (top left) and $NUV - r$ (top right) encoded in colour for all 2dF red sequence cluster galaxies in the sample. The same plots are shown for Coma and Perseus galaxies on the bottom left and bottom right panels for comparison. Photometric uncertainty in colour is $\lesssim 0.2$ magnitudes.

4

The UV Upturn in Abell 1689 at $z = 0.18$

Most studies of the UV upturn at higher redshifts have focused on characterising the phenomenon in the brightest cluster galaxies (BCG); however there have only been a handful of cluster-wide surveys of the upturn in galaxies with a wide range of luminosities in the local Universe, e.g. Coma and Virgo. It is important to extend the analysis of the upturn to standard ETGs (not just BCGs) at higher redshifts, as studies have shown that these galaxies may have had a different formation channel from BCGs and hence may host different stellar populations.

In this chapter, the strength of the upturn will be analysed in the Abell 1689 cluster of galaxies at $z \sim 0.18$ (corresponding to a lookback time of 2.2 Gyrs) down to L^* and beyond. The results are then compared to those of Coma in order to investigate whether the upturn has evolved significantly in the general ETG population over this redshift range.

This chapter has been published in and is largely reproduced from Ali et al. (2018b).

4.1 Introduction

The evolution of the UV upturn with redshift has been a key area of research ever since the discovery of the phenomenon, as it can help constrain the various proposed models of the upturn.

However, due to limitations in detector sensitivities and the overall faintness of ETGs in the UV compared to optical wavebands, only the BCGs and very luminous ETGs have been observed in the UV at higher redshifts.

BCGs are found at the centre of galaxy clusters, generally at the peak of the cluster X-ray emission (Jones & Forman 1984), and as their name suggests, are the most luminous and massive galaxies in the cluster. They appear similar to elliptical galaxies, with a mostly quiescent stellar population. In some instances, BCGs may also have an extended halo of stars, in which case they are referred to as cD galaxies (e.g Tonry 1987; Jordán et al. 2004). Due to their unconventionally large size, BCGs are hypothesised to have had a different formation history compared to standard cluster elliptical galaxies. Among the different formation channels, the one that is most consistent with observations seems to be *galactic cannibalism* (Searle et al. 1973; Tovmassian & Andernach 2012). In this scenario, cD galaxies formed at early times through the *heirarchical merging* of galaxies that fell into the cluster core along primordial filaments (e.g. Dubinski 1998; Torlina et al. 2007). Mergers of red galaxies have been observed at low redshift (van Dokkum 2005), which has led to the hypothesis that cD galaxies have increased 3-4 times in stellar mass at $z \leqslant 1$ through mostly dry mergers (i.e. do not trigger strong star-formation) between quiescent, red and dead galaxies (e.g. Aragon-Salamanca et al. 1998), leading to the massive galaxies observed today.

Compared to this, standard ellipticals can form through two main channels. Firstly, they are thought to have formed from the *monolithic collapse* of an initial gas cloud at very high redshifts ($z \gtrsim 5$), leading to a short period of intense star-formation, followed by passive evolution since (Larson 1975; Bower et al. 1999; De Lucia et al. 2006). This hypothesis strongly supports the existence of a tight red sequence in clusters at high redshifts ($z \sim 2$, e.g. Newman et al. 2014), as well as the fundamental plane relationship, and their evolution with redshift (Kodama et al. 1998). Secondly, both simulations and observations suggest that ellipticals can also from the minor mergers of two galaxies (Farouki & Shapiro 1982; Negroponte & White 1983).

Due to the likely different formation channels between BCGs and standard ETGs, it is possible that there exist some differences in their overall stellar populations despite having similar optically red colours. Thus the evolution of the upturn should be explored in both BCGs and standard ETGs at higher redshift as the onset and strength of the upturn may be different in each case.

Beyond the local Universe but still in the low redshift regime ($z \sim 0.1 - 0.5$), most previous

work has concentrated on BCGs and very bright ETGs in clusters because of limitations in telescope aperture or detector sensitivity. Brown et al. (1998a, 2003) studied the evolution of the upturn in a handful of the most luminous cluster ETGs at $z = 0.375$ and $z = 0.33$. Interestingly, in the first case ($z = 0.375$) they found that the $FUV - V$ colour remained roughly consistent with similar $z = 0$ galaxies. However, in the subsequent study ($z = 0.33$) they found that the $FUV - V$ colour appeared redder compared to local galaxies. The different results for cluster galaxies at roughly the same epoch may be due to the stochastic nature of the upturn, but Brown et al. suggest that it may also be due to a systematic offset in their earlier study in which a solar blind camera was not used during the imaging of the cluster. However, it is difficult to pinpoint the cause given the very small sample sizes of a few galaxies in each case. Ree et al. (2007) also performed a similar study on BCGs at $z < 0.2$ and found a fading of the upturn with redshift. Conversely, Donahue et al. (2010) used a sample of REXCESS BCGs between $z = 0.06 - 0.18$ to show that the upturn remains consistent in their sample after taking into account the general scatter observed in the $FUV - optical$ colour of upturn sources. More recently Boissier et al. (2018) recovered similar results of a consistent upturn strength in a sample of several tens of BCGs out to $z \sim 0.35$ behind the Virgo cluster.

Of the various models of the upturn, the metal-poor hypothesis is the most easily testable as the upturn in this case is expected to disappear completely beyond low redshift (by $z \sim 0.25$) due to the requirement of large ages for metal-poor stars to become UV bright (Park & Lee 1997). The presence of a significant fraction of low metallicity stars in massive ETGs is already excluded by the observation of their strong metal lines, which imply that the dominant population is solar or super-solar in abundance. Furthermore, the observations in chapter 2 show that the contribution of the upturn population spectral energy distribution, if parameterised as a black body, is more prominent and hotter in the more massive and more metal rich galaxies. This is contrary to what one would expect in a low-metallicity scenario. A low metallicity model would imply that a blue HB population should only appear at the lowest redshifts, and certainly be missing in observations of even moderate-redshift galaxies, contrary to previous work which detected upturns in the most massive galaxies over the past ~ 5 Gyrs, e.g. in the work of Brown et al. (1998a, 2000a, 2003).

In chapters 2 and 3, I explored the strength of upturn in the red sequence galaxy populations of local clusters, including Coma. In this and the next chapter, I will explore the evolution of the upturn in cluster red sequence galaxies over a range of higher redshifts and for a range of

Filter	Proposal ID	PI	Total exp. time/s
ACS F475W	9289	Ford	9500
ACS F625W	9289	Ford	9500
WFC3 F225W	12931	Siana	27710
WFC3 F275W	12201	Siana	73360
WFC3 F336W	12931	Siana	33075

Table 4.1: Table giving details of the images extracted from HLA for each of the HST filters. Further information regarding the ACS and WFC3 images can be found in Mieske et al. (2004) and Alavi et al. (2016) respectively.

luminosities, not just BCGs. Here the focus will be on the galaxy population of Abell 1689 at $z = 0.18$, one of the richest and most massive clusters known (Bautz-Morgan type II-III), well studied for its strong gravitational lensing of background galaxies (e.g. Halkola et al. 2006), as well as for hosting the largest globular cluster population (upwards of 160,000) discovered thus far within a cluster (Alamo-Martínez et al. 2013). At the initiation of this project, it was the only cluster at $z \sim 0.2$ with suitable archival HST ACS and WFC3 imaging data in the required bands and of sufficient depth to reach below the L^* point in the luminosity function. This allows for the spread in the upturn strength of galaxies in Abell 1689 to be directly compared to those in local clusters (chapter 2) down to L^* and beyond. Otherwise, we can take this cluster as a typical exemplar of massive clusters at this redshift. This study will also allow for the metal-poor hypothesis to be tested for the general early-type population, given that if metal-poor stars are the source of the upturn in these galaxies, the upturn should already show strong fading at the redshift being surveyed.

4.2 Data & Photometry

For Abell 1689, suitable optical and UV imaging data was available from the HST archive. The optical data consists of images taken with the Hubble Space Telescope (HST)'s Advanced Camera for Surveys (ACS) through the F475W and F625W filters of the WFC channel, corresponding approximately to the rest-frame B and V filters at this redshift. The ACS has a field of view of $202'' \times 202''$ for the WFC channel and a pixel scale of $0.05''/pixel$[1]. Archived images in both filters were extracted from the Hubble Legacy Archive (HLA). The program IDs and PI identifications are reported in Table 4.1, together with exposure times and other relevant

[1] See Avila (2017) for details of the ACS.

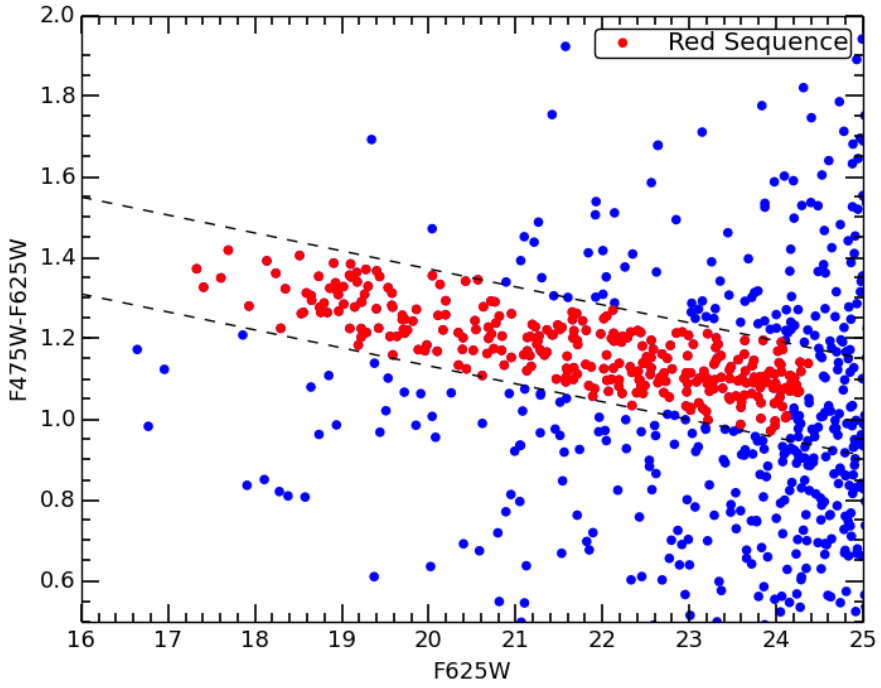

Figure 4.1: Optical $F475W - F625W$ vs. $F625W$ colour-magnitude diagram. The red sequence galaxies are denoted by red filled circles and have photometric uncertainty of < 0.05 magnitudes in their optical colour.

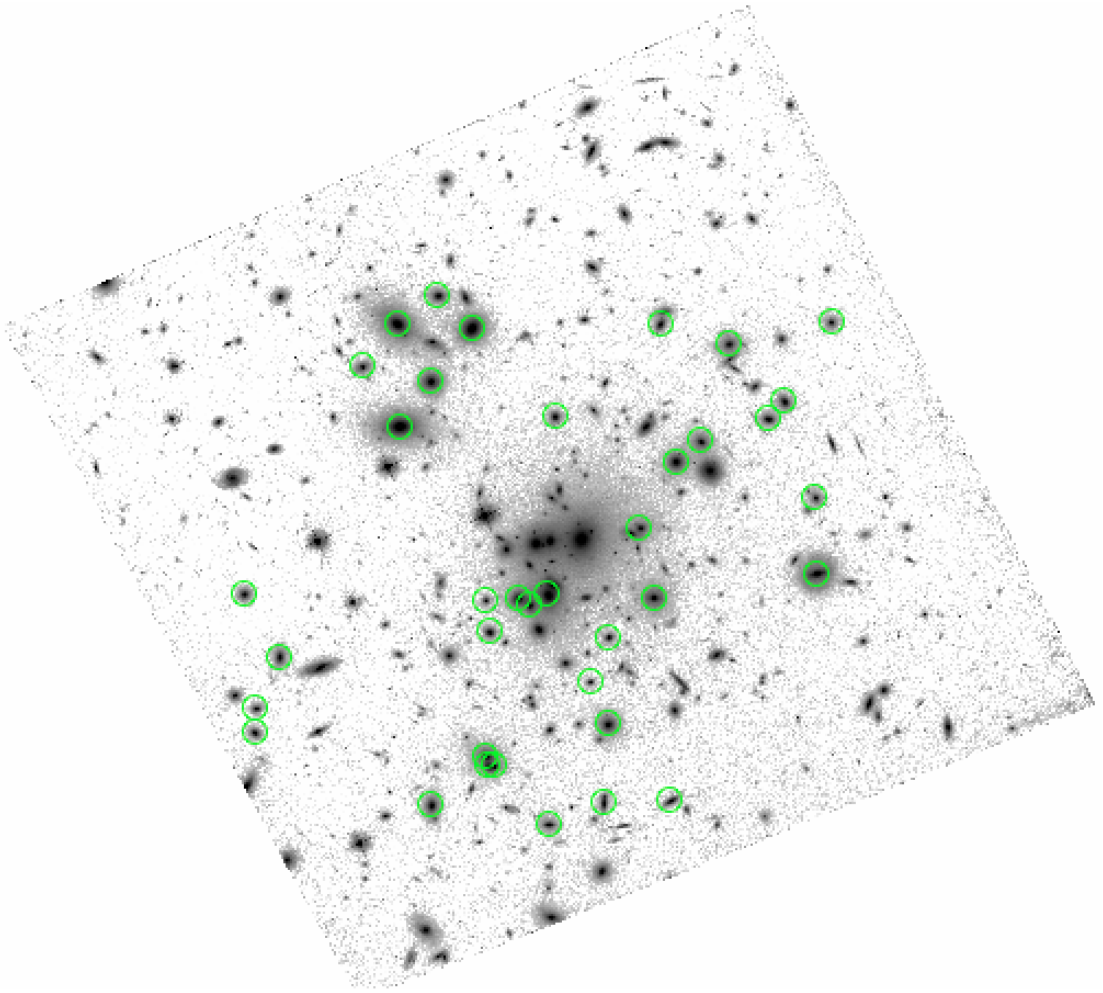

Figure 4.2: F625W image of Abell 1689 as an illustration. Highlighted are the red sequence galaxies detected in all UV and optical bands and plotted in Fig. 4.4 (top).

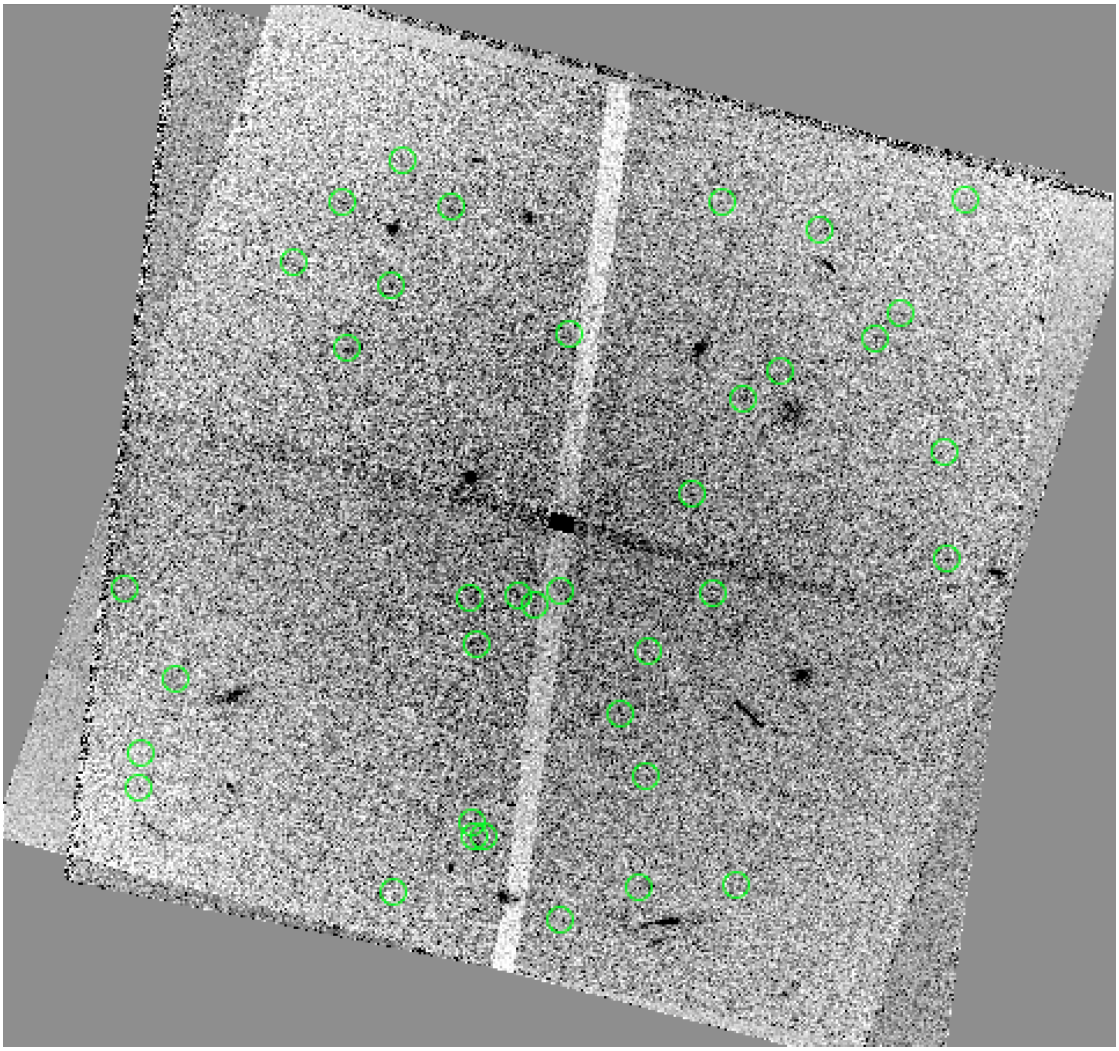

Figure 4.3: F225W image of Abell 1689 as an illustration. Highlighted are the red sequence galaxies detected in all UV and optical bands and plotted in Fig. 4.4 (top).

information.

The ACS F475W and F625W were level 3 HLA mosaics, which are combined images from multiple HST visits covering a large contiguous area of the sky. Level 3 data are produced through the DrizzlePac pipeline which removes geometric distortions, positions the image north up, corrects for sky background variations, removes cosmic rays and combines and projects multiple images on to one common frame with the same pixel scale as the detector. Details of the whole drizzling process is given in the DrizzlePac handbook (Gonzaga 2012). As Level 3 data have already been pre-processed by the pipeline, photometry could be carried out on them without any need for further corrections to the images.

SEXTRACTOR (Bertin & Arnouts, 1996) was used to carry out aperture photometry (through a metric 7.5kpc diameter aperture) on the F475W and F625W images, deriving also the Kron (1980) magnitudes in each band. The red sequence is clearly visible in Fig. 4.1. Because there is no complete redshift survey for this cluster, I make the reasonable assumption here that all bright resolved galaxies falling in the region of parameter space coincident with the cluster red sequence are cluster members. CLASH-VLT spectroscopy of rich clusters at similar redshifts indicates that $> 95\%$ of apparent red sequence galaxies at these magnitudes are genuine cluster members (De Propris et al., 2016). I do not consider red sequence galaxies fainter than F625W> 24 as the possibility of contamination by foreground or background objects significantly increases at this point. Given the tight red sequence down to the selection limit, contamination from non-cluster members is therefore unlikely to be significant.

Ultraviolet observations were made using using the Wide Field Camera 3 (WFC3) with the F225W, F275W and F336W filters of the UVIS channel, corresponding to rest frame 1900Å, 2300Å and 2850Å respectively. The WFC3 has a field of view of $162'' \times 162''$ for the UVIS channel and a pixel scale of $0.04''$/pixel[2]. The WFC3 images through these filters are provided by the archive as Level 2 data, which are identical to Level 3 data in how they are processed with the exception that the combined images are limited to the same HST visit. In order to achieve the maximum depth possible for each band, I aligned and combined all Level 2 frames in each filter using the *imalign* and *imcombine* functions within *IRAF*. Exemplar optical and UV images of Abell 1689 are shown in Figs. 4.2 and 4.3.

The different pixel scales of the optical and UV images precluded the use of SEXTRACTOR

[2]Details of the WFC3 detector is given in Dressel (2017).

in dual mode to obtain UV photometry in the manner as for the optical data. Instead, *IRAF*'s *apphot* package was used to place apertures of fixed 7.5kpc diameter on to the RA and DECs of all the red sequence objects determined from the optical data onto the F225W, F275W and F336W images to measure their corresponding magnitudes in these bands. I then made a 5σ signal to noise cut on the detected objects and checked them by eye to ensure they were indeed real. In total a sub-sample of 37 optically-selected red sequence galaxies were detected in every UV band (these were also the brightest objects in the optical sample). Of these, approximately half had redshifts tabulated in NED[3] and they were all confirmed cluster members. These represent the 37 optically-brightest galaxies of a sample of 176 red sequence galaxies within the field-of-view of the UV frames. The non UV-detected galaxies had upper limits to their UV-optical colours which do not constrain the presence or otherwise of an upturn. The detected objects typically displayed visually identifiable rest-frame UV emission only over the central ~ 1 arcsec, simply reflecting the relative surface brightness sensitivity to $z = 0.18$ ellipticals of the HST data in the different bands. At the redshift of Abell 1689, I detect F225W emission from all ellipticals with optical luminosities down to the $\sim L^*$ level (Bañados et al. 2010).

4.3 Results

4.3.1 UV-to-optical colour-magnitude diagrams

Fig. 4.4 (top) is a plot of the $F225W - F625W$ (rest-frame $\sim 1900 - V$) colours against the absolute F625W (rest-frame V band) magnitudes. There is a spread of approximately 2 magnitudes in this colour. While not a conventional means of measuring the strength of the upturn, this colour has similar sensitivity to the upturn as the standard $1550 - V$ (GALEX $FUV - V$) colour more normally used to measure its strength. Consequently, the spread of ~ 2 magnitudes in $1900 - V$ is comparable to that in the $1550 - V$ colour of red sequence galaxies found in Coma, Fornax, Perseus and Virgo clusters (chapter 2, Boselli et al. 2005). We can also make a more direct comparison with the UVOT $UVW2 - V$ ($\sim 1900 - V$) colours of Coma galaxies from chapter 2 for the same luminosity range as the Abell 1689 sample, where the galaxies show a somewhat smaller scatter of ~ 1.5 magnitudes. It is important to note that while the *spread* in the $UVW2 - V$ and $F225W - F625W$ colours between the two clusters may be comparable, the actual colour values can not as easily be compared. This is due to the

[3] ned.ipac.caltech.edu

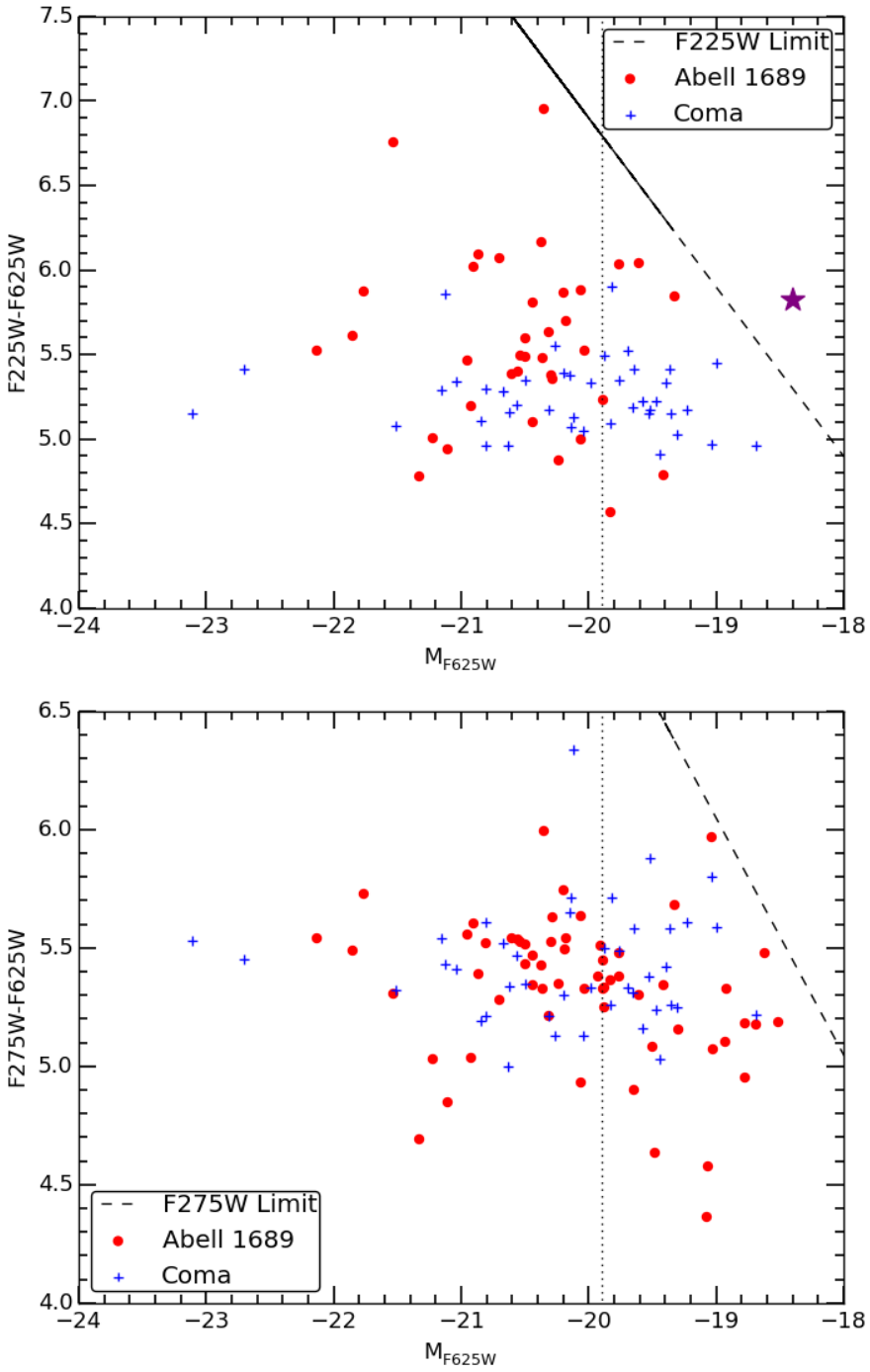

Figure 4.4: $F225W - F625W$ (top) and $F275W - F625W$ (bottom) vs. M_{F625W} colour-magnitude diagrams for the Abell 1689 red sequence galaxies (red filled circles). Photometric uncertainties in colours are < 0.15 magnitudes. The purple starred data point represents the $F225W - F625W$ colour of the stacked galaxies between $M_{F625W} \approx$-19 and -18. Also plotted (blue crosses) is photometry of Coma red sequence galaxies from chapter 2 obtained in similar rest-frame bands (*i.e.* UVOT $UVW2 - V$, top, and GALEX $NUV - V$, bottom) in the same absolute magnitude range as for the Abell 1689 sample. The vertical dotted line denotes the L^* point for Abell 1689. See text for details.

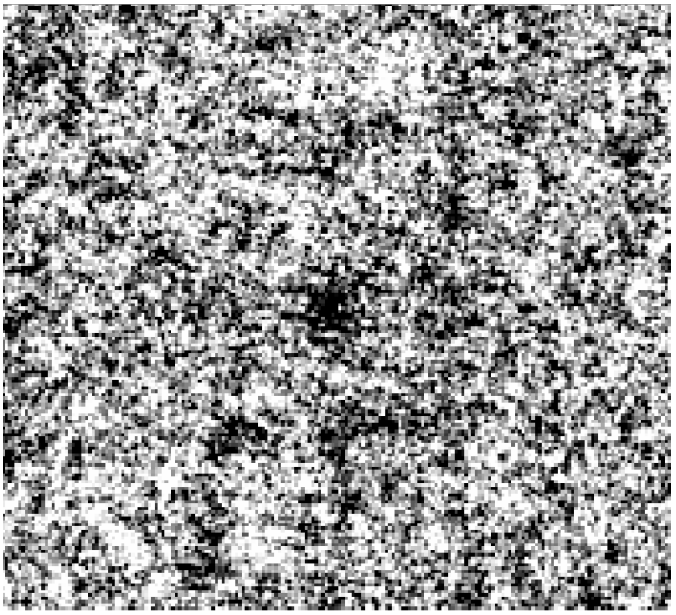

Figure 4.5: $F225W$ image of stacked red sequence galaxies between M_{F625W} ≈-19 and -18 as plotted in Fig. 4.4 (top). A clear $> 5\sigma$ detection can be seen in the stacked image even though the individual galaxies are undetected at this level.

inherent differences in the shape and bandwidths of the HST WFC3 F225W and UVOT UVW2 filter responses, which have FWHMs of 500Å and 657Å respectively. These differences lead to an underlying variation in the measured colours independent of any upturn.

I also stacked the non-detected galaxies in the F225W band between M_{F625W} ≈-19 and -18 to get a detection, from which the average $F225W - F625W$ colour of the galaxies just beyond the detection limit could be determined. This is plotted as the purple star in Fig. 4.4 (top) and the stack itself is shown in Fig. 4.5. As can be seen, the colour is consistent with some of the redder detected galaxies in the overall sample, which is to be expected given that the upturn tends to get weaker with decreasing mass/luminosity (Boselli et al. 2005; Smith et al. 2012).

It should be noted that my sample of Abell 1689 galaxies does not contain the two brightest (central) galaxies. This is due to the final UV image of the cluster having a 'dead' zone at its centre, resulting from the range of rotations and offsets of individual data frames not fully compensating for the gap between individual detectors (Fig. 4.3). As seen from previous studies, locally the largest galaxies – particularly BCGs – tend to have some of the bluest UV-optical colours, and as such the strongest upturns (Burstein et al. 1988), though the results of Brown et al. (1998a, 2000a, 2003) and Ree et al. (2007) noted earlier may indicate some evolution for

these objects.

Also plotted in Fig. 4.4 (bottom) is the $F275W - F625W$ (rest frame $\sim 2300 - V$) colours of the galaxies against the absolute F625W magnitudes. While not as sensitive to the upturn as the GALEX $FUV - V$ used in chapter 2, previous studies of red sequence galaxies (Schombert 2016, e.g.) have shown that the $NUV - V$ colour is also affected quite strongly by the hot HB stars that are the likely source of the upturn. In the discussion section I further justify this choice, showing that the $NUV - V$ colour probes the upturn and does not depend significantly on the underlying stellar populations. Since in the rest frame of Abell 1689, the HST $F275W - F625W$ colour is very similar to that of the the GALEX $NUV - V$ measured for the sample of Coma galaxies with the same absolute magnitude range as that for Abell 1689, these results can be directly compared, as seen in Fig. 4.4 (bottom). Both the Abell 1689 and Coma galaxies show a near identical spread of ~ 1.5 magnitudes and have very similar $NUV - V / F275W - F625W$ colours. This immediately suggests that if the range in this colour is due to upturns of varying strengths, the range in upturn strength has not evolved drastically over the past ~ 2.2 Gyrs. In addition, it is clear that this is true for the *whole* population of galaxies, and not just the brightest galaxies as seen in previous studies (Brown et al., 1998a, 2000a, 2003).

At first glance, these results seem to be in disagreement with those of Ree et al. (2007), who found that the upturn fades with redshift in the range of $z = 0 - 0.2$, but is in agreement with Donahue et al. (2010), who found that the upturn does not evolve in that same redshift range. However, these previous studies were performed only on BCGs. When a much larger sample of ETGs down to L^* (and beyond) is considered, I find that the strength of the upturn phenomenon does not appear to evolve significantly out to $z = 0.2$.

4.3.2 UV-to-optical SEDs of Abell 1689 galaxies

Fig. 4.6 shows the photometry of the 37 galaxies in my sample that were detected in all WFC3 and ACS bands. The observed $F225W - F625W$, $F275W - F625W$, $F336W - F625W$ and $F475W - F625W$ colours are plotted against the equivalent rest-frame central wavelength of each filter, to create UV-to-optical SEDs that span the wavelength range between ~ 1500Å and ~ 5500Å. Even though the SEDs of the Abell 1689 galaxies are sampled by fewer points in the UV than for those of the lower redshift Coma galaxies from chapter 2, I plot both sets of SEDs in order to compare as many data points between the two clusters as possible. Also plotted is the SED of IC4040, a typical star-forming galaxy from the Coma cluster. The SED of this galaxy is

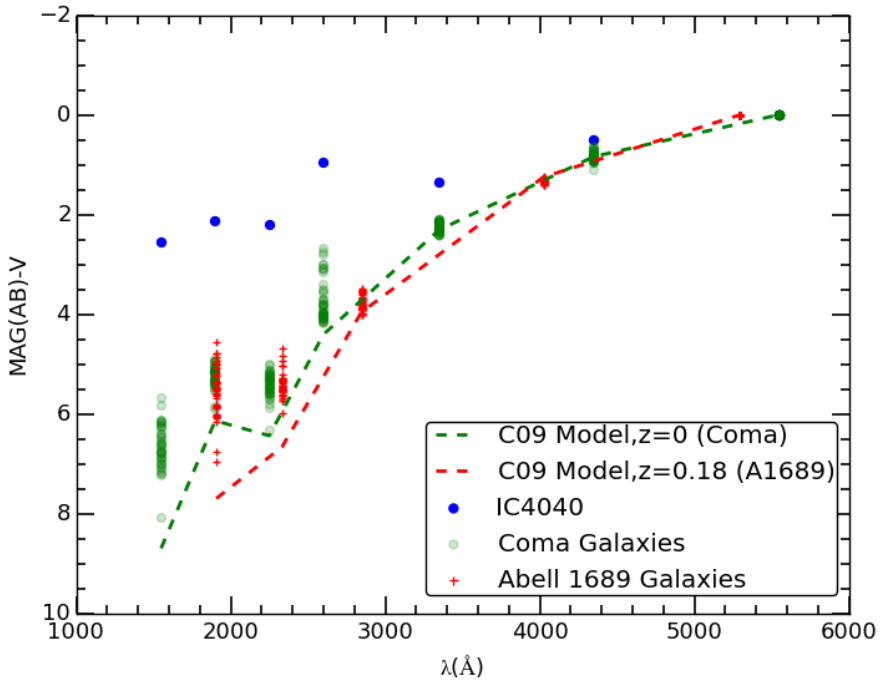

Figure 4.6: UV to optical SEDs of Abell 1689 red sequence galaxies, IC4040 (a starforming galaxy) and an old metal-rich SSP (with no star formation) from the C09 model. Also plotted are similar UV to optical SEDs of Coma red sequence galaxies for comparison. Photometric uncertainties in colours are < 0.15 magnitudes.

much flatter between the UV and optical than those of red sequence galaxies, which is a result of the fundamental difference between the source of UV luminosity in star-forming and quiescent galaxies.

Also included in Fig. 4.6 is the SED of a 'red and dead' SSP from Conroy et al. (2009) (C09 henceforth) with solar metallicity and a formation redshift of $z_f = 4$, which represents a system completely dominated by a conventional old stellar population and therefore having a very weak UV output. The same C09 model is used for both dashed curves. The offset between them is due to its convolution with the appropriate (rest-frame) filter bandpasses for the two sets of observations and the difference in age between Coma and Abell 1689. Although other models for synthetic SSPs exist, the advantage of using C09 is that it specifically does not attempt to model in an ad-hoc fashion any post main-sequence stellar population that contributes to a galaxy's UV emission (see chapter 2).

The SEDs of IC4040 and C09 represent the two opposite extremes of ongoing star formation and no star formation at all, which can then be compared to my sample of red sequence galaxies. It is then possible to form intermediate SEDs between these two extremes by adding in a proportion of the IC4040 SED to that of the C09 model. Given that the range in optical colours of the selected Abell 1689 red sequence galaxies is strongly limited (covering a range of no more than 0.1 magnitudes in $F336W - F625W$), this constrains the maximum proportion of IC4040 SED that can be included. Adding this maximal amount to the C09 SED leads to a combined SED that is redder in UV-optical colours than those measured for my red sequence galaxies, implying that the UV flux is dominated by emission not arising from ongoing star formation, as similarly found in chapter 2.

As already noted, the galaxies in the Abell 1689 sample have a very tight spread of ~ 0.1 magnitudes in their optical colour. However, at wavelengths shorter than 3000Å, the spread in the colours gradually become larger, increasing to several magnitudes at the shortest wavelength (1900Å). Clearly, the large scatter seen in the UV colours is absent in the optical colours. This suggests that the sub-population of stars responsible for the scatter in the UV has little to no effect on the optical output of these galaxies. Furthermore, the C09 SSP fits the optical data extremely well, but in the UV the same model has colours at least as red as the reddest of the observed galaxies. Given that the C09 SSP replicates the contribution of the conventional old stellar population, this indicates that such a population has a very minor effect on the overall UV emission of red sequence galaxies, as one would expect. Ultimately, the comparison of the

results with models suggest (as in chapter 2) that these red sequence galaxies are formed of a majority old stellar population that emits strongly in the optical, superimposed with a similarly old sub-population of (likely) He-enhanced hot HB stars that emit strongly in the UV. The large range in the UV-optical colours reflects the different strengths of the upturn in different galaxies, which in turn appears to be linked directly to the temperature and number of hot HB stars within the galaxies (see chapter 2).

When compared with Coma, the spread in the optical colours of Abell 1689 red sequence galaxies is similarly tight, ~ 0.1 magnitudes. As discussed previously, the spread in the $F275W - F625W$ (Abell 1689) and GALEX $NUV - V$ (Coma) colours are also remarkably similar. In the case of the $F225W - F625W$ (Abell 1689) and UVOT $UVW2 - V$ colours (Coma), the exact values between the two clusters can not be directly compared due to the large inherent difference in the bandpasses of the HST F225W and UVOT UVW2 filters, which is illustrated by the large difference in the $\sim 1900 - V$ colour of ~ 1.5 magnitudes in the underlying C09 model when convolved through each filter. Such a big difference in the model colours does not exist (nor was it expected to exist given the bandpasses) for any of the other data points. However, the spread in the two colours are comparable.

As discussed in chapter 2, the Coma galaxies have an unexpectedly large spread of 2 magnitudes in the $UVW1 - V$ $(2600 - V)$ colour, larger than all other shorter wavelength UV colours. It was surmised that this may be an issue with a subset of the UVOT UVW1 dataset, rather than the true photometry of the galaxies. The majority of the Coma galaxies could be well fitted by a C09 SSP as shown in Fig. 4.6 combined with a blackbody of a specific temperature and normalisation to account for the UV emission. Those galaxies that could not be fit with such a 2-component model were the ones with the unusually blue $UVW1 - V$ colours ($\leqslant 3.8$ mags) - the discrepant $UVW1$ magnitudes specifically degraded any fit. From the current data, the $F336W - F625W$ (rest frame $\sim 2800 - V$) colour of the Abell 1689 galaxies should be closely related to that of the $UVW1 - V$ $(2600 - V)$ colour for the Coma galaxies. The former colour has a smaller range than the latter, and when those objects in Coma that are not well-fitted by a two component model are excluded, the ranges become comparable. This lends credence to the argument in chapter 2 that the overly large spread in $UVW1 - V$ in the Coma galaxies is caused by an issue with a subset of the UVW1 data.

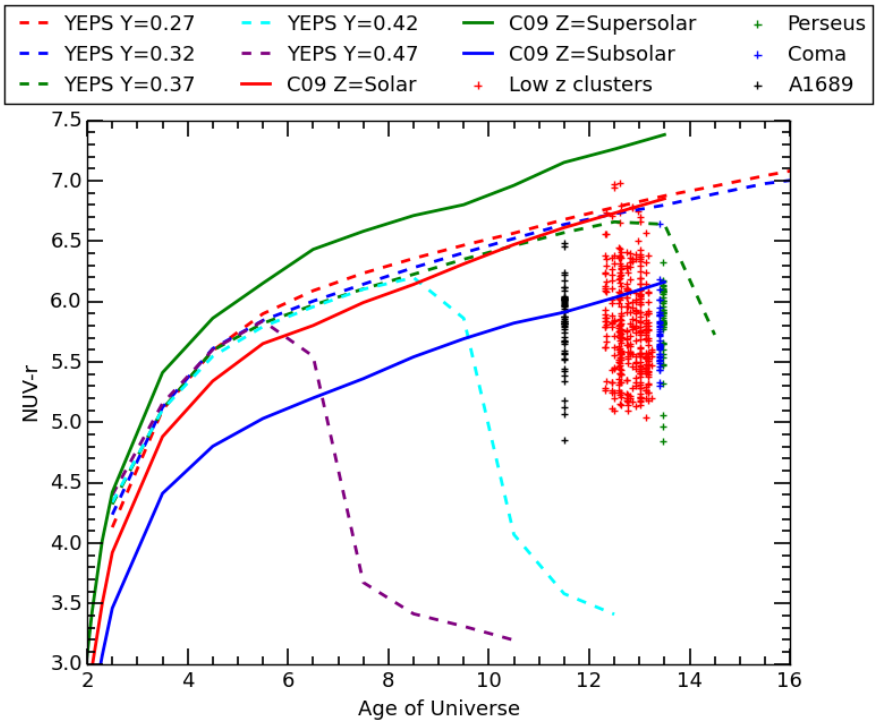

Figure 4.7: YEPS spectrophotometric models (assuming $z_f = 4$ and $Z = Z_\odot$) showing the evolution of the GALEX $NUV - r$ colour over the age of the Universe for a range of Helium abundances. Also included in the plot are the predictions from the C09 model with the following metallicities: Z=$Z_\odot$, $0.56Z_\odot$ and $1.78Z_\odot$. Plotted on top are the $NUV - r$ colours of Coma, Perseus, Abell 1689 and the 20 2dF cluster red sequence galaxies from chapters 2 and 3. Photometric uncertainties in colours are < 0.2 magnitudes.

4.4 Discussion

As discussed in the introduction and in chapter 2, we can interpret these results in terms of the presence of a He-enriched HB population within the galaxies giving rise to their upturns. Recently Chung et al. (2017) published synthetic photometry for a series of Simple Stellar Populations with varying levels of Helium abundance (Y) and metallicity (Z) as a function of time since burst (referred to here as YEPS models, after the name of the project). These models can be used to interpret the results obtained in this chapter and place constraints on the age and/or Helium enrichment of any population giving rise to the upturn.

Fig.4.7 shows the evolution of the GALEX $NUV - r$ colour with lookback time as given by the YEPS spectrophotometric models for a range of He-enriched populations as dashed lines. It should be noted that the photometry from the YEPS models are tabulated by Chung et al.

(2017) for a range of Y_{ini}, which is defined as the initial Helium content of the SSP at $Z = 0$. This parameter is related to the Helium abundance through the following equation: $Y = Y_{ini} + \Delta Y/\Delta Z \times Z$. I adopt the values of $\Delta Y/\Delta Z = 2$ and $Z = 0.02$ (solar metallicity) to calculate the Y for the models as shown in Fig. 4.7, and use these values in the discussion henceforth. Also assumed is a formation redshift of $z_f = 4$. A later formation redshift shifts these evolutionary tracks to the right, trading decreased age for increased Y at a given colour. Age and Y are degenerate in these colours for these models because higher Y populations have shorter main sequence lifetimes. I then plot the $NUV - r$ colours of Coma and Perseus from chapter 2 and low redshift red sequence galaxies from twenty further $z \lesssim 0.1$ 2dF clusters from chapter 3. Also added is the $F275W - F625W$ colours of the Abell 1689 galaxies, suitably k-corrected to the rest-frame $\sim NUV - r$. The overall distribution of points demonstrates a lack of evolution for the UV upturn out to $z \sim 0.2$ (with a $\sim 2.2\ Gyr$ range in lookback time) - the range in the $NUV - r$ of $1 \sim 1.5$ mags, which is a measure of the upturn strengths, is consistent between all the clusters in the redshift range being surveyed.

The observed range in the $NUV - r$ colour is also consistent with the predictions from the YEPS models. The reddest objects can be explained as those with little or no contribution from a significantly He-enhanced HB population. Conversely, the bluest require an additional population with $Y > 0.40$ if the formation redshift was $z_f \sim 4$ or higher, and an even stronger enrichment if the population formed at lower redshift. It should be noted that the model colours shown in Fig. 4.7 are for uniformly He-enhanced populations of a given Y and fixed $Z = Z_{\odot}$. In reality, the observed data is for real red sequence galaxies that have a majority 'red and dead' population with a standard Helium fraction that is close to primordial, combined with a sub-population of He-enhanced stars with a range of Y. As such, the observed colours do not (and should not) reach the bluest colours shown by the models. Because of the age-Y degeneracy, it is possible in theory to have populations with very high Y values (as seen in the $Y = 0.42$ and $Y = 0.47$ models), which become UV-bright after ~ 7 and ~ 4 Gyrs main sequence lifetimes respectively. These populations could therefore form at much lower redshifts ($z \sim 1$). However, given the fact that the He-enhanced sub-population is not an insignificant fraction (of order 10%) of the galaxies' overall stellar population (chapter 2) and that most cluster red sequences appear to be already established by a redshift of $z \sim 2$ (e.g. Newman et al. 2014), any appreciable star formation would seem to have been completed at much higher redshifts (i.e. more than 10 Gyrs ago).

The upturn typically becomes obvious as a separate component of the SED at ≤ 2500Å and strengthens to at least ~ 1500Å. Although measurements in the NUV band (rest frame $F275W$ for Abell 1689) can be significantly influenced by the upturn, it may also partially be affected by the output from the main sequence. Consequently it is potentially sensitive to variations in the age and metallicity of the entire stellar population. To test whether variation in these main sequence parameters can explain the observed range in the $NUV - r$ colour seen in my clusters, I plot in Fig. 4.7 alongside the YEPS models, the evolution of $NUV - r$ against the age of the Universe as given by the C09 models (which have no upturn component) for three different metallicities - Z=$Z_{\odot}$, 0.56$Z_{\odot}$ and 1.78$Z_{\odot}$ (i.e. solar, sub-solar and super-solar) with $z_f = 4$. As can be seen from the plot, the C09 model with solar metallicity matches closely the YEPS model with $Y = 0.27$, since the latter has no upturn compared to the models with higher Y. The super-solar and sub-solar models have $NUV - r$ colours that are ~ 0.5 mags redder and bluer than the solar metallicity model respectively. Since the galaxies probed are almost all at or above the L^* point, the majority will have solar or super-solar metallicities. This is supported by Price et al. (2011) who showed that all Coma galaxies above L^* (i.e. the ones plotted in Fig. 4.7) have metallicities between Z=1-2$Z_{\odot}$. In chapter 2, an attempt was made to fit blackbodies+C09 models with sub-solar metallicities to the SEDs of the aforementioned Coma galaxies, but these all gave poor fits (see chapter 2 for further details). Thus the $NUV - r$ colours given by the Z=0.56$Z_{\odot}$ metallicity C09 model is unlikely to be appropriate for any of the galaxies in my sample. In any event, the model is still not blue enough to account for the entire range of $NUV - r$ colours observed in these clusters even if the entire stellar population of a galaxy has this metallicity. If such a population is mixed in with a super-solar population (in order to satisfy all previous evidence for higher overall metallicities), the mismatch in the range of colours is even worse.

As noted earlier, the age of the main sequence population is the third parameter besides metallicity and Helium enhancement to potentially have a significant effect on the $NUV - r$ colour. As can be seen from the time-evolution of the colours of all C09 models, the change in the $NUV - r$ colour is ~ 0.1 per Gyr. Recent studies by Jørgensen et al. (2017) have found a lack of any appreciable star formation in cluster galaxies at $z < 2$ and formation redshifts for such galaxies between $2 < z_f < 6$ depending on the choice of diagnostics used in its estimation. Furthermore, red sequence galaxies in clusters show a consistent small spread in optical colours up to at least $z \sim 2$ and even higher, and hence have SEDs that were dominated by passively

evolving populations since then (Glazebrook et al. 2017).

Given that the C09 models shown in Fig. 4.7 have $z_f = 4$, this would only allow the age of the population to realistically be ~ 1 Gyr younger or older if the formation redshift was allowed to range between $2 < z_f < 6$, which would only change the $NUV - r$ colour by ~ 0.1 mags. This change in $NUV - r$ caused by the age of the population is once again clearly insufficient to account for the total spread in colour observed in my clusters. While the $NUV - r$ colour can be affected by the metallicity and age of the main sequence population, for the cluster galaxy population studied here, variation in this colour must still be dominated by the hot HB stars that are believed to be the primary driving force behind the upturn.

It should be noted that the strength and onset of the upturn also depends on Reimers mass loss parameter (Reimers 1975, 1977), η, as the properties of a star on the HB are influenced by the mass of its surviving envelope (i.e. the higher the mass loss during the RGB phase, the higher the surface temperature of the star in the HB). The YEPS models used here assume $\eta = 0.63$, which is calibrated using the inner-halo globular clusters of the Milky Way. However, observations by Dalessandro et al. (2012) have shown the existence of a few Milky Way globular clusters such as 47 Tuc which have UV-optical colours much redder than those predicted by the YEPS models with the lowest Y, despite having lower metallicities than the models shown here. This discrepancy can be accounted for by assuming a lower value of η, which would make the UV-optical colours redder. The majority of the observed galaxies have $NUV - r$ colours that fall within the range predicted by the YEPS models, with the reddest ones being accounted for by higher metallicity models, implying that the $\eta \sim 0.6$ is not unreasonable for most of these galaxies. Nevertheless, the value chosen for η could bring an uncertainty of the order $\sim$1 Gyr to the age of the models of a given metallicity.

While there is an appreciable population of low metallicity Galactic globular clusters that demonstrate upturns (either with or without He-enhanced HB populations), there are few nearby observational models for systems with high Z (commensurate with ETGs) and high Y. As such, I use the YEPS models in Fig. 4.7 to make plausible estimates of $Y = 0.40 \sim 0.41$ and $z_f = 4 \sim 6$ for the He-enhanced sub-populations in the observed cluster galaxies. If so, Fig. 4.7 implies that the strength of such upturns should diminish in higher redshift cluster populations because there is insufficient time to form the most He-enriched HBs (see Brown et al., 1997, et seq.). To a limited extent (given the available time), this could be countered by an even earlier formation redshift. Clearly, the strength of the evolution in UV upturns at higher redshifts is a

crucial diagnostic of the viability of the He-enhanced HB explanation for these upturns and as such I will explore this issue in an observational analysis of higher redshift clusters in the next chapter.

While the focus has been on explaining the results through the existence of a He-enhanced HB population in these galaxies, the observed lack of evolution over this time interval is still consistent with alternative models for the UV upturn, such as the binary model of Han et al. (2007) or a metallicity-dependent mass loss fraction on the red giant branch. It is not consistent with the predictions of the low-metallicity model proposed by Yi et al. (1997, 1998), as this model predicts that the upturn should show strong fading at $z \sim 0.2$ and disappear completely by $z \sim 0.25$. Again, observations of higher redshift clusters should help to further discriminate between these models.

4.5 Conclusions

By determining the range of UV-optical colours displayed by the population of red sequence galaxies drawn from HST observations of Abell 1689 at $z = 0.18$, I demonstrate that it is comparable to that seen for the same population in lower redshift clusters, including Coma.

The origin of this range is therefore likely to be the same in these clusters and is due to the variation in the strength of UV upturn seen in their galaxies. In common with previous work, I can interpret this UV upturn as originating from a metal rich He-enhanced HB population of variable strength in each galaxy. Given this interpretation, the lack of variation in the range of colours across ~ 2.2 Gyr of lookback time can constrain a combination of the level of Helium enhancement in the stellar subpopulation and the time since formation of the population and galaxies. In particular the results imply $Y \geqslant 0.40$ for a formation redshift of $z_f \sim 4$ and significantly higher for later formation. Earlier formation still requires a reasonable level of helium enhancement ($Y \sim 0.38$).

The results cannot currently rule out other origins for the UV upturns, but subsequent observations of red sequence populations in higher redshift clusters should test all of these scenarios.

5

The UV Upturn in $z = 0.3, 0.55$ & 0.7 clusters

Building upon the results that have been presented thus far, this chapter will expand the study on the evolution of the upturn to the highest redshift clusters currently observed in the UV, with deep enough datasets such that the output from the standard early-type population can be probed. Given the redshift regime reached in this study (6.3 Gyrs in lookback time), all models of the upturn can be tested, as each of them predict some form of evolution (or non-evolution in the case of the binary model) during this epoch, allowing for the most likely mechanism giving rise to the upturn in ETGs to be pinpointed.

This chapter has been published in and is largely reproduced from Ali et al. (2018c).

5.1 Introduction

Studies of the UV upturn at moderate-high redshift ($z > 0.5$) have been few and far between due to past detector sensitivity not being strong enough to pick up faint UV sources at higher redshifts. As such, all investigations have been limited to BCGs (or very bright cluster ETGs), which naturally have the largest UV output due to their massive size compared to normal ETGs, as discussed in previous chapters. The first key paper that explored the upturn at moderate

redshift was by Brown et al. (2000b), who observed four of the most luminous ellipticals in the galaxy cluster CL 0016+16 ($z \sim 0.55$) and found that while the upturn was still present in these galaxies, the $FUV-V$ colour was redder (i.e. upturn was weaker) compared to equivalent $z = 0$ galaxies. As with Brown et al.'s other work, it should be noted that due to the extremely small size of the sample, it could suffer heavily from stochasticity. More recently, a spectroscopic study of a much larger sample of massive SDSS-III/BOSS galaxies ($\log M^*/M_\odot > 11.5$) by Le Cras et al. 2016 found that the upturn exists in galaxies out to $z \sim 1$, though its frequency in ETGs decreases with redshift, particularly at $z > 0.6$. They also recover a temperature range between 10,000-25000K for the upturn population, consistent with the temperatures derived in chapter 2 for Coma galaxies.

The four key models of the upturn as detailed in chapter 1 are metal-poor HB stars, metal-rich HB stars from increased mass loss in the RGB, HB stars created through mass loss due to binary interactions, and He-enriched HB stars. The evolution of the upturn at moderate-high redshift ($z > 0.5$), as explored in this chapter, should allow us to confidently discriminate between these scenarios, given that most models diverge in their predictions around this redshift. For example, if metal poor stars are responsible, the envelope mass quickly becomes too large for stars to evolve onto the *blue* HB, irrespective of their metallicity, only lower mass stars have the potential to evolve onto the blue HB. Consequently the upturn should disappear above some relatively low redshift (Park & Lee 1997). Conversely, in the binary scenario, the upturn should always be present, back to the earliest times (Han et al. 2007). If enhanced mass loss on the RGB is driving the upturn, then the upturn should appear at a moderate redshift and become stronger over time. Finally, if He-rich (metal-rich) stars are responsible, the upturn appears rapidly at moderate redshifts (Chung et al. 2017; Tantalo et al. 1996) and remains roughly constant thereafter, thus making it a sensitive probe of the epoch of galaxy formation and the degree of He-enrichment. Unlike a low metallicity population, the increased He abundance is required if high metallicity stars are to evolve onto the blue HB. Because the progenitors of HB stars have masses such that they take about 8 Gyrs to reach the zero-age line for Helium burning stars, assuming that the responsible population is He-enhanced implies that observations of the upturn at $z \sim 0.6$ probe conditions in early galaxies at $z > 4$. However, we should note that there is currently no well established theoretical mechanism that gives rise to the high He abundances in these populations. Nevertheless, there is clear observational proof that such stars exist in the nearby Universe (see review by Bastian & Lardo 2018 and the discussion section below).

In this chapter, the upturn is explored in even higher redshifts compared to Abell 1689 (z=0.18). With the advent of the Hubble Frontier Fields survey (Koekemoer et al. 2017) and deep optical+UV imaging of multiple galaxy clusters, it is finally possible to perform a detailed analysis of the galaxies at $z = 0.31$ (Abell 2744; lookback time of 3.5 Gyrs) and $z = 0.55$ (MACSJ0717+3745 and MACSJ1149+2223; lookback time of 5.4 Gyrs). Outside of the Frontier Fields clusters, deep observations of SDSSJ1004+4112 at $z = 0.68$ (lookback time of 6.3 Gyrs) have also been made using HST, which can allow for us to push the analysis of cluster-wide surveys of the upturn at the furtherest redshift to date. Each of the Frontier Fields clusters are well known for being highly rich in ETGs and act as massive gravitational lensing sources, such that $6 < z < 10$ galaxies have been discovered behind them, ones that are believed to be responsible for the epoch of reionization (McLeod et al. 2016; Livermore et al. 2017). SDSSJ1004+4112, while not as massive/rich as the Frontier Fields clusters, is still a relatively massive cluster ($\sim 3\times10^{14} M_{\odot}$ – Oguri et al. 2012) demonstrating both strong and weak gravitational lensing effects. As was the case with all previous clusters presented in this thesis, galaxies down to the $\sim L^*$ level and beyond are probed in all 4 of the clusters presented in this chapter, through both individual and stacking analyses.

5.2 Dataset

For this analysis I required a sample of clusters that had sufficiently deep rest-frame optical and UV data available in the Hubble Legacy Archive. Only a very limited number of clusters above $z > 0.2$ have thus far been observed in suitable UV wavebands by WFC3 to depths that are sufficient to characterise the upturn in red sequence galaxies, and it is this that dictates my choice of clusters. Rest-frame optical images for the clusters analysed in this chapter were all taken with the Hubble Space Telescope's (HST) Advanced Camera for Surveys (ACS). Abell 2744 ($z = 0.31$), MACSJ0717+3745 and MACSJ1149+2223 (both $z = 0.55$) are part of the Hubble Frontier Field sample, providing very deep optical and infrared images for these clusters. I used images in filters F606W and F814W for these clusters, corresponding approximately to rest frame g (4630Å) and r (6220Å) for Abell 2744 and to rest frame B (3930Å) and V (5270Å) for the two $z = 0.55$ clusters. For SDSSJ1004+4112 at $z = 0.68$, observations were carried out in filters F555W and F814W, corresponding to rest-frame u (3300Å) and g (4850Å) respectively. All of these images were retrieved from the Hubble Legacy Archive as fully processed data on

Cluster	z	Filter	Proposal ID	PI	Total exp. time/s
Abell 2744	0.308	ACS F814W	13495	Lotz	104270
Abell 2744	0.308	ACS F606W	13495	Lotz	23632
Abell 2744	0.308	WFC3 F275W	13389	Siana	22720
MACSJ1149+2223	0.543	ACS F814W	13504	Lotz	104177
MACSJ1149+2223	0.543	ACS F606W	13504	Lotz	24816
MACSJ1149+2223	0.543	WFC3 F336W	13389	Siana	22080
MACSJ1149+2223	0.543	WFC3 F275W	13389	Siana	22080
MACSJ0717+3745	0.535	ACS F814W	13498	Lotz	114591
MACSJ0717+3745	0.535	ACS F606W	13498	Lotz	27015
MACSJ0717+3745	0.535	WFC3 F336W	13389	Siana	22720
MACSJ0717+3745	0.535	WFC3 F275W	13389	Siana	22720
SDSSJ1004+4112	0.68	ACS F814W	10509	Kochanek	5360
SDSSJ1004+4112	0.68	ACS F555W	10509	Kochanek	7978
SDSSJ1004+4112	0.68	WFC3 F275W	11732/12324	Kochanek	25914

Table 5.1: Table giving details on all the images retrieved from HLA for the four clusters being analysed.

which photometry could be performed directly. See Table 5.1 for a full summary of the data, including Proposal IDs, PIs, exposure times, etc.

Ultraviolet data in F275W and F336W were taken for Abell 2744, MACSJ0717+3745 and MACSJ1149+2223 using the Wide Field Camera 3 (WFC3). These correspond to rest frame central wavelengths of ~ 2100Å for Abell 2744 (F275W) and ~ 1750Å and ~ 2150Å for the two $z = 0.55$ clusters (F275W & F336W). For SDSSJ1004+4112 ($z = 0.68$) the F275W image corresponds to a rest-frame wavelength of ~ 1650Å. As with the optical data, these images were retrieved as fully processed data from the Hubble Legacy Archive, and multiple frames from each filter were combined together using *IRAF*'s *imcombine* function, on which photometry was then performed. Refer to Table 5.1 for a full summary of the datasets used. These images have the potential to probe the evolution of the upturn over the past 7 Gyrs. If the upturn arises from a post main sequence population, this in turn is a probe of star formation at much earlier epochs in these galaxies. Exemplar optical and UV images of one of the clusters (MACSJ1149+2223) are shown in Figs. 5.2 and 5.3.

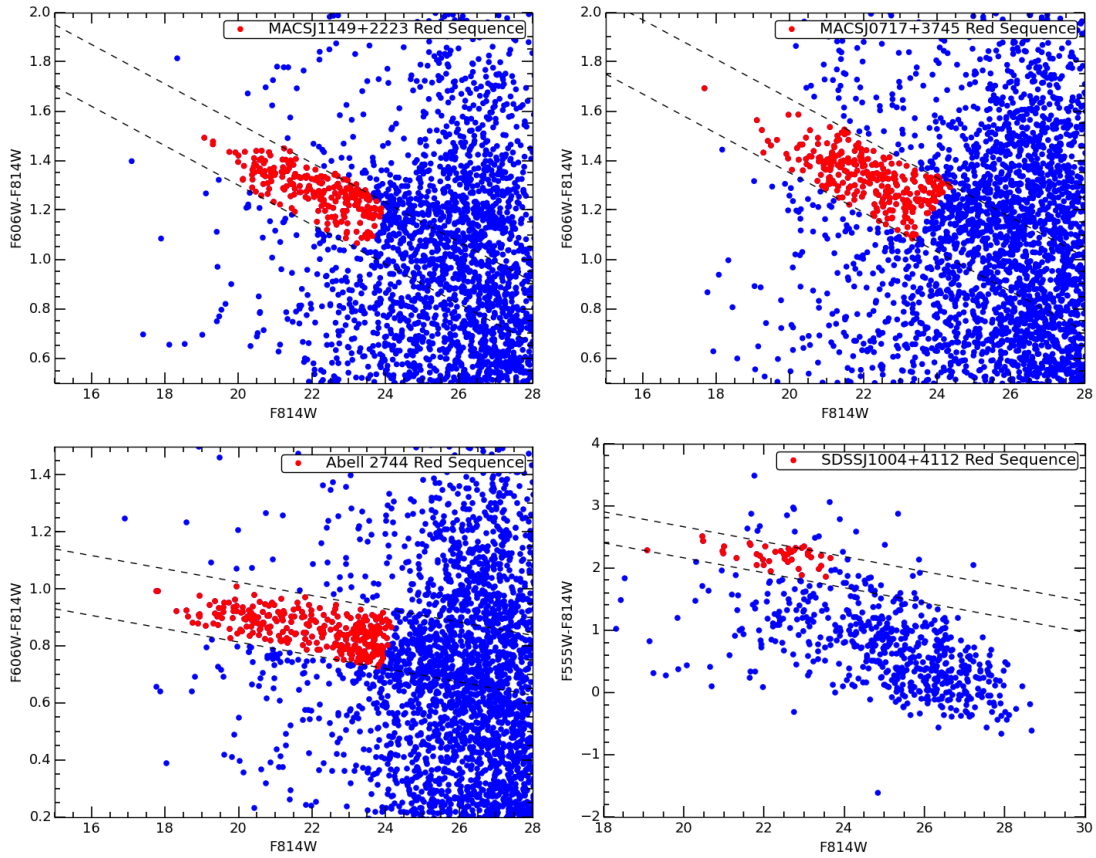

Figure 5.1: Optical $F606W - F814W$ vs. $F814W$ or $F555W - F814W$ vs. $F814W$ colour-magnitude diagrams for MACSJ1149+2223, MACSJ0717+3745, Abell 2744 and SDSSJ1004+4112. The red sequence is denoted with the red filled circles within the dashed lines and have photometric uncertainties of < 0.05 magnitudes in their optical colours. The equations of the selection mid-lines are as follows - MACSJ1149+2223: $y = -0.08x + 1.825$; MACSJ0717+3745: $y = -0.08x + 1.9$; Abell 2744: $y = -0.023x + 1.035$; SDSSJ1004+4112: $y = -0.12x + 2.65$, where x is the $F814W$ magnitude and y is the relevant colour.

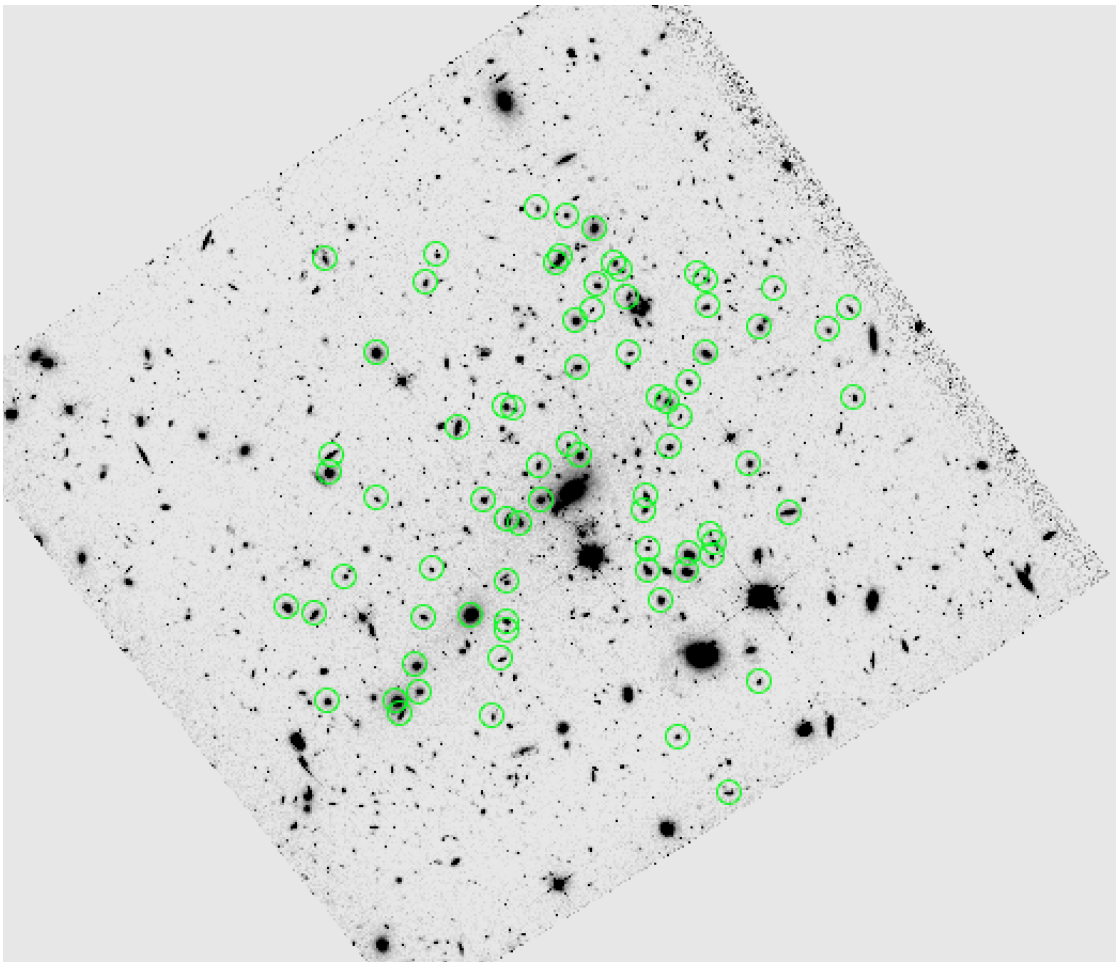

Figure 5.2: Exemplar F814W image of MACSJ1149+2223. Highlighted are the red sequence galaxies detected in the F336W band and plotted in Fig. 5.4 (bottom).

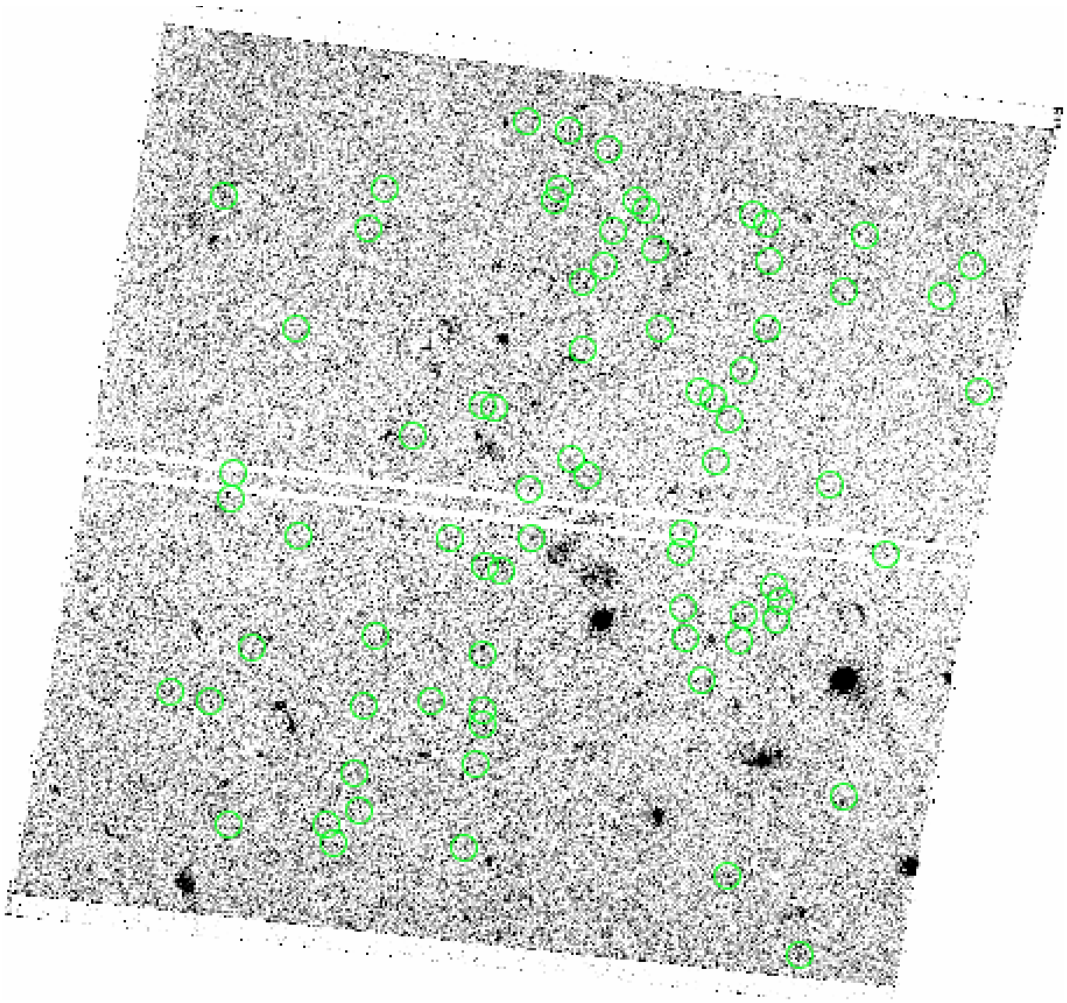

Figure 5.3: Exemplar F336W image of MACSJ1149+2223. Highlighted are the red sequence galaxies detected in this band and plotted in Fig. 5.4 (bottom).

5.2.1 Colour-magnitude diagrams

As in the previous chapters, I used the red sequence to select quiescent cluster members in all clusters. This has already been shown to be an efficient method to identify ETGs in clusters, with a high degree of fidelity (e.g, see De Propris et al. 2016; Rozo et al. 2015). Galaxies belonging to these tight red sequences appear to show no evidence of current or recent star formation, even in high redshift clusters at $z > 1$ (e.g., Mei et al. 2006). I used SEXTRACTOR (Bertin & Arnouts, 1996) to perform photometry on all optical images listed in Table 5.1 and measure Kron (1980) style total magnitudes and aperture magnitudes within a metric diameter of 7.5 kpc. Fig. 5.1 shows the optical colour-magnitude diagrams for the clusters, where a tight red sequence of cluster members is identified (see figure caption). All photometrically selected objects were then checked by eye to ensure that the final sample only included objects that appeared to have early-type morphology, rejecting objects that were clearly (reddened or red) late-type galaxies. Red sequences up to $M_{F814W} \sim 24$ are selected, as beyond this point the likelihood of contamination from non-cluster foreground or background galaxies increases significantly.

For the selection of the red sequence in the three clusters at $z \leqslant 0.55$, a width of $0.2 \sim 0.3$ in the optical colours was used to be consistent with the red sequence selection of low redshift clusters in the previous chapters, where similar rest-frame colours were used in the selection. For Abell 2744, MACSJ1149+2223 and MACSJ0717+3745, the $F606W - F814W$ vs. $F275W/F336W - F814W$ was plotted to check whether there was any correlation between the optical and NUV colours. None was found. This indicates that small changes to the width of the red sequence selection would not significantly affect the spread in the observed UV-optical colours in the clusters. For SDSSJ1004+4112, a slightly larger width of 0.5 magnitudes in $F555W - F814W$ is used since the rest-frame colour corresponds to $u - g$, and it is known that the scatter in the red sequence increases towards shorter wavelengths. Indeed, the scatter in the red sequence in this cluster is the same as that in Coma (Eisenhardt et al. 2007) for this rest-frame colour.

The UV magnitudes were then measured for all our red sequence galaxies in each cluster. Given that the UV data was obtained by a different instrument with a different plate scale etc, it was not possible to use SEXTRACTOR in dual image model with the optical data as the master image. I therefore placed metric (7.5 kpc) apertures on the RA and DEC positions of optically-selected red sequence galaxies using *IRAF*'s APPHOT package, after checking the

relative alignment of optical and UV images using bright stars. A 5σ cut was adopted for detection and all objects were also checked by eye to verify that they were really detected in the UV images. In Abell 2744 53 galaxies were detected in F275W of the 155 red sequence galaxies selected in the optical that were in the field of view of the UV frame. For MACSJ1149+2223 I detected 75 galaxies in F336W and 12 in F275W out of 160, whereas in MACSJ0717+3745 (with higher extinction) these numbers are 39 and 11 in each UV filter, respectively, out of 188 red sequence galaxies. In SDSSJ1004+4112 only 2 galaxies in F275W were detected out of 40 red sequence objects. For all clusters I was able to detect UV emission from galaxies with optical luminosities at least down to L^*.

5.3 Evolution of the UV upturn

I first consider the evolution of the upturn using the rest-frame $NUV - V$ colour that has also been used in the previous chapters. Although this is not as sensitive to the upturn strength as the standard $FUV - V$ colour, previous studies have shown that $NUV - V$ in red sequence galaxies is mainly produced by the hot HB stars that are recognised as the source of the upturn (Schombert, 2016). In chapter 4, I confirmed that the $NUV - V$ colour is indeed mainly produced by hot HB stars and is not influenced heavily by the main sequence age and metallicity of the underlying stellar population in quiescent galaxies. This is further developed below in the discussion. For the clusters in this chapter, the rest-frame NUV approximately lies within the F275W (Abell 2744) and F336W (MACSJ0717+3745 and MACSJ1149+2223) filters, which have greater sensitivity than bluer HST filters closer to the original FUV filter. For SDSSJ1004+4112, the F275W image corresponds more closely to FUV than the NUV in the rest-frame.

5.3.1 NUV-optical

Fig. 5.4 (top) shows the $F275W - F814W$ (approximately $NUV - r$) against M_{F814W} colour-magnitude diagram for red sequence galaxies in Abell 2744 ($z = 0.31$). I find a spread of 1.5 magnitudes in the $NUV - r$ colour, which is perfectly consistent with that measured in Coma and Abell 1689 in previous chapters. This suggests that there has been no evolution of the upturn strength at least to this redshift.

Also plotted is the observed $F336W - F814W$ colours vs. M_{F814W} for the two $z = 0.55$

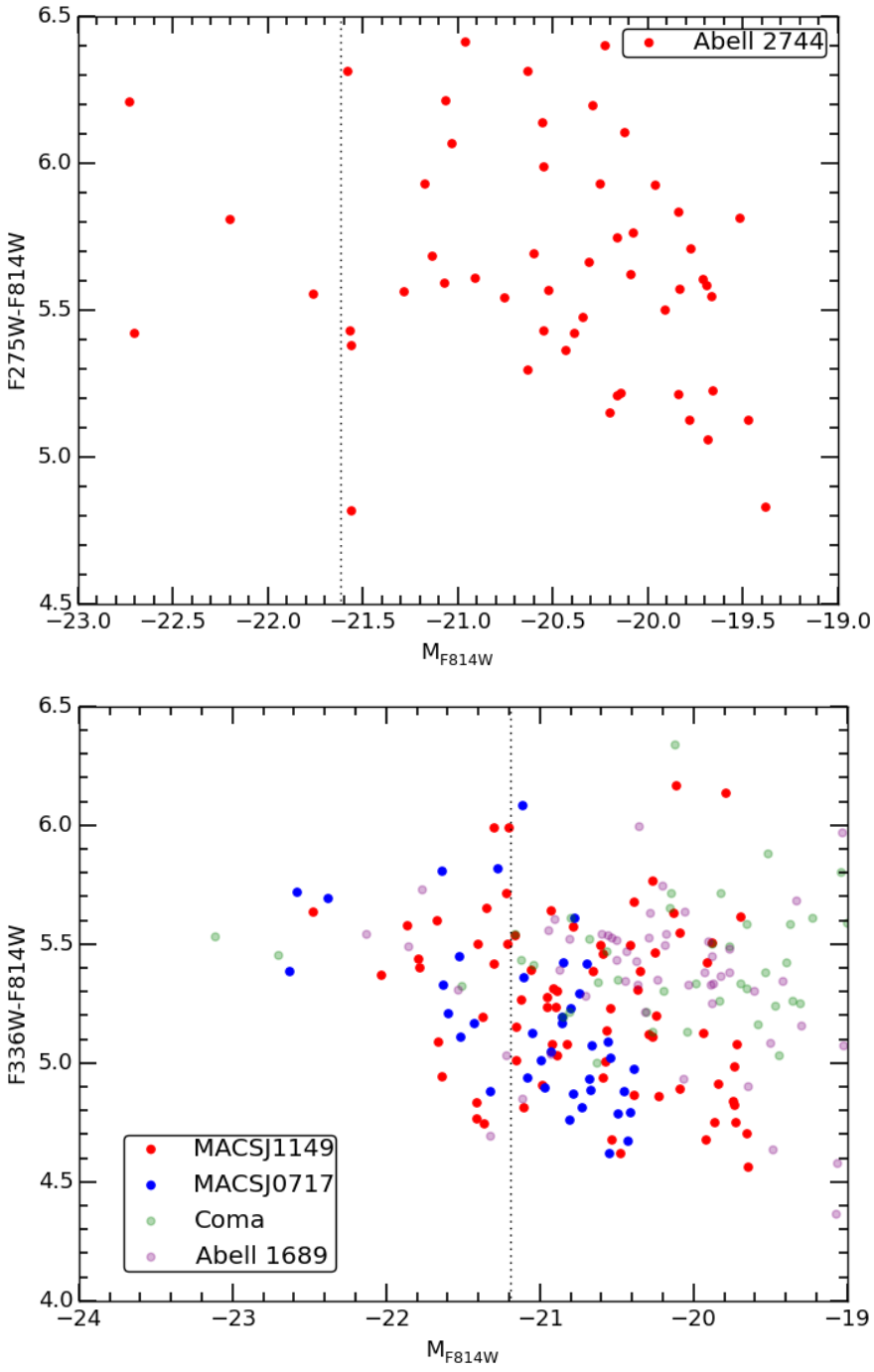

Figure 5.4: *Top:* $F275W - F814W$ vs. M_{F814W} for Abell 2744. *Bottom:* $F336W - F814W$ vs. M_{F814W} for MACSJ1149+2223 and MACSJ0717+3745. Also plotted are the same rest frame colours for Coma and Abell 1689 for comparison. The vertical dotted lines in each plot denote the $F814W$ L^* point for each respective cluster (De Propris et al., 2013). All photometric errors in colour are < 0.15 magnitudes unless explicitly plotted. There is no significant difference in the colour spread of galaxies across the entire redshift range.

clusters in Fig. 5.4 (bottom), which is equivalent to $NUV - V$. For comparison, I also plot the same colours in Coma and Abell 1689 in the same absolute magnitude range as sampled in MACSJ0717+3745 and MACSJ1149+2223. These objects appear to have the same range in colour $4.5 < NUV - V < 6$ at all redshifts. This indicates that at least to $z = 0.55$ the upturn has not evolved significantly. By itself, this result rules out a low metallicity hot HB population as the origin for the upturn, as such stars would only reach the hot HB at significantly lower redshift – they should not be present in $z = 0.55$ populations.

5.3.2 FUV-optical

For MACSJ1149+2223 and MACSJ0717+3745 the archival HST imaging in the F275W filter corresponds to rest-frame 1750Å (at $z = 0.55$), close to the classical definition of the FUV band used to characterise the upturn. I plot the observed, reddening-corrected $F275W - F814W$ vs. M_{F814W} for both clusters in Fig. 5.5 (top), which is roughly equivalent to rest-frame $m_{1750} - V$.

In MACSJ1149+2223 and MACSJ0717+3745 I was only able to clearly detect (at least to 5σ and visually confirmed) the galaxies with the strongest upturns, resulting in 12 and 11 objects in each cluster, respectively. Recall that at any V magnitude the spread in the upturn colour is of the order of 1.5$\sim$2 mags. This means we are not detecting the entire population of galaxies exhibiting upturns because of the detection limit – i.e. a galaxy with no upturn would have a UV magnitude significantly below the detection limit, as shown in Fig. 5.5 (top). In this figure we can also see the equivalent colours for Coma and Perseus, k-corrected to the F275W filter at $z = 0.55$, following Chung et al. (2017). Only the strongest upturn galaxies from Coma and Perseus would lie above the detection limit at this redshift.

In order to explore the rest of the upturn population in these clusters, I produced mean stacks of the non UV-detected red sequence galaxies in these clusters in the F275W filter. For each galaxy I extracted an $8''$ by $8''$ cutout from the HST image, at the RA and DEC position established from the F814W image. Stacking the 5 optically brightest galaxies lacking individual UV detections (to my 5σ limit) in MACSJ1149+2223 and the 7 optically brightest UV non-detections in MACSJ0717+3745 achieves a $> 5\sigma$ detection in the stacked F275W data in both cases. I then made further stacks from optically fainter sources by combining as many galaxies as necessary (in order of F814W magnitude) to produce stacks with approximately the same combined F814W flux as the first stack. This process was repeated until I reached galaxies as faint as $M_{F814W} \approx -19.5$ (limit also reached in Coma, Perseus, Fornax and the compilation

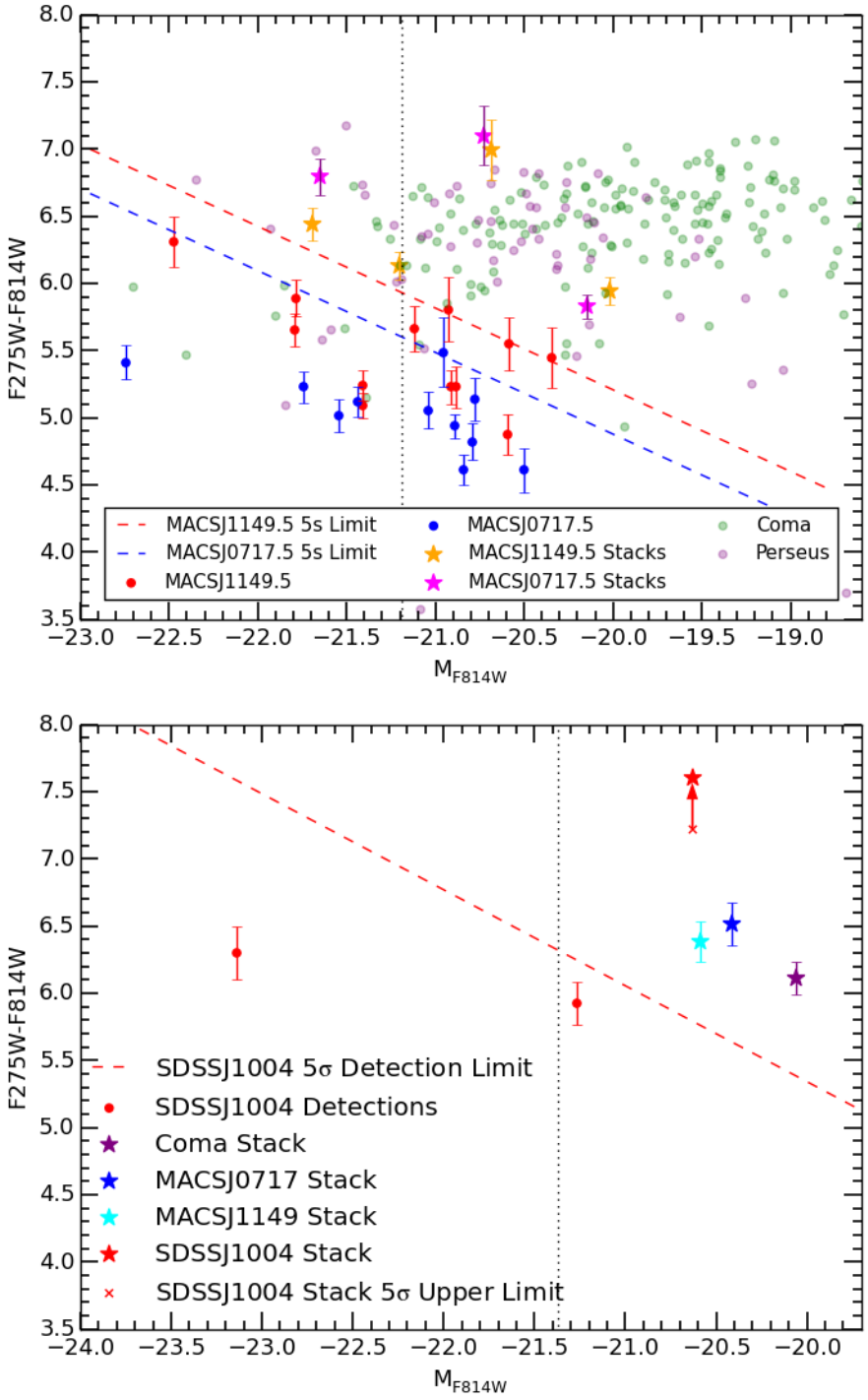

Figure 5.5: *Top:* $F275W - F814W$ vs. M_{F814W} for MACSJ1149+2223 and MACSJ0717+3745. The magenta and orange starred data points are stacked non-detections from each cluster. Also plotted are the same rest frame colours for Coma and Perseus for comparison. *Bottom:* $F275W - F814W$ vs M_{F814W} for SDSSJ1004+4112. Also plotted for comparison are the blue, cyan and purple starred points, which represent the stacked colours between M_{F814W} ∼-19.7 to -21.7 for Coma, MACSJ1149+2223 and MACSJ0717+3745. The dashed lines are the UV 5σ detection limits for each cluster. The vertical dotted lines denote the $F814W$ L^* point for each respective cluster (De Propris et al., 2013). The mean colour of galaxies in SDSSJ1004+4112 is at least 1 magnitude redder than at $z \leqslant 0.55$, showing that the upturn is either very weak or no longer present at this epoch.

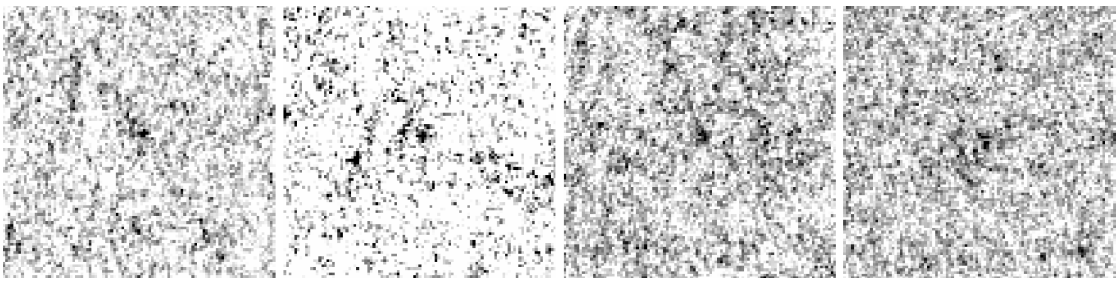

Figure 5.6: 4" by 4" stacks of all non-detected MACSJ1149+2223 red sequence galaxies in the $F275W$ band. The stacks are divided into 4 bins ranging between $-19.5 \lesssim M_{F814W} \lesssim -21.5$ as plotted in Fig. 5.5 (top). Each of the stacks demonstrate at least a 5σ detection.

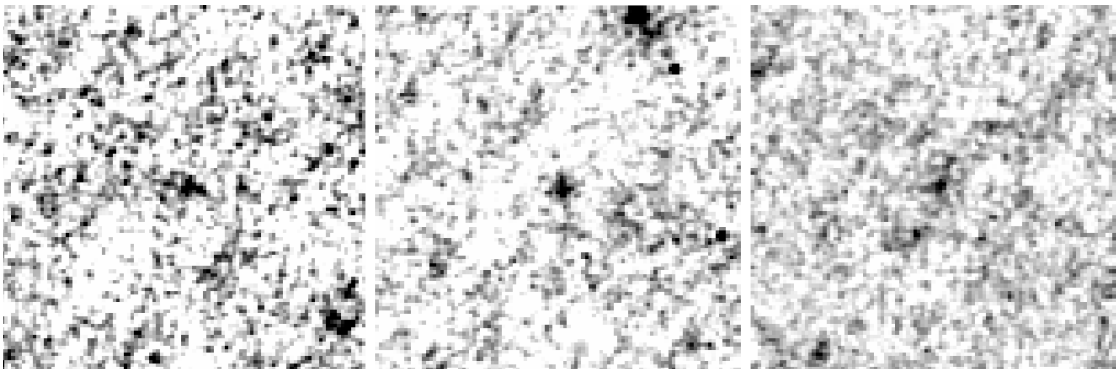

Figure 5.7: 4" by 4" stacks of all non-detected MACSJ0717+3745 red sequence galaxies in the $F275W$ band. The stacks are divided into 3 bins ranging between $-19.5 \lesssim M_{F814W} \lesssim -21.5$ as plotted in Fig. 5.5 (top). Each of the stacks demonstrate at least a 5σ detection.

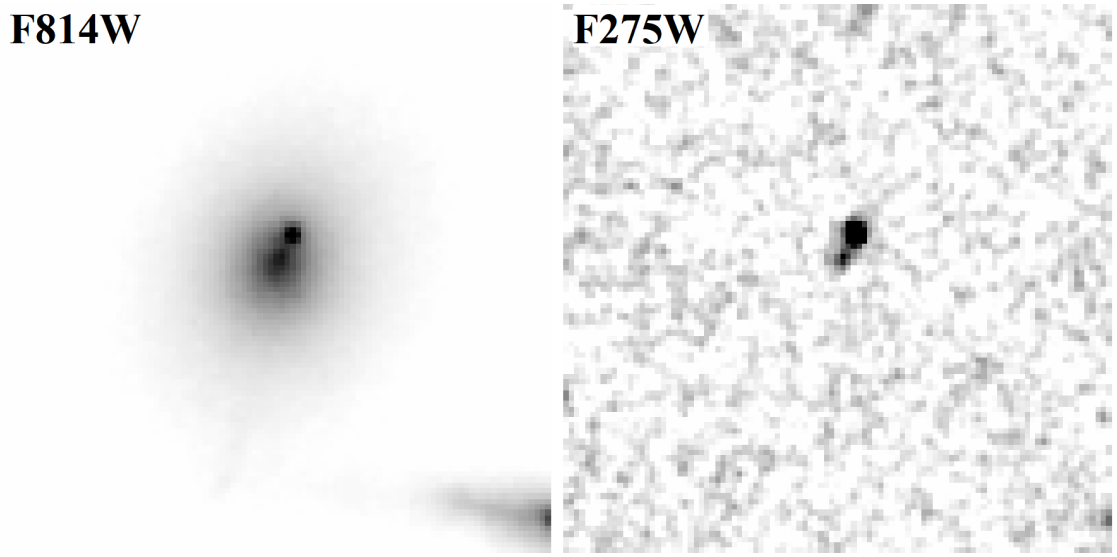

Figure 5.8: 5" by 5" and 4" by 4" images of the SDSSJ1004+4112 BCG in the F814W (optical) and F275W (UV) bands respectively. The bright point-like source to the north-east of the BCG in F814W is a lensed quasar at $z = 1.74$. The quasar is much bluer than the BCG in $F275W - F814W$ and this affects the quality of the latter's photometry in F275W. This is reflected in the uncertainty in the applied error bar to the photometry of the BCG.

of 20 2dFGRS clusters previously). This resulted in a total of 4 stacks for MACSJ1149+2223 made up of 5, 8, 15 and 26 galaxies (shown in Fig. 5.6) and 3 stacks for MACSJ0717+3745 consisting of 7, 18 and 32 galaxies (shown in Fig. 5.7). This procedure means that if galaxies of different optical brightnesses had, on average, the same UV-optical colours, each stack should be detected in the UV at the same level, although given the numbers in each stack, clearly there would be stochastic variation due to small number statistics. I plot the $F275W - F814W$ colour of these stacks against F814W, where the F814W used is the mean magnitude of the galaxies contributing to that stack, in Fig. 5.5 (top). The range of colour seen in these stacks is similar to that seen in the range of individual colours for upturn systems drawn from Coma and Perseus, $5.5 < FUV - V < 7$. In combination with the small number of individual detections, this behaviour implies that the upturn has undergone no significant evolution to $z = 0.55$ (at least for these clusters), as already established from the $NUV - V$ data presented in the previous subsection and shown in Figs. 5.4 and 5.10.

a) SDSSJ1004+4112: The Rise of the Upturn

For SDSSJ1004+4112 archival HST imaging in the F275W filter was used, corresponding to rest-frame 1650Å (at $z = 0.68$). In Fig. 5.5 (bottom), I plot $F275W - F814W$ against F814W, corresponding roughly to rest-frame $m_{1650} - g$. Brighter than L^*, only one of three galaxies meeting the optical cut was individually detected in the UV at $> 5\sigma$, which is the brightest cluster galaxy. However, photometry for this object was complicated by the presence of a $z = 1.47$ lensed quasar image projected close to the centre of the galaxy (Inada et al., 2003). Both the quasar and the galaxy were detected in the UV, with the brightest emission arising from the point source (Fig. 5.8). Consequently, for this object I calculated the optical and UV fluxes in apertures that excluded the region contaminated by the quasar, so the brightest data point in Fig. 5.5 (bottom) is the colour of the central region of the BCG with minimal contamination from the quasar. I estimate the uncertainty on this value to be approximately 0.2 mags. Besides the BCG, there is one other galaxy (at $\sim L^*$) detected at a $> 5\sigma$ level in the UV. The detections are shown as filled red circles in Fig. 5.5 (bottom).

At fainter optical magnitudes there were no individual UV detections, but given the 5σ limit shown in Fig. 5.5 (bottom), we may not expect there to be any if emission arises from upturns of comparable strength to those seen at lower redshift. Given this, it was only possible to search for a general upturn population by carrying out a stacking procedure on the fainter red sequence galaxies in this cluster, similar to that used in the analysis of the $z = 0.55$ systems. In this case, I simply stacked the optical and UV images from the 20 red sequence galaxies with optical magnitudes in the range $-19.7 < M_{F814W} < -21.7$ (excluding the one $> 5\sigma$ detection in this interval), a range similar to that explored in the analysis of the lower redshift clusters. This was therefore representative of the general population of objects contributing to the upturn in local clusters, without including fainter dwarfs whose low metallicity may produce significant flux in the UV from lower metallicity old stellar populations or recent star formation. No detection is observed in the stacked UV image to a 5σ UPPER LIMIT to optical-UV colour of $F275W - F814W > 7.2$. A possible $\sim 3\sigma$ detection may be present (Fig. 5.9 with a colour of $F275W - F814W = 7.6$ for the stacked flux from the 20 galaxies. Both the 5σ upper limit and the potential 3σ detection are plotted in Fig. 5.5 (bottom).

As is apparent from Fig. 5.5 (top), the 5σ limit to the stacked colour is as red or redder than the individual colours of Coma and Perseus red sequence galaxies in the same rest-frame bands to the same luminosity limit. To further understand the significance of this, I combined

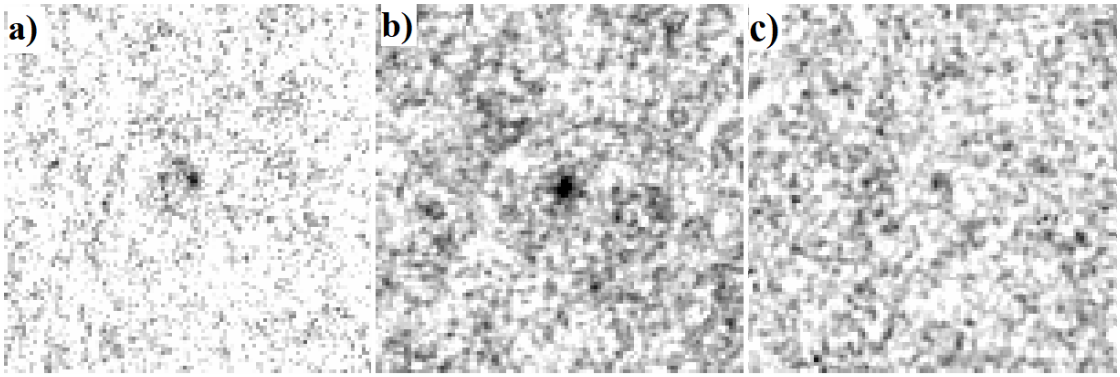

Figure 5.9: 4" by 4" stacks of all galaxies between M_{F814W} ∼-19.7 to -21.7 in MACSJ1149+2223 (a), MACSJ0717+3745 (b) & SDSSJ1004+4112 (c) in the F275W band. The stacks of MACSJ1149+2223 and MACSJ0717+3745 both demonstrate $> 5\sigma$ detections, while the SDSSJ1004+4112 stack corresponds to a $\sim 3\sigma$ detection.

the fluxes in both the UV and optical of all galaxies in Coma within the same g-band luminosity range as SDSSJ1004+4112 (corrected for passive evolution using the fiducial model by Conroy et al. 2009) and plot the resulting equivalent $F275W - F814W$ colour in Fig. 5.5 (bottom). The resultant colour is a magnitude bluer than the 5σ upper limit and ~ 1.5 magnitudes bluer than the possible detection for the $z = 0.68$ stack (see Fig. 5.9). I also repeated this process for MACSJ0717+3745 and MACSJ1149+2223, stacking only non-detections (to avoid the biased sample of detected objects in these clusters, that must be among the galaxies with the stronger upturns). These stacks have clear detections at the 5σ level, the values of which are also plotted in Fig. 5.5 (note that k-corrections were made to the colours to convert them to the equivalent of $z = 0.68$ and $F275W - F814W$). These stacks are again bluer than the upper limit for the stacked galaxies in SDSSJ1004+4112. The stacked images are displayed in Fig. 5.9. Barring the two individually-detected objects in the $z = 0.68$ cluster, one of which is the BCG, the upturn appears to have significantly faded in the general cluster red sequence population between $z = 0.55$ and $z \sim 0.7$ in a relatively rapid fashion, as predicted by the high metallicity (and He-enhanced) models of Bressan et al. (1994) and Tantalo et al. (1996).

Additionally of note is that MACSJ0717+3745 suffers from significantly higher Galactic extinction than the other clusters (about 0.4 mags in F275W). By chance, the effect of this extra dust extinction nearly compensates for the higher distance modulus of SDSSJ1004+4112, especially given that the two images have similar exposure times of about 25ks. If both systems had similar upturn populations, we might then expect to see similar detection statistics for these

populations. Despite this, I obviously detect more galaxies to a similar observed UV detection in MACSJ0717+3745 than in SDSSJ1004+4112, and in stacking the non-detections, I generate clear detections in F275W at a level that is significantly bluer than the upper limit to the non-detection of the equivalent stack in SDSSJ1004+4112. This is further evidence that the upturn has significantly faded across this redshift range - if it didn't we would have expected the two raw UV data sets to be more similar than they are.

It should also be noted that I rejected several galaxies brighter than $M_{F814W} = -21$ on morphological grounds that made the initial optical colour cut for the red sequence in SDSSJ1004+4112. One appeared to be an interacting system and others appeared to have disks that were too structured or edge-on systems too thin to be S0 galaxies. However, these could eventually evolve into classical lower red sequence galaxies (e.g. De Propris et al. 2016) and so I might be excluding a section of the cluster galaxy population that exhibit upturn populations at these redshifts. However, none of these were individually detected at the 5σ level in the UV and so it is unlikely that these systems exhibit upturns of a strength comparable to lower redshift cluster red sequence galaxies of comparable optical luminosity.

My analysis of this whole sample of clusters out to $z \sim 0.7$ therefore implies that the upturn arose across a ~ 1 Gyr period between $z \sim 0.7$ and $z \sim 0.5$ in the general population of galaxies down to $\sim L^*$ in the optical. In the next section I explore the consequences of these findings for galaxy formation and evolution.

5.4 Discussion

5.4.1 Helium rich stars as the source of the UV upturn

The results demonstrate that the range and strength of the upturns in typical cluster red sequence galaxies remain constant between $z = 0$ and $z = 0.55$. The $FUV - V$ and/or $NUV - V$ colours (measures of the upturn strength) between low redshift clusters such as Coma and Perseus are nearly identical to those of Abell 2744 ($z = 0.308$) as well as MACSJ1149+2223 and MACSJ0717+3745 ($z = 0.55$). Assuming a hot HB origin for the upturn, this phenomenon should show an eventual decline with increasing redshift that corresponds to the age at which a blue HB can first start to form, and as such the upturn has not had enough time since the galaxy formed to develop from stars evolving off of the RGB. The upturn should develop rapidly once the turnoff mass reaches a point that allows for the HB to form (Tantalo et al. 1996). In my

analysis of SDSSJ1004+4112, I find that the number of galaxies demonstrating an upturn of similar strength as cluster galaxies at $z \leqslant 0.55$ decreases significantly by $z = 0.68$ - all but two of the brightest galaxies show little to no detectable upturn in rest-frame $1650 - g$ colour at this redshift even after stacking galaxies in a bin spanning 2 magnitudes around the L^* point. Stacking galaxies in the same magnitude range in Coma, MACSJ1149+2223 and MACJ0717+3745 demonstrate strong upturns in each case as discussed earlier. Particularly strong evidence for the fading comes from the fact that MACSJ0717+3745 has an extinction in its $F275W$ band of approximately 0.4 magnitudes, which compensates for the difference in the distance modulus between $z = 0.55$ and $z = 0.68$, thus making the depth of the data effectively identical to that of SDSSJ1004+4112 in the UV. Despite this, clear detections are made in the UV with and without stacking in MACSJ0717+3745, while very few galaxies with a clear upturn detection are seen in SDSSJ1004+4112, despite SDSSJ1004+4112 having a longer total exposure time in $F275W$ compared to MACSJ0717+3745. These results indicate that for typical $\sim L^*$ cluster red sequence galaxies, the upturn emerges at around $z = 0.7$. The individual detection of two of the most massive galaxies (including the BCG) may indicate that their upturns develop earlier, possibly because these are the galaxies with the oldest stellar populations in the cluster. This is consistent with the results of Le Cras et al. (2016) who identified evidence for upturns out to $z \sim 1$ in some (but not all) of the most massive (stellar masses above $10^{11.5}\mathrm{M}_{\odot}$) BOSS ETGs. Alternatively, we could simply be seeing the impact of stochasticity as the upturn starts to develop over a limited range in time across the cluster's galaxy population. Regardless, the upturn must then be fully developed in typical red sequence cluster galaxies by $z = 0.55$ in order to explain the observations in MACSJ1149+2223 and MACSJ0717+3745. The difference in look-back time between these two redshifts is ~ 1 Gyr, a timescale which approximately matches the predictions made by Tantalo et al. (1996) and Chung et al. (2017) for the rapid appearance of an upturn sub-population once the hot HB starts to form.

My data to $z = 0.55$ is broadly consistent with previous work by Brown et al. (1998b, 2000b, 2003) on the brightest galaxies in clusters in the sense that both sets of studies detect upturns in cluster populations out to this redshift. Le Cras et al. (2016) use a series of indices (developed by Fanelli et al. 1992) to measure the strength of the hot HB population in BOSS Luminous Red Galaxies and show evidence for a decline in the upturn strength at $z > 0.6$, though with a subset of the most massive galaxies showing an upturn even at $z = 1$. A caveat on this is that some of the indices used in their work also have some sensitivity to star formation, and Roseboom et al.

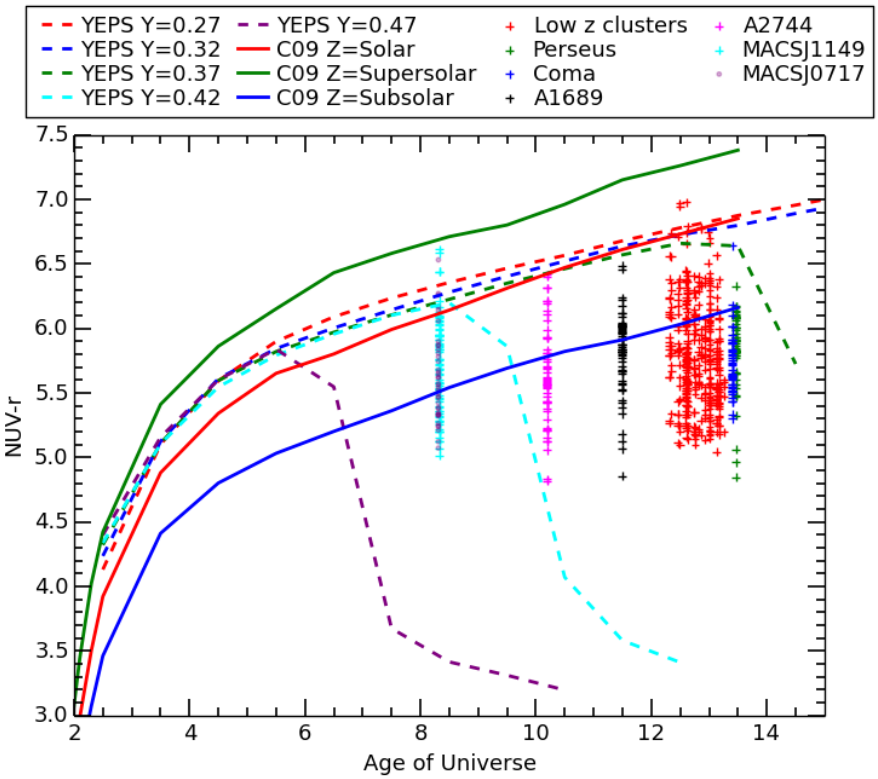

Figure 5.10: YEPS spectrophotometric models (assuming $z_f = 4$ and $Z = Z_\odot$) showing the evolution of the GALEX $NUV - r$ colour over the age of the universe for a range of Helium abundances. Also included in the plot are the predictions from the C09 model with the following metallicities: Z=$Z_\odot$, $0.56Z_\odot$ and $1.78Z_\odot$. Plotted on top are the $NUV - r$ colours of red sequence galaxies in Coma, Perseus, Abell 1689, Abell 2744, MACSJ1149+2223, MACSJ0717+3745 and 20 2dF clusters between $0 \leqslant z \leqslant 0.1$ as detailed in the text. Photometric uncertainties in colours are < 0.2 magnitudes. The upturn is detected at least to $z = 0.55$ with unchanged strength for galaxies down to the $\sim L^*$ level.

(2006) has shown that there is a large fraction of post-starburst galaxies in the LRG sample.

Given the rapid onset of the upturn at $z \sim 0.7$ which then remains consistent up to present day with a range of upturn strengths, the observations can be best explained through the presence of a He-enhanced sub-population of HB stars (superimposed on top of the majority 'red and dead' population that dominates ETGs) for which a transition in the upturn strength is expected at a moderate redshift, as will be shown below. I will also discuss why other proposed sources of the upturn cannot fully explain my observations.

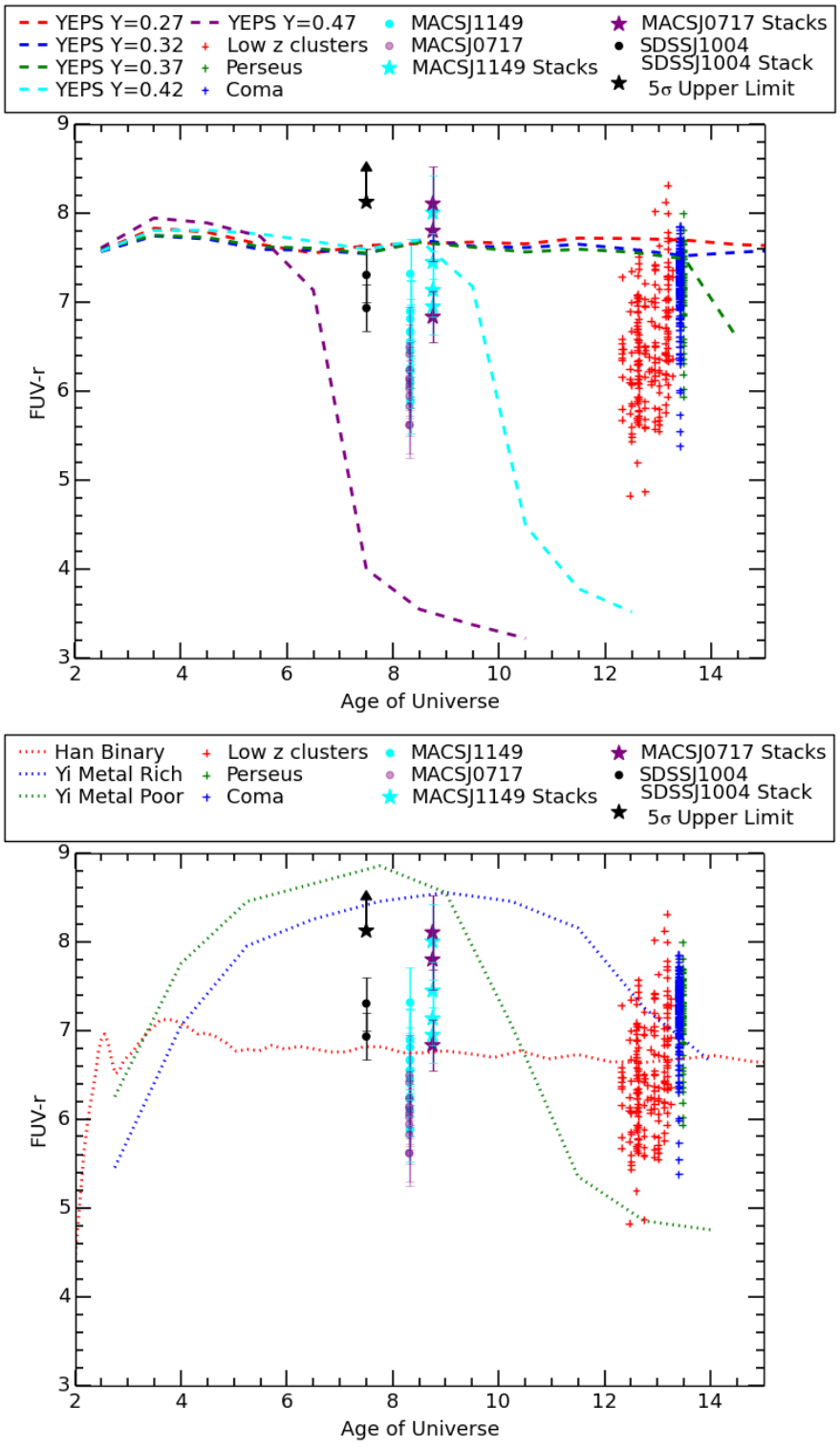

Figure 5.11: *Top*: YEPS spectrophotometric models (assuming $z_f = 4$ and $Z = Z_\odot$) showing the evolution of the GALEX $FUV - r$ colour over the age of the Universe for a range of Helium abundances. Plotted on top are the $FUV - r$ colours of Coma, Perseus, 20 2dF clusters, MACSJ1149+2223, MACSJ0717+3745 and SDSSJ1004+4112 with appropriate k-corrections as detailed in the text. For the $z = 0.55$ clusters, both the individual detections and the stacks (shifted slightly to the right for visual clarity) are plotted from Fig. 5.5. *Bottom*: Same photometric results but this time plotted against the $FUV - r$ colours from the binary model of Han et al. (2007), as well as the metal-rich and metal-poor models of Yi et al. (1999) (Model A and C from their Fig. 7). Photometric uncertainties in colours are < 0.2 magnitudes unless explicitly plotted. The detection of a decrease in the strength of the upturn at $z > 0.65$ implies that a metal-rich He-rich subpopulation with $Y > 0.42$ and $z_f \geqslant 4$ is present in cluster early-type galaxies at a mass fraction of $\sim 10\%$ and is inconsistent with other proposed sources (metal-poor stars, close binaries or mass loss).

5.4.2 The ages and Helium abundances of galaxies

Assuming a He-enhanced HB origin for the upturn, it is then possible to interpret the results within the framework of stellar population synthesis models which allow for a variation in He-abundance, specifically the YEPS models (Chung et al., 2017). These are a series of Simple Stellar Populations that evolve with age depending on the He-abundance (Y) and metallicity (Z). These allow us to make predictions on the age and Y of the sub-populations which can give rise to the upturn in the galaxies being investigated. As before, I note here that Chung et al. (2017) tabulate the YEPS models for a range of Z and Y_{ini}, defined as the initial Helium content of an SSP for which notionally $Z = 0$. The He-abundance, Y, in an actual model is then related to these parameters by $Y = Y_{ini} + 2Z$. I used this relation to calculate Y for the models and use these values in the discussion hereafter.

Fig. 5.10 shows the evolution of the GALEX $NUV-r$ colour against the age of the Universe as predicted by the YEPS models with a range of Y values. Z=$Z_{\odot}$ and a redshift of formation for the stellar population of z_f=4 are assumed. I also plot the time evolution of the same colour for models from Conroy et al. (2009), C09 henceforth, for three different metallicities: Z=$Z_{\odot}$, $0.56Z_{\odot}$ and $1.78Z_{\odot}$, i.e. solar, sub-solar and super-solar. Once again a z_f=4 is assumed for all models. The C09 models have no He-enhancement and as such have no contribution from a hot HB sub-population. Their $NUV - r$ colours are purely driven by the passive evolution of a canonical old stellar population that is thought to be the dominant stellar population in ETGs. The solar metallicity C09 model evolves nearly identically to the $Y = 0.27$ YEPS model, because the latter does not develop an upturn by the present day, unlike the higher Y models. Consequently, neither of these models show the characteristic increase in the UV flux at late ages expected from a He-enhanced population. The YEPS models are for a population which has a single value of Y, i.e. the predicted colours are for a stellar population where *all* stars have the same He-abundance. As shown in chapter 2, it is likely that cluster red sequence galaxies, even those with the strongest upturns, can be modeled with a He-enhanced population of a few percent of the total, the rest being the conventional stellar population of the type modeled in C09. Consequently, we should not expect to see colours as extreme as the bluest YEPS model predictions. The ~ 2 mag difference in the bluest observed $NUV - r$ and YEPS predictions is consistent with a He-enhanced population of order ~ 10 percent of the total stellar population in these galaxies. The YEPS models are tabulated for five discrete values of Y at each Z and so in the following I linearly interpolate between these values of Y where necessary.

Also plotted in Fig. 5.10 are the rest-frame $NUV - r$ colours of Coma and Perseus cluster galaxies from chapter 2, the red sequence galaxies from 20 2dFGRS clusters at $z \lesssim 0.1$ from chapter 3, and those for the Abell 1689 population from chapter 4. Finally I plot the rest-frame $NUV - r$ colours of the red sequence populations of Abell 2744, MACSJ1149+2223 and MACSJ0717+3745 from this chapter, allowing us to compare the evolution of the observed upturn between $z = 0$ and $z = 0.55$ in a large range of cluster galaxies with the predictions from the models. For the $z = 0.55$ clusters, where the observed optical band corresponds to the rest-frame $V-$band, the optical photometry was transformed to r through a k-correction of $V - r = 0.4$ derived from C09, to match the $NUV - r$ colour of the models.

From first glance one can see that in all clusters out to $z = 0.55$ the $NUV - r$ colours range between $\sim 5 - 6.5$ in each case. The clear implication is that the range and strengths of upturns have not evolved in any significant manner over this redshift range. Comparing these results to the YEPS models, I find that most of the reddest galaxies in my sample match the $NUV - r$ colours of the solar metallicity C09 model and the YEPS $Y = 0.27$ model, i.e. the models with little or no upturn. The few galaxies that have redder colours than these models can be easily accommodated with a slightly super-solar metallicity model. This is expected as the majority of galaxies in my sample are giant ellipticals and S0s, which are very likely to have solar or super-solar metallicities (see Price et al. 2011 for an analysis of the metallicity in Coma galaxies). Alternatively, the galaxies in my sample with the bluest $NUV - r$ colours constrain the parameters of valid YEPS models through the onset of the hot HB. The bluest galaxies at $z = 0.55$ constrain any He-enhanced model to have $Y > 0.42$ and, if we interpolate between the tabulated values plotted in Fig. 5.10, $Y \geqslant 0.45$ provided that z_f=4 or lower. Although the constraint on Y can be reduced by increasing z_f, because $z = 4$ is only about 1 Gyr after the first galaxies are thought to have formed, any relaxation still requires a significant He-enhancement.

This prediction for Y is further reinforced by the observed fading in the rest-frame $1650 - g$ colour in SDSSJ1004+4112. Note that data points for SDSSJ1004+4112 could not be directly plotted in Fig. 5.10 as the rest-frame UV data for this system probes the region around 1650Å and any transformation to rest-frame NUV requires a large and, crucially, model dependent k-correction. Galaxies containing a few percent of stars with $Y \sim 0.45$ would be relatively red in the $NUV - r$ at $z = 0.68$ (age of Universe $\sim$ 7.5 Gyrs) because the He-enhanced population would have colours barely different from the majority population at this point, but then get rapidly bluer over the next Gyr, so that by $z = 0.55$ the most extreme members of

the population would be blue enough to cover the entire range of $NUV - r$ colours seen in MACSJ1149+2223 and MACSJ0717+3745. As noted above, an earlier formation redshift can be traded for slightly less He-enrichment ($Y = 0.43 \sim 0.44$ at z_f=6-8), but studies by Jørgensen et al. (2017) suggest formation redshifts between $2 < z_f < 6$ for cluster galaxies.

Fig. 5.11 (top) is a similar plot, but this time for the $FUV - r$ colours predicted by the YEPS models and the observed photometry in all of my clusters with appropriate data, including the values for the photometry of the stacks displayed in Fig. 5.5 (top) and the upper limit from Fig. 5.5 (bottom). The $FUV - r$ C09 models are not plotted - difference in metallicity has little effect on this colour for C09 at $z < 1$ and these colours track those of the low Y YEPS models with an offset due to the different values of the RGB mass loss parameter (η) used in each case. The photometry for the $z = 0.55$ and $z = 0.68$ clusters (observed through the F275W filter) needed to be transformed to rest-frame 1550Å. This transformation was minimal for the SDSSJ1004+4112 photometry (from 1650 to 1550Å) and larger for the two lower redshift clusters (from 1750 to 1550Å). In order to carry out this transformation, I linearly interpolated the range in $1550 - 1650$ and $1550 - 1750$ from the range of $FUV - NUV$ colours displayed by the YEPS models, as well as upturn galaxies in low redshift clusters (typically $1 < FUV - NUV < 2$). I chose a correction appropriate to $FUV - NUV = 1.5$ and added error bars reflecting the full range and therefore maximum uncertainty in potential colours, combined with the measured photometric uncertainties.

Fig. 5.11 (bottom) shows the same photometric results as Fig. 5.11 (top) but now plotted against the evolution of the $FUV - r$ colours as predicted by the binary model of Han et al. (2007) and the metal-rich and metal-poor models from Yi et al. (1999). The lack of evolution to $z = 0.55$ is clearly inconsistent with the predictions of the low metallicity model, as the upturn only develops about 2 Gyrs ago in this case. Similarly, the detection of a transition in the presence of upturns at $z = 0.7$ falsifies the binary evolution model of Han et al. (2007), as such a transition is not expected to be observed, except at very high redshift. Finally, increasing mass loss as a function of metallicity is also less appealing as an explanation, as there is no reason for the rise of the upturn to take place at any particular redshift, and there is also evidence that mass loss on the RGB is not dependent on metal abundance (Miglio et al., 2012; Salaris et al., 2016), while the upturn is observed to correlate with metallicity in ETGs (Burstein et al. 1988). Of the commonly discussed models that seek to explain the upturn and specifically those discussed in this and previous chapters, my observations therefore appear to support only the hypothesis that

the upturn derives from He-rich HB stars, where the transition in upturn strength is a primary prediction of that model.

It is also very clear from this plot that even the two detected galaxies in SDSSJ1004+4112 are redder in $FUV - r$ than the extremes of the range seen in all lower redshift clusters, and the photometry of the non (or barely) detected stack, which contains the combined light from the majority of the red sequence galaxies around L^*, is consistent with little to no upturn. This is completely inconsistent with the results from the lower redshift clusters - the 5σ limit from the SDSSJ1004+4112 stack is as red or redder than the reddest galaxies in all the other clusters. Of note is the much smaller number of the red sequence galaxies in this cluster (in comparison to the other Frontier Fields clusters). Although unlikely, since none of the galaxies in the stack are individually detected to even a 3σ level, small number statistics may still affect the results to some degree. The only way that this cluster shows similar behaviour to those at lower redshift is that its BCG has a similar strength upturn to the other BCGs, perhaps indicating the different fundamental properties of BCGs relative to the rest of the cluster early-type population.

As noted in the previous chapters, these results also have implications for the minimum stellar mass of the galaxies at the earliest stages in their evolution. The results presented here and interpreted in terms of a He-enhanced population origin for the upturn imply that the upturn population is formed by $z = 4$ at the latest *in situ* (see also Goudfrooij 2018). The work done in chapter 2 implies that this population accounts for several percent (and potentially up to ~ 20 per cent in the most extreme objects) of the total stellar mass of each galaxy. For the most massive of the cluster red sequence galaxies today this implies minimum stellar masses at $z = 4$ of order 10^{10} $M_\odot$. This value is almost certainly even larger if, as seems plausible, any He-rich subpopulation is produced from a previous stellar generation (with yields as in globular clusters, the initial generation of stars providing the enrichment must be about 20 times more massive than the second generation – e.g. D'Antona et al. 2016).

All of the above discussion assumes a single value for metallicity and formation redshift for the YEPS models, but in Fig. 5.12 I show the effect of different metallicities and formation redshifts on the YEPS model with $Y = 0.42$ (from Fig. 5.11) as an example. As can be seen from the plots, while the onset of the upturn does depend on these parameters, it is clear that for the models to fit the observed behaviour of the upturn, early formation redshifts ($z_f \geqslant 4$) and comparatively high metallicities (i.e. solar or above) are generally required, supporting my choice of z_f and metallicity in the above discussion.

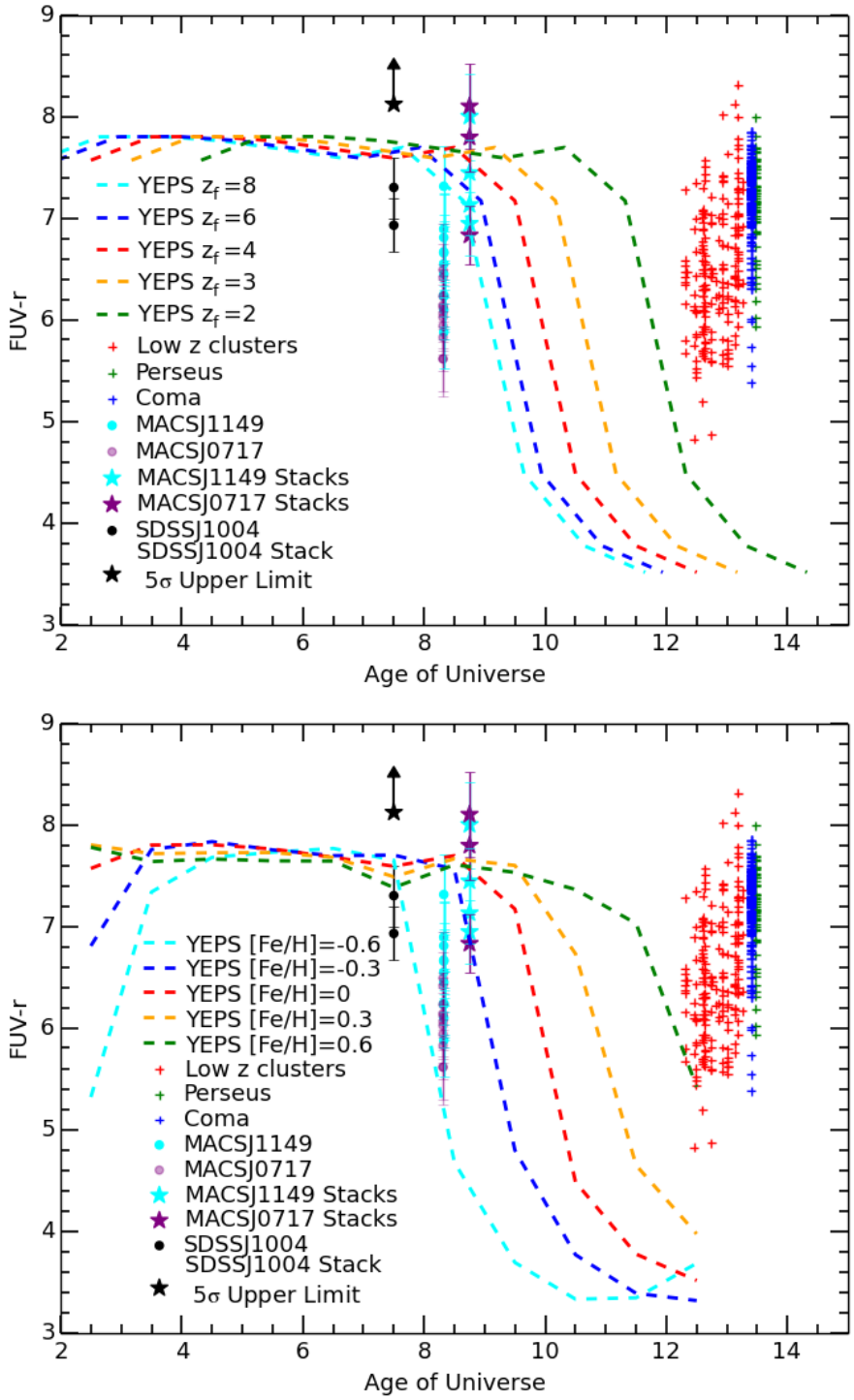

Figure 5.12: YEPS spectrophotometric model for $Y = 0.42$ (from Fig. 5.11 as an example with the same photometric results) showing the evolution of the GALEX $FUV - r$ colour over the age of the Universe for a range of formation redshifts and metallicities. These plots show that for a given Y, later formation redshifts or increasing the metallicity delays the onset of the upturn and vice versa.

5.4.3 Alternative explanations and caveats

The hot HB populations in second parameter globular clusters are generally believed to be He-rich, from both direct and indirect evidence. The observations in this and previous chapters imply that such hot HB stars are also present in some numbers in ETGs. It is reasonable to assume that these are again He-rich, as this is consistent with the evidence presented thus far and with observations of comparatively metal-rich bulge globular clusters in our Galaxy (e.g. Piotto et al. 2005, 2007). Goudfrooij (2018) suggests that these He-rich stars were formed within now dissolved metal-rich globular clusters, whose FUV-bright counterparts are observed around M87 and other galaxies (Peacock et al. 2017). In order to achieve the observed $FUV - V$ colours we require high He abundances, especially given the high metallicities of ETGs; these are comparable to the more extreme stars in Omega Centauri, NGC2808, NGC6388 and NGC6441. The origin of the extra Helium is still in dispute for the Milky Way Globular cluster systems, and even more so for galaxies (Karakas et al. 2006; Maeder & Meynet 2006; Cassisi et al. 2009; Moehler et al. 2011; Ventura et al. 2013; Chantereau et al. 2016). Massive (3-5$M_{\odot}$) AGB stars (Denissenkov et al. 1997) or Fast Rotating Massive Stars (Denissenkov & Merryfield 2011; Denissenkov et al. 2013) have been proposed as candidate polluters, although neither explains the detailed abundance patterns and both require a somewhat contrived star formation history (see review by Bastian & Lardo 2018). However, the balance of observational evidence favours a He-rich subpopulation as the most likely explanation, even if the origin of the Helium enhancement is uncertain.

There are several other parameters that can potentially affect the $NUV - r$ colour of a galaxy besides the presence of an upturn stellar population, particularly the metallicity and age of the main sequence population, which could in theory account for the observed spread in the $NUV - r$ colour. In chapter 4 I explained in detail why these parameters cannot be the strongest driving factors behind the scatter in $NUV - r$, and that it is the upturn that dominates this colour in red sequence galaxies. Here I summarise the key points in my arguments (see chapter 4 for further details). By comparing my results with C09 models of solar, sub-solar and super-solar metallicities as seen in Fig. 5.10, I found that even a comparatively low metallicity model ($0.56Z_{\odot}$), despite being unrealistic for most of my giant elliptical/S0 population around the L^* point (which are likely to have Z=1-2$Z_{\odot}$ as shown for Coma by Price et al. 2011), still cannot account for the full range in $NUV - r$ colours shown by the galaxies. Furthermore, as can be seen from any of the C09 models in Fig. 5.10, a change in age of the SSP by 1 Gyr only brings

about a change of 0.1 mags in $NUV - r$. Given that most cluster red sequences seem to be established by $z \sim 2$ (Newman et al. 2014; Glazebrook et al. 2017), and most star-formation in these galaxies seems to have stopped before $z = 2$ (Kodama et al. 1998; Jørgensen et al. 2017), my reasonable estimate of z_f=4 can only shift by approximately 1 Gyr, clearly insufficient to account for the observed spread in $NUV - r$. As such, an extra component of upturn is required to explain the full spread in $NUV - r$ seen in all of the clusters.

One final parameter that can affect the estimate of age and Y of the stellar populations from the YEPS models is the Reimers' mass loss parameter - η (Reimers 1975, 1977). Once again the effect of this parameter is discussed in greater detail in chapter 4, but in summary, the choice of the mass loss parameter can directly affect the strength and onset of the upturn (since a higher mass loss on the RGB leads to a higher surface temperature of the star in the HB). The η parameter primarily affects the $FUV - NUV$ colour, giving rise to the offset between the $FUV - r$ colours in the C09 and YEPS $Y = 0.27$ (non-upturn) models as noted earlier. The YEPS models plotted in Fig. 5.10 assume $\eta = 0.63$ as calibrated using Milky Way globular clusters, which is also reasonable for the majority of my galaxies. But changing the value of this parameter could likely bring about an uncertainty of ~ 1 Gyr in the age of my models.

Finally, I note here the main caveats in my results. SDSSJ1004+4112 is only one cluster for which the decline in the upturn has been observed in the general red sequence population; suitable data does not yet exist for other clusters at the same or higher redshift. Although SDSSJ1004+4112 is an optically poorer system (in terms of the number of red sequence galaxies selected) than many of the other clusters studied in this and previous chapters, it is still a relatively massive cluster ($\sim 3 \times 10^{14} M_{\odot}$ – Oguri et al. 2012) showing significant strong and weak gravitational lensing. My comparison of $FUV - V$ colours for galaxies in Coma, Perseus and Fornax - which themselves span a decade in mass - shows that this colour does not depend on environment. I have also used 20 clusters at $z \lesssim 0.1$ from 2dFGRS where FUV and NUV colours have been measured for a complete sample of spectroscopically identified members down to $M_K = -21$, with SDSS and PanStarrs1 optical colours. The $FUV - r$ colour of their red sequence galaxies was found to not depend on cluster velocity dispersion or X-ray luminosity, and therefore the results in SDSSJ1004+4112 are likely to apply to the general population of galaxies at its redshift. In other words, the upturn phenomenon is internal to galaxies, and therefore unrelated to star formation history as affected by the cluster environment. A similar result was obtained by Yi et al. (2011), Loubser & Sánchez-Blázquez (2011) and Boissier

et al. (2018) who also suggested that the upturn is intrinsic to galaxies and not related to their environments.

While the fading in the upturn is therefore very likely to take place at around $z = 0.7$ given the limited time required to evolve a He-enhanced hot HB prior to this, it is possible that SDSSJ1004+4112 may be an outlier, also because it is not as rich in high mass red sequence galaxies as the two $z = 0.55$ systems it is compared to. In order to fully confirm my results, it would be best to observe several more clusters in the UV at $z = 0.7 - 1$. This small redshift window is particularly important as it is during this time that the upturn is likely to be developing while the observed epoch is late enough that the bulk of the population is passively evolving (and therefore comparatively red). Regardless of the observed fading in the upturn at $z = 0.7$, which places an upper limit on the amount of He-enhancement required to produce the observed upturn, a Y of 0.45 (or higher for later formation redshifts than z_f=4) is necessary to account for the upturn seen in MACSJ1149+2223 and MACSJ0717+3745 at $z = 0.55$, along with all other clusters at lower redshifts.

5.5 Conclusions

I have measured the evolution of the UV upturn to $z = 0.7$ from archival UV images of four clusters. I detect no evolution in the strength and range of the upturn exhibited by cluster red sequence galaxies out to $z = 0.55$ but then observe a strong decline to $z = 0.7$. This behaviour rules out most of the theoretical models for the origin of the upturn, but is predicted by those where the increased UV emission arises from a population of He-enhanced stars which have evolved onto the (hot) horizontal branch. This implies that a fraction of the stellar population in such galaxies (perhaps up to $\sim 10 - 20\%$ for the those with the strongest upturns) has high ($Y \geqslant 0.45$) Helium abundance and large formation ages ($z_f \geqslant 4$), and that objects at these redshifts had *in situ* stellar masses of the order of $10^{10}\ M_{\odot}$ at these early epochs.

6

Conclusion

The UV upturn is a rise in the spectra of early-type galaxies shortward of 2500Å down to the Lyman limit. It is caused by a minority, yet exotic population of hot horizontal branch stars. Given that the upturn appears to be ubiquitous feature in all old and quiescent galaxies, it is important to understand the characteristics of the sub-population driving the phenomenon, and its evolution. This understanding is paramount to better guide the theories of galaxy formation, evolution and chemical enrichment as a whole.

The key objectives achieved in this PhD project were as follows:

- To characterise the hot HB population, the main driver of the upturn, within cluster ETGs in the local Universe.
- To explore the effect of the cluster environment on the upturn.
- To analyse the evolution of the upturn in a large sample of cluster ETGs with varying luminosities, spanning a wide redshift range between $0 < z < 0.7$.
- To compare the observed evolution of the upturn to the predictions from all major models for the origin of the upturn, in order to determine the most likely mechanism that is giving rise to the hot HB stars in cluster ETGs.

6.1 Characteristics of the UV Upturn

In chapter 2, the red sequence in Coma, Fornax and Perseus clusters were selected from their optical $g-r$ or $B-V$ colour-magnitude diagrams. These are quiescent, 'red and dead' galaxies with little to no ongoing star-formation activity - objects that are known to exhibit the UV upturn. To analyse the upturn, the GALEX $FUV-V$ colour of the red sequence was measured, going well below the L^* point for each cluster. The $6 < FUV-V < 8$ for giant ellipticals was broadly consistent between all three clusters (as well as Virgo from Boselli et al. 2005), indicating that the upturn is a ubiquitous feature in all cluster ETGs at low redshift. In the case of Fornax, the UV output from a subset of the dwarf elliptical population was also picked up, which showed much bluer $FUV-V$ colours with decreasing luminosity compared to their giant elliptical counterparts, most likely due to ongoing star-formation in this galaxy type (also consistent with the findings by Boselli et al. 2005 in Virgo).

Focusing on the central Coma cluster galaxies, these were observed in the UV by both GALEX (FUV and NUV) and UVOT ($UVW2$ and $UVW1$) detectors, giving contiguous coverage between ∼1000-3000Å in the UV. When combined with the optical U, B, V data from UVOT, it was possible to create comparatively detailed UV-to-optical SEDs for a subset of the overall Coma red sequence galaxies, ones that were observed by both GALEX and UVOT. The SEDs were then fitted with a canonical C09 SSP model (assuming $z_f = 4$ and $Z = Z_\odot$) that replicates the output from the majority 'red and dead' population, superimposed with a black-body of variable temperature and extinction (following the Milky Way law from Cardelli et al. 1988), which simulates the output from the hot HB population giving rise to the upturn. The model fitting procedure yielded a range of temperatures between 10,000-21,000K for the upturn population and a fraction of blue HB to turnoff stars between 4-20%. The temperature of the hot HB, as well as the fraction of blue HB to turnoff stars were correlated with the galaxy luminosity/mass, i.e. more massive metal-rich galaxies tended to consist of both a hotter and larger fraction of blue HB population. These results are broadly consistent with the findings of Brown et al. (1997) and Le Cras et al. (2016). Assuming a He-enhanced origin for the hot HB population, the YEPS spectrophotometric models (Chung et al. 2017) predict $Y = 0.38$ for the galaxies studied at this redshift (with $z_f = 4$ and $Z = Z_\odot$). This also implies at least $\sim 0.5 \times 10^{10}\ M_\odot$ of the He-enriched sub-population needs to be in place by $z \sim 4$ if the estimated Y is reasonable.

In chapter 3, the effect of cluster environment on the strength of the upturn was tested in 20

2dF clusters of a variety of sizes and richness. For each of these clusters, similar to chapter 2, the red sequence was determined from the SDSS $g - r$ or UKST $B_J - R_F$ colours. Subsequently for the red sequence members, the GALEX $FUV - r$ and $NUV - r$ were also calculated, both a measure of the upturn strength, which had values between $5.5 < FUV - r < 7.5$ and $5 < NUV - r < 6.5$. The $\sim$ 2 and $\sim$ 1.5 magnitude ranges in each colour respectively are consistent with the results from Coma, Fornax and Perseus, further providing evidence that the upturn is a ubiquitous feature in all cluster ETGs. The $FUV - r$ and $NUV - r$ colours were then plotted against the velocity dispersion and X-ray luminosity of each cluster, as well as the clustercentric distances and line-of-sight velocities of the galaxies - parameters which are defined by the cluster environment. In each case, no correlation was found indicating that the strength of the upturn is unaffected by the cluster environment and that this phenomenon is intrinsic to ETGs, a conclusion that was reached for BCGs by Donahue et al. (2010) and Boissier et al. (2018). The test was repeated for Coma and Perseus ETGs and nearly identical results were recovered for those clusters as well.

6.2 Evolution of the UV Upturn

In chapter 4, the strength of the upturn in the Abell 1689 ($z = 0.18$) cluster of galaxies was explored. The HST $F225W - F625W$ and $F275W - F625W$ colours (rest-frame $\sim 1900 - V$ and $\sim 2300 - V$) demonstrated spreads of $\sim$ 2 and $\sim$ 1.5 magnitudes respectively, which were comparable to the Coma $UVW2 - V$ and $NUV - V$ colours. Using HST F225W, F275W, F336W, F475W and F625W data, UV-to-optical SEDs of Abell 1689 red sequence galaxies encompassing $1500 < \lambda < 5500$ were generated. The SEDs of Abell 1689 galaxies appeared mostly similar to the Coma SEDs from chapter 2 despite the difference in redshift between the clusters, strongly suggesting that the strength in the upturn has not evolved significantly over the past 2.2 Gyrs. Assuming a He-enriched origin for the hot HB stars and comparing the observed results with the YEPS spectrophotometric models gave an estimate of $Y = 0.40 - 0.41$ for $z_f = 4 \sim 6$ and $Z = Z_\odot$. An even higher Y is necessary to account for the upturn in Abell 1689 compared to the lower redshift clusters because the He-enhanced stars would need to evolve on to the hot HB faster in the former case, which is only possible through the shorter MS lifetimes at higher Y.

Chapter 5 expanded further on this work by examining the evolution of the upturn in four

more clusters out to $z \approx 0.7$. These include Abell 2744 ($z = 0.31$), MACSJ0717+3745 ($z = 0.55$), MACSJ1149+2223 ($z = 0.54$) and SDSSJ1004+4112 ($z = 0.68$), reaching a lookback time out to 6.3 Gyrs. For the optically selected red sequence members in Abell 2744, MACSJ0717+3745 and MACSJ1149+2223, the $F275W - F814W$ (Abell 2744) and $F336W - F814W$ (MACSJ0717+3745 and MACSJ1149+2223) were calculated, corresponding roughly to rest-frame $NUV - r$ and $NUV - V$ respectively. These colours were found to be dominated by the output from the hot HB (upturn) population and were consistent with those of Coma, Perseus and other low redshift clusters studied in the earlier chapters. Furthermore, for MACSJ0717+3745, MACSJ1149+2223 and SDSSJ1004+4112, $F275W - F814W$ roughly corresponded to $FUV - V$ after performing some minor k-corrections. Due to the large distance to these clusters, only a handful of the brightest upturn galaxies were directly detected in the $F275W$ band. However, by performing a stacking analysis of all the non-detected galaxies across multiple bins spanning several magnitudes in range, extending to and beyond the L^* point, it was possible to get multiple $\geqslant 5\sigma$ detections for the stacks in $F275W$ for both MACSJ0717+3745 and MACSJ1149+2223. These stacks remarkably showed colours that were roughly comparable to those of low redshift cluster galaxies, indicating that the prevalence and incidence of the upturn persisted out $z = 0.55$ without showing any signs of significant evolution.

When the same analysis was repeated for SDSSJ1004+4112, only 2 galaxies, one of which was the BCG was directly detected above a 5σ level in $F275W$. These had $FUV - V$ colours similar to lower redshift clusters. A potential $\sim 3\sigma$ detection was found for the stack consisting of all non-detected red sequence members, with a $FUV - V$ colour over a magnitude redder than that of the $z = 0.55$ and Coma clusters. These results indicate that the upturn has faded significantly in the general ETG population between $z = 0.55$ and $z = 0.68$, but for the very brightest galaxies, ones that are likely to have formed the earliest, the upturn still remains intact. This is perhaps indicative of the time taken between BCG and ETG formation. The latter result is in line with Le Cras et al. (2016), who found that the upturn is present in the very brightest/massive ETGs up to $z = 1$, though its frequency in these galaxies decreases significantly above $z = 0.6$.

Finally, all of the aforementioned results were put into the framework of the four main models for the UV upturn - metal-poor, enhanced mass loss, binary and He-enrichment. Comparing the observed results with the model predictions, the following conclusions were reached:

- The metal-poor HB model is clearly unfeasible for explaining the observed upturn as it predicts that the upturn should disappear at a low redshift ($z \approx 0.25$), while the upturn is observed consistently in all ETGs out to at least $z = 0.55$, and in BCGs at $z = 0.68$.
- The binary model also does not match the observed data, given that it predicts that the upturn strength should remain constant out to very high redshifts ($z \approx 3$), when in reality the upturn is observed to fade strongly between $z = 0.55$ and $z = 0.68$ in the majority red sequence population.
- Enhanced mass loss in the RGB also does not seem to be supported by the data, as the upturn in this case should gradually get stronger from moderate to low redshift after its onset at $z \sim 0.5$. In observations of clusters at a range of redshifts, the upturn strength seems to remain roughly constant out to $z = 0.55$, before rapidly fading away in the next 1-1.5 Gyrs (though this fading is only observed in one cluster thus far).
- He-enrichment is the only model that appears to be consistent with the observations. Assuming a very high Y of 0.45 ($z_f = 4$ and $Z = Z_{\odot}$) reproduces an upturn population by the models that turns on at $z \sim 0.7$ and becomes blue enough within ~ 1 Gyr to account for the full range in $FUV - V$ seen in the $z \leqslant 0.55$ clusters. For later formation redshifts and/or higher metallicities, Y would need to be even higher and vice versa.

It should be noted that while the results presented in this thesis strongly suggest a He-enhanced origin for the upturn over all other models, there is still no self-consistent theoretical explanation as to how such a high $Y(> 0.45)$ can be present in ETGs. Some models have been suggested, such a dissolved metal-rich globular clusters being the source of the He-enhanced stars in ETGs, but none of the models can fully replicate all observed parameters simultaneously. Recent spectroscopic observations of local star clusters have directly proven the existence of He-enhanced RGB/HB stars (e.g. Dupree et al. 2011; Marino et al. 2014), which strengthens the plausibility of the upturn being driven by He-enhanced hot HB stars, but more theoretical and observational work still needs to be undertaken in order to find a plausible mechanism that can explain the predicted high He content in metal-rich systems. Given that the upturn is a strong function of age, such high levels of $Y(\geqslant 0.45)$ if truly present in galaxies at $z_f \geqslant 4$ would require canonical models of galaxy formation and chemical enrichment to be revised.

6.3 Future Work

In this project, the fading of the upturn at $z = 0.68$ was observed in only one galaxy cluster, which was markedly poorer in terms of richness compared to all other lower redshift clusters studied. Thus it is possible that the results from this cluster may be an outlier. To confirm the results, another rich cluster would need to be observed in the small redshift window of $z \sim 0.7 - 1$, during which time the upturn is still expected to be developing, while the epoch is still late enough such that the overall population is quiescent and passively evolving. UV data for such a cluster does not currently exist in any relevant archives. To that end, we have recently submitted a proposal to undertake HST observations of the massive rich cluster MS1054-0321 at $z = 0.83$ in the F275W (rest-frame 1500Å) band, with a total integration time of 175ks to reach an AB magnitude of 28.5 at 5σ level. This cluster already has deep V, I and z data from HST, as well as ground based and Spitzer data in many other wavebands. If observed, it will be possible to probe the upturn in the general red sequence population at $z = 0.83$, where it should be almost entirely non-existent apart from potentially in the BCG. If true, it should also place a strong upper limit on the He-enrichment parameter, Y, in ETGs.

Another avenue for further work in this area would be to expand the study of the upturn to field galaxies. In chapter 3 I concluded that the upturn in ETGs is unaffected by the environment of the host cluster, and that the He-enhancement occurs intrinsically within the galaxies at very high redshift, potentially before they even became part of clusters. If this is true, then field ETGs should also exhibit an upturn. To test this hypothesis, an initial attempt was made to analyse the $FUV - r$ colours of a large sample of GAMA galaxies with available GALEX data at $z < 0.1$. However, given the already smaller ETG population in the field compared to clusters and after making a similar optical $g - r$/$u - r$ cut as with cluster red sequences to determine quiescent ETGs in the field, I was left with a very small number of galaxies in the sample (< 50), for which the $FUV - r$ colour showed a larger spread of ~ 3 magnitudes compared to the ~ 2 magnitudes of cluster ETGs. In general there were a lot more field ETGs with bluer $FUV - r$ colours than cluster ETGs. This preliminary analysis suggests that field ETGs likely have some level of residual star-formation, making their overall optical and UV colours bluer. To properly extend this study, it would be best to perform the analysis on a large sample of field early-type spirals, which are much more common in the field compared to ETGs. As demonstrated in the early work of Brown et al. (1997), the bulge of early-type spirals such as M31 demonstrate a

strong upturn, given the similarity between the stellar populations in the bulge of spirals and ellipticals. If the bulge to disk ratio is known for the field galaxies, it may be possible to separate the UV emission from the bulge and the disk in early-type spirals in the local Universe. That would in turn allow us to find if the UV upturn exists in old stellar populations outside of dense environments. Though such an analysis may be challenging due to potential gas flow from bulge to disk.

Bibliography

Abadi M. G., Moore B., Bower R. G., 1999, MNRAS, 308, 947

Alam S., et al., 2015, ApJS, 219, 12

Alamo-Martínez K. A., et al., 2013, ApJ, 775, 20

Alavi A., et al., 2016, ApJ, 832, 56

Ali S. S., Bremer M. N., Phillipps S., De Propris R., 2018a, MNRAS, 476, 1010

Ali S. S., Bremer M. N., Phillipps S., De Propris R., 2018b, MNRAS, 478, 541

Ali S. S., Bremer M. N., Phillipps S., De Propris R., 2018c, MNRAS, 480, 2236

Aragon-Salamanca A., Baugh C. M., Kauffmann G., 1998, MNRAS, 297, 427

Avila R. J., 2017, Advanced Camera for Surveys Instrument Handbook for Cycle 25 v. 16.0

Bañados E., Hung L.-W., De Propris R., West M. J., 2010, ApJ, 721, L14

Badenes C., et al., 2017, preprint, (arXiv:1711.00660)

Barazza F. D., Jogee S., Marinova I., 2008, ApJ, 675, 1194

Bastian N., Lardo C., 2018, Annual Review of Astronomy and Astrophysics, 56, 83

Baum W. A., 1959, PASP, 71, 106

Bautz L. P., Morgan W. W., 1970, ApJ, 162, L149

Bedin L. R., Piotto G., Anderson J., Cassisi S., King I. R., Momany Y., Carraro G., 2004, ApJ, 605, L125

Bekki K., 2011, MNRAS, 412, 2241

Bekki K., 2012, ApJ, 747, 78

Bertin E., Arnouts S., 1996, A&AS, 117, 393

Bertola F., Capaccioli M., Holm A. V., Oke J. B., 1980, ApJ, 237, L65

Bertola F., Capaccioli M., Oke J. B., 1982, ApJ, 254, 494

Bertola F., Bressan A., Burstein D., Buson L. M., Chiosi C., di Serego Alighieri S., 1995, ApJ, 438, 680

Blanton M. R., Moustakas J., 2009, ARA&A, 47, 159

Boesgaard A. M., Jensen E. E. C., Deliyannis C. P., 2009, AJ, 137, 4949

Boesgaard A. M., Lum M. G., Deliyannis C. P., 2015, ApJ, 799, 202

Boissier S., Cucciati O., Boselli A., Mei S., Ferrarese L., 2018, A&A, 611, A42

Boselli A., et al., 2005, ApJ, 629, L29

Bower R. G., Lucey J. R., Ellis R. S., 1992, MNRAS, 254, 601

Bower R. G., Terlevich A., Kodama T., Caldwell N., 1999, in Carral P., Cepa J., eds, Astronomical Society of the Pacific Conference Series Vol. 163, Star Formation in Early Type Galaxies. p. 211 (arXiv:astro-ph/9808325)

Bragaglia A., Tosi M., Andreuzzi G., Marconi G., 2006, MNRAS, 368, 1971

Bragaglia A., et al., 2010, ApJ, 720, L41

Bressan A., Chiosi C., Fagotto F., 1994, ApJS, 94, 63

Brodie J. P., Strader J., 2006, ARA&A, 44, 193

Brown T. M., Ferguson H. C., Davidsen A. F., Dorman B., 1997, ApJ, 482, 685

Brown T. M., Ferguson H. C., Stanford S. A., Deharveng J.-M., 1998a, ApJ, 504, 113

Brown T. M., Ferguson H. C., Deharveng J.-M., Jedrzejewski R. I., 1998b, ApJ, 508, L139

Brown T. M., Bowers C. W., Kimble R. A., Ferguson H. C., 2000a, ApJ, 529, L89

Brown T. M., Bowers C. W., Kimble R. A., Sweigart A. V., Ferguson H. C., 2000b, ApJ, 532, 308

Brown T. M., Ferguson H. C., Smith E., Bowers C. W., Kimble R. A., Renzini A., Rich R. M., 2003, ApJ, 584, L69

Brown P. J., Breeveld A. A., Holland S., Kuin P., Pritchard T., 2014, Ap&SS, 354, 89

Brunzendorf J., Meusinger H., 1999, A&AS, 139, 141

Bureau M., et al., 2011, MNRAS, 414, 1887

Burstein D., Bertola F., Buson L. M., Faber S. M., Lauer T. R., 1988, ApJ, 328, 440

Butcher H., Oemler Jr. A., 1978a, ApJ, 219, 18

Butcher H., Oemler Jr. A., 1978b, ApJ, 226, 559

Buzzoni A., Bertone E., Carraro G., Buson L., 2012, ApJ, 749, 35

Cardelli J. A., Clayton G. C., Mathis J. S., 1988, ApJ, 329, L33

Carlberg R. G., et al., 1997, ApJ, 485, L13

Carraro G., Benvenuto O. G., 2017, ApJ, 841, L10

Carretta E., 2012, in Chemical Evolution of the Milky Way. p. 12

Carter D., Pass S., Kennedy J., Karick A. M., Smith R. J., 2011, MNRAS, 414, 3410

Cassisi S., Salaris M., Anderson J., Piotto G., Pietrinferni A., Milone A., Bellini A., Bedin L. R., 2009, ApJ, 702, 1530

Catelan M., 2009, Astrophysics and Space Science Proceedings, 7, 175

Chaboyer B., Green E. M., Liebert J., 1999, AJ, 117, 1360

Chantereau W., Charbonnel C., Decressin T., 2015, A&A, 578, A117

Chantereau W., Charbonnel C., Meynet G., 2016, A&A, 592, A111

Chantereau W., Usher C., Bastian N., 2018, MNRAS, 478, 2368

Charbonnel C., 2016, in Moraux E., Lebreton Y., Charbonnel C., eds, EAS Publications Series Vol. 80, EAS Publications Series. pp 177–226 (arXiv:1611.08855), doi:10.1051/eas/1680006

Chung C., Yoon S.-J., Lee Y.-W., 2017, ApJ, 842, 91

Code A. D., 1969, PASP, 81, 475

Code A. D., Welch G. A., 1979, ApJ, 228, 95

Colless M., Dunn A. M., 1996, ApJ, 458, 435

Conroy C., Gunn J. E., White M., 2009, ApJ, 699, 486

D'Antona F., Bellazzini M., Caloi V., Pecci F. F., Galleti S., Rood R. T., 2005, ApJ, 631, 868

D'Antona F., Ventura P., Caloi V., D'Ercole A., Vesperini E., Carini R., Di Criscienzo M., 2010, ApJ, 715, L63

D'Antona F., Vesperini E., D'Ercole A., Ventura P., Milone A. P., Marino A. F., Tailo M., 2016, MNRAS, 458, 2122

D'Ercole A., Vesperini E., D'Antona F., McMillan S. L. W., Recchi S., 2008, MNRAS, 391, 825

Dalessandro E., Schiavon R. P., Rood R. T., Ferraro F. R., Sohn S. T., Lanzoni B., O'Connell R. W., 2012, AJ, 144, 126

Danese L., de Zotti G., di Tullio G., 1980, A&A, 82, 322

De Lucia G., Springel V., White S. D. M., Croton D., Kauffmann G., 2006, MNRAS, 366, 499

De Propris R., 2000, MNRAS, 316, L9

De Propris R., 2017, MNRAS, 465, 4035

De Propris R., Phillipps S., Bremer M. N., 2013, MNRAS, 434, 3469

De Propris R., Bremer M. N., Phillipps S., 2016, MNRAS, 461, 4517

Denissenkov P. A., Merryfield W. J., 2011, ApJ, 727, L8

Denissenkov P. A., Weiss A., Wagenhuber J., 1997, A&A, 320, 115

Denissenkov P. A., Herwig F., Truran J. W., Paxton B., 2013, ApJ, 772, 37

Diaferio A., Geller M. J., Rines K. J., 2005, ApJ, 628, L97

Donahue M., et al., 2010, ApJ, 715, 881

Donas J., et al., 2007, ApJS, 173, 597

Dorman B., O'Connell R. W., Rood R. T., 1995, ApJ, 442, 105

Dressel L., 2017, Wide Field Camera 3 Instrument Handbook for Cycle 25 v. 9.0

Dressler A., 1980a, ApJS, 42, 565

Dressler A., 1980b, ApJ, 236, 351

Dressler A., 1984, ARA&A, 22, 185

Dressler A., et al., 1997, ApJ, 490, 577

Drinkwater M. J., et al., 2000, A&A, 355, 900

Dubinski J., 1998, ApJ, 502, 141

Dupree A. K., Avrett E. H., 2013, ApJ, 773, L28

Dupree A. K., Strader J., Smith G. H., 2011, ApJ, 728, 155

Eisenhardt P. R., De Propris R., Gonzalez A. H., Stanford S. A., Wang M., Dickinson M., 2007, ApJS, 169, 225

Ellis R. S., Smail I., Dressler A., Couch W. J., Oemler Jr. A., Butcher H., Sharples R. M., 1997, ApJ, 483, 582

Fanelli M. N., O'Connell R. W., Burstein D., Wu C.-C., 1992, ApJS, 82, 197

Farouki R. T., Shapiro S. L., 1982, ApJ, 259, 103

Ferguson H. C., Sandage A., 1988, AJ, 96, 1520

Ferrarese L., et al., 2016, ApJ, 824, 10

Ferraro F. R., Sollima A., Pancino E., Bellazzini M., Straniero O., Origlia L., Cool A. M., 2004, ApJ, 603, L81

Forbes D. A., Sánchez-Blázquez P., Phan A. T. T., Brodie J. P., Strader J., Spitler L., 2006, MNRAS, 366, 1230

Forbes D. A., et al., 2018, Proceedings of the Royal Society of London Series A, 474, 20170616

Gadotti D. A., de Souza R. E., 2006, ApJS, 163, 270

Gallagher III J. S., Ostriker J. P., 1972, AJ, 77, 288

García Pérez A. E., et al., 2013, ApJ, 767, L9

Genzel R., Tacconi L. J., Rigopoulou D., Lutz D., Tecza M., 2001, ApJ, 563, 527

Giavalisco M., 2002, ARA&A, 40, 579

Giavalisco M., Macchetto F. D., Madau P., Sparks W. B., 1995, ApJ, 441, L13

Giavalisco M., Steidel C. C., Macchetto F. D., 1996, ApJ, 470, 189

Gil de Paz A., et al., 2007, ApJS, 173, 185

Glazebrook K., et al., 2017, Nature, 544, 71

Gonzaga S., 2012, The DrizzlePac Handbook

Goudfrooij P., 2018, ApJ, 857, 16

Graham A. W., Guzmán R., 2003, AJ, 125, 2936

Gratton R. G., Carretta E., Bragaglia A., 2012, A&A Rev., 20, 50

Greggio L., Renzini A., 1990, ApJ, 364, 35

Gunn J. E., Gott III J. R., 1972, ApJ, 176, 1

Halkola A., Seitz S., Pannella M., 2006, MNRAS, 372, 1425

Hammer D., Hornschemeier A. E., Mobasher B., Miller N., Smith R., Arnouts S., Milliard B., Jenkins L., 2010, ApJS, 190, 43

Han Z., Podsiadlowski P., Maxted P. F. L., Marsh T. R., Ivanova N., 2002, MNRAS, 336, 449

Han Z., Podsiadlowski P., Maxted P. F. L., Marsh T. R., 2003, MNRAS, 341, 669

Han Z., Podsiadlowski P., Lynas-Gray A. E., 2007, MNRAS, 380, 1098

Harris W. E., Ciccone S. M., Eadie G. M., Gnedin O. Y., Geisler D., Rothberg B., Bailin J., 2017, ApJ, 835, 101

Holden B. P., Stanford S. A., Eisenhardt P., Dickinson M., 2004, AJ, 127, 2484

Howes L. M., et al., 2014, MNRAS, 445, 4241

Howes L. M., et al., 2015, Nature, 527, 484

Hubble E. P., 1926, ApJ, 64

Hubble E. P., 1936, Realm of the Nebulae

Inada N., et al., 2003, Nature, 426, 810

Jeong H., et al., 2009, MNRAS, 398, 2028

Jeong H., et al., 2012, MNRAS, 423, 1921

Jester S., et al., 2005, AJ, 130, 873

Johnson H. M., 1979, ApJ, 230, L137

Jones C., Forman W., 1984, ApJ, 276, 38

Jordán A., Côté P., West M. J., Marzke R. O., Minniti D., Rejkuba M., 2004, AJ, 127, 24

Jørgensen I., Chiboucas K., Berkson E., Smith O., Takamiya M., Villaume A., 2017, AJ, 154, 251

Karakas A. I., Fenner Y., Sills A., Campbell S. W., Lattanzio J. C., 2006, ApJ, 652, 1240

Karick A. M., Drinkwater M. J., Gregg M. D., 2003, MNRAS, 344, 188

Kaviraj S., Sohn S. T., O'Connell R. W., Yoon S.-J., Lee Y. W., Yi S. K., 2007, MNRAS, 377, 987

Kennicutt Jr. R. C., 1992, ApJS, 79, 255

Kennicutt Jr. R. C., 1998, ARA&A, 36, 189

Kent S. M., Sargent W. L. W., 1983, AJ, 88, 697

Kodama T., Arimoto N., Barger A. J., Arag'ón-Salamanca A., 1998, A&A, 334, 99

Koekemoer A. M., et al., 2017, in American Astronomical Society Meeting Abstracts #230. p. 316.13

Komiyama Y., et al., 2002, ApJS, 138, 265

Kormendy J., 1979, ApJ, 227, 714

Kormendy J., 1982, Morphology and dynamics of galaxies; Proceedings of the Twelfth Advanced Course, Saas-Fee, Switzerland, March 29-April 3, 1982 (A84-15502 04-90). Sauverny, Switzerland, Observatoire de Geneve, 1983, p. 113-288., 12, 113

Kormendy J., 1985, ApJ, 295, 73

Kravtsov A. V., Borgani S., 2012, ARA&A, 50, 353

Kravtsov A. V., Vikhlinin A., Nagai D., 2006, ApJ, 650, 128

Kron R. G., 1980, ApJS, 43, 305

Larson R. B., 1975, MNRAS, 173, 671

Larson R. B., Tinsley B. M., Caldwell C. N., 1980, ApJ, 237, 692

Lauer T. R., Faber S. M., Ajhar E. A., Grillmair C. J., Scowen P. A., 1998, AJ, 116, 2263

Le Cras C., Maraston C., Thomas D., York D. G., 2016, MNRAS, 461, 766

Lee Y.-W., Joo J.-M., Sohn Y.-J., Rey S.-C., Lee H.-C., Walker A. R., 1999, Nature, 402, 55

Lee Y.-W., et al., 2005a, ApJ, 619, L103

Lee Y.-W., et al., 2005b, ApJ, 621, L57

Lima Neto G. B., Lagana T. F., Andrade-Santos F., Machado R. E. G., 2014, preprint, (arXiv:1406.1496)

Linden S. T., et al., 2017, ApJ, 842, 49

Livermore R. C., Finkelstein S. L., Lotz J. M., 2017, ApJ, 835, 113

Loubser S. I., Sánchez-Blázquez P., 2011, MNRAS, 410, 2679

Maeder A., Meynet G., 2006, A&A, 448, L37

Mamon G. A., 1987, ApJ, 321, 622

Maoz D., Filippenko A. V., Ho L. C., Macchetto F. D., Rix H.-W., Schneider D. P., 1996, ApJS, 107, 215

Marino A. F., et al., 2014, MNRAS, 437, 1609

Markwardt C. B., Tueller J., Skinner G. K., Gehrels N., Barthelmy S. D., Mushotzky R. F., 2005, ApJ, 633, L77

Martin D. C., et al., 2005, ApJ, 619, L1

McCarthy I. G., Frenk C. S., Font A. S., Lacey C. G., Bower R. G., Mitchell N. L., Balogh M. L., Theuns T., 2008, MNRAS, 383, 593

McLeod D. J., McLure R. J., Dunlop J. S., 2016, MNRAS, 459, 3812

Mei S., et al., 2006, ApJ, 644, 759

Michard R., Andreon S., 2008, A&A, 490, 923

Mieske S., et al., 2004, AJ, 128, 1529

Miglio A., et al., 2012, MNRAS, 419, 2077

Milone A. P., et al., 2015, ApJ, 808, 51

Milone A. P., et al., 2018, MNRAS, 481, 5098

Moehler S., Dreizler S., Lanz T., Bono G., Sweigart A. V., Calamida A., Nonino M., 2011, A&A, 526, A136

Møller P., Stiavelli M., Zeilinger W. W., 1995, MNRAS, 276, 979

Moore B., Katz N., Lake G., Dressler A., Oemler A., 1996, Nature, 379, 613

Morrissey P., et al., 2007, ApJS, 173, 682

Moss C., Whittle M., 1993, ApJ, 407, L17

Munari E., Biviano A., Borgani S., Murante G., Fabjan D., 2013, MNRAS, 430, 2638

Negroponte J., White S. D. M., 1983, MNRAS, 205, 1009

Nelan J. E., Smith R. J., Hudson M. J., Wegner G. A., Lucey J. R., Moore S. A. W., Quinney S. J., Suntzeff N. B., 2005, ApJ, 632, 137

Newman A. B., Ellis R. S., Andreon S., Treu T., Raichoor A., Trinchieri G., 2014, ApJ, 788, 51

Norgaard-Nielsen H. U., Kjaergaard P., 1981, A&A, 93, 290

Norris J. E., 2004, ApJ, 612, L25

O'Connell R. W., 1999, ARA&A, 37, 603

O'Connell R., 2005, The PERSEUS Cluster in the Ultraviolet, GALEX Proposal

Oconnell R. W., Thuan T. X., Puschell J. J., 1986, ApJ, 303, L37

Oguri M., Bayliss M. B., Dahle H., Sharon K., Gladders M. D., Natarajan P., Hennawi J. F., Koester B. P., 2012, MNRAS, 420, 3213

Ohl R. G., et al., 1998, ApJ, 505, L11

Oke J. B., Bertola F., Capaccioli M., 1981, ApJ, 243, 453

Park J.-H., Lee Y.-W., 1997, ApJ, 476, 28

Pasquini L., Mauas P., Käufl H. U., Cacciari C., 2011, A&A, 531, A35

Pastorello N., Forbes D. A., Foster C., Brodie J. P., Usher C., Romanowsky A. J., Strader J., Arnold J. A., 2014, MNRAS, 442, 1003

Peacock M. B., Zepf S. E., Kundu A., Chael J., 2017, MNRAS, 464, 713

Peimbert M., Luridiana V., Peimbert A., 2007, ApJ, 666, 636

Peng F., Nagai D., 2009, ApJ, 705, L58

Peng E. W., et al., 2006, ApJ, 639, 95

Percival S. M., Salaris M., 2011, MNRAS, 412, 2445

Piotto G., et al., 2002, A&A, 391, 945

Piotto G., et al., 2005, ApJ, 621, 777

Piotto G., et al., 2007, ApJ, 661, L53

Poole T. S., et al., 2008, MNRAS, 383, 627

Pozzetti L., et al., 2010, A&A, 523, A13

Price J., Phillipps S., Huxor A., Smith R. J., Lucey J. R., 2011, MNRAS, 411, 2558

Rawle T. D., Smith R. J., Lucey J. R., Hudson M. J., Wegner G. A., 2008, MNRAS, 385, 2097

Recio-Blanco A., Aparicio A., Piotto G., de Angeli F., Djorgovski S. G., 2006, A&A, 452, 875

Ree C. H., et al., 2007, ApJS, 173, 607

Reed M. D., Stiening R., 2004, PASP, 116, 506

Reimers D., 1975, Memoires of the Societe Royale des Sciences de Liege, 8, 369

Reimers D., 1977, A&A, 61, 217

Renzini A., 2006, ARA&A, 44, 141

Renzini A., 2008, MNRAS, 391, 354

Rich R. M., et al., 2005, ApJ, 619, L107

Rizzo F., Fraternali F., Iorio G., 2018, MNRAS, 476, 2137

Roberts M. S., Haynes M., 1994, in Meylan G., Prugniel P., eds, European Southern Observatory Conference and Workshop Proceedings Vol. 49, European Southern Observatory Conference and Workshop Proceedings. p. 197

Roming P. W. A., et al., 2005, Space Sci. Rev., 120, 95

Roseboom I. G., et al., 2006, MNRAS, 373, 349

Rozo E., Rykoff E. S., Becker M., Reddick R. M., Wechsler R. H., 2015, MNRAS, 453, 38

Sadat R., Blanchard A., Kneib J.-P., Mathez G., Madore B., Mazzarella J. M., 2004, A&A, 424, 1097

Saffer R. A., Bergeron P., Koester D., Liebert J., 1994, ApJ, 432, 351

Sakamoto K., Okumura S. K., Ishizuki S., Scoville N. Z., 1999, ApJ, 525, 691

Salaris M., Cassisi S., Pietrinferni A., 2016, A&A, 590, A64

Sandage A., 1961, The Hubble Atlas of Galaxies

Sandage A., Visvanathan N., 1978a, ApJ, 223, 707

Sandage A., Visvanathan N., 1978b, ApJ, 225, 742

Sanders D. B., Soifer B. T., Elias J. H., Madore B. F., Matthews K., Neugebauer G., Scoville N. Z., 1988, ApJ, 325, 74

Sanders J. S., Fabian A. C., Sun M., Churazov E., Simionescu A., Walker S. A., Werner N., 2014, MNRAS, 439, 1182

Saro A., Mohr J. J., Bazin G., Dolag K., 2013, ApJ, 772, 47

Schechter P., 1976, ApJ, 203, 297

Schlafly E. F., Finkbeiner D. P., 2011, ApJ, 737, 103

Schombert J. M., 2016, AJ, 152, 214

Searle L., Sargent W. L. W., Bagnuolo W. G., 1973, ApJ, 179, 427

Serra A. L., Diaferio A., 2013, ApJ, 768, 116

Smith R. J., Lucey J. R., Carter D., 2012, MNRAS, 421, 2982

Sohn S. T., O'Connell R. W., Kundu A., Landsman W. B., Burstein D., Bohlin R. C., Frogel J. A., Rose J. A., 2006, AJ, 131, 866

Sollima A., Pancino E., Ferraro F. R., Bellazzini M., Straniero O., Pasquini L., 2005, ApJ, 634, 332

Stanek R., Rasia E., Evrard A. E., Pearce F., Gazzola L., 2010, ApJ, 715, 1508

Stanford S. A., Eisenhardt P. R., Dickinson M., 1998, ApJ, 492, 461

Tailo M., et al., 2017, MNRAS, 465, 1046

Tantalo R., Chiosi C., Bressan A., Fagotto F., 1996, A&A, 311, 361

Taranu D. S., Hudson M. J., Balogh M. L., Smith R. J., Power C., Oman K. A., Krane B., 2014, MNRAS, 440, 1934

Thomas D., Maraston C., Bender R., Mendes de Oliveira C., 2005, ApJ, 621, 673

Thomas D., Maraston C., Schawinski K., Sarzi M., Silk J., 2010, MNRAS, 404, 1775

Tonry J. L., 1987, in de Zeeuw P. T., ed., IAU Symposium Vol. 127, Structure and Dynamics of Elliptical Galaxies. pp 89–96

Torlina L., De Propris R., West M. J., 2007, ApJ, 660, L97

Tovmassian H. M., Andernach H., 2012, MNRAS, 427, 2047

Truemper J., 1993, Science, 260, 1769

Ventura P., Di Criscienzo M., Carini R., D'Antona F., 2013, MNRAS, 431, 3642

Visvanathan N., Sandage A., 1977, ApJ, 216, 214

Wen Z. L., Han J. L., 2011, ApJ, 734, 68

White S. D. M., Briel U. G., Henry J. P., 1993, MNRAS, 261, L8

Williams K. A., Canton P. A., Bellini A., Bolte M., Rubin K. H. R., Gianninas A., Kilic M., 2018, preprint, (arXiv:1807.09315)

Yaron O., Kovetz A., Prialnik D., 2008, in Deng L., Chan K. L., eds, IAU Symposium Vol. 252, The Art of Modeling Stars in the 21st Century. pp 261–262, doi:10.1017/S1743921308022965

Yi S. K., 2008, in Heber U., Jeffery C. S., Napiwotzki R., eds, Astronomical Society of the Pacific Conference Series Vol. 392, Hot Subdwarf Stars and Related Objects. p. 3 (arXiv:0808.0254)

Yi S., Demarque P., Oemler Jr. A., 1997, ApJ, 486, 201

Yi S., Demarque P., Oemler Jr. A., 1998, ApJ, 492, 480

Yi S., Lee Y.-W., Woo J.-H., Park J.-H., Demarque P., Oemler Jr. A., 1999, ApJ, 513, 128

Yi S. K., et al., 2005, ApJ, 619, L111

Yi S. K., Lee J., Sheen Y.-K., Jeong H., Suh H., Oh K., 2011, ApJS, 195, 22

York D. G., et al., 2000, AJ, 120, 1579

de Boer K. S., 1982, A&AS, 50, 247

de Freitas Pacheco J. A., Barbuy B., 1995, A&A, 302, 718

de Vaucouleurs G., 1963, ApJS, 8, 31

van Dokkum P. G., 2005, AJ, 130, 2647

van Dokkum P., Conroy C., Villaume A., Brodie J., Romanowsky A. J., 2017, ApJ, 841, 68